

This is to certify that the

dissertation entitled

EFFECT OF MULTI-FUNCTIONAL INHIBITORS
ON THE ELECTROCHEMISTRY WITHIN A CORROSION CRACK
presented by

Hiroyuki Omura

has been accepted towards fulfillment of the requirements for

ph.D degree in Metallurgy

Major professor

Robert Summitt

Date 6 August 1984



RETURNING MATERIALS:
Place in book drop to remove this checkout from your record. FINES will be charged if book is returned after the date stamped below.

EFFECT OF MULTI-FUNCTIONAL INHIBITORS ON THE ELECTROCHEMISTRY WITHIN A CORROSION CRACK

Ву

Hiroyuki Omura

A DISSERTATION

Submitted to
Michigan State University
in partial fulfillment of the requirements
for the degree of
DOCTOR OF PHILOSOPHY

Department of Metallurgy, Mechanics and Materials Science

ABSTRACT

EFFECT OF MULTI-FUNCTIONAL INHIBITORS ON THE ELECTROCHEMISTRY WITHIN A CORROSION CRACK

By

Hiroyuki Omura

The electrochemical and mass transport mechanisms in stress corrosion cracking, which depend on the rate of metal dissolution and production of hydrogen, have been used to establish analytically the electrode potential distribution within the crack. When crack growth occurs by enhanced anodic dissolution of the plastically strained tip, the electrode potential at the crack tip always is more active than at the crack mouth because of the electric potential gradient which exists in the electrolyte within the crack. This also gives rise to additional or alternate electrochemical reactions such as hydrogen evolution and anodic dissolution at the crack tip. Futhermore, because of the potential difference from the crack mouth, the electrochemical driving force becomes more favorable for the development of corrosion inside the crack.

The analysis predicts the distribution of electrode potential within a crack, and theoretical results have been compared with experimental measurements recorded from a model electrode system. Under free corrosion, a small potential difference may cause a concentration change of Cl ion and increase the chloride attack. In order to reduce the chloride and hydrogen attack, multifunctional inhibitors, such as borax-nitrite with small amounts of surfactant such as MBT or amino-methyl-propanol, are excellent inhibitors. The surfactant interferes in the dissolution reaction and blocks active chloride ion and hydrogen ion by interacting synergistically with the passive film produced by the borax-nitrite, which results in development of a stronger and thicker protective film.

ACKNOWLEDGMENT

The author would like to express his deep gratitute and appeciation to his academic advisor, Dr. Robert Summitt whose guidance and assistance were invaluable throughout the authors graduate program and especially during the course of this investigation.

Thanks are also due the other members of the authors guidance committee, Dr. J. Martin, Dr. K. N. Subramanian and Dr. A. Timnick for their inspiration.

Thanks are extended to U. S. Air Force, Wright-Aeronautical Laboratories, NASA Lewis Research Center, U. S. Army Construction Engineering Research Laboratories, U. S. Office of Naval Research, the Department of Metallurgy, Mechanics and Materials Science, and the Division of Engineering Research at Michigan State University for the financial assistance rendered during the Doctoral program.

TABLE OF CONTENTS

| | | Page |
|------------|---------------------------------|------|
| LIST OF TA | ABLES | iv |
| LIST OF F | IGURES | v |
| I. | INTRODUCTION | 1 |
| II. | THEORETICAL BACKGROUND | 11 |
| III. | EXPERIMENTAL TEST PROCEDURE AND | |
| | APPARATUS | 25 |
| IV. | EXPERIMENTAL RESULTS | 40 |
| v. | DISCUSSION | 85 |
| VI. | CONCLUSION | 105 |
| REFERENCE | S | 108 |

LIST OF TABLES

| Table | | Page |
|-------|-------------------------------------------|--------------|
| 1 | Chemical Analysis of Test Specimen | . 35 |
| 2 | Mechanical Properties of 7075-T6 Al Alloy | . 36 |
| 3 | The Inhibitors and Surfactant | . 3 9 |
| 4 | Chemical Composition of Tap Water | . 47 |

LIST OF FIGURES

| Figure | | Page |
|--------|-------------------------------------------------------------------------------------------------------------------------------------------|------|
| 1 | Theoretical Electrochemical System with Two Oxidation-Reduction Reactions | 17 |
| 2 | Motion of Electrolyte ions in a Crack | 22 |
| 3 | Simplified Experimental System | 26 |
| 4 | Bare Surface Specimen | 29 |
| 5 | A Modified Artificial Crevice | 29 |
| 6 | Block Diagram of Simplified Experimental System in Control E Operation | 31 |
| 7 | Steady-State Open-Circuit Potential for 7075 T6 Al Alloy in 1.0 wt.% NaCl Solution | 33 |
| 8 | Modified WOL-type Constant Deflection Specimen | 38 |
| 9 | Anodic Polarization of 7075 T6 Al Alloy in Dilute Sodium Chloride Solution Without Stirring at $20^{\circ}\text{C} \pm 2^{\circ}\text{C}$ | 41 |
| 10 | Cathodic Polarization of 7075 T6 Al Alloy in 1 wt.% NaCl Solution Without Stirring at $20^{\circ}\text{C} \pm 2^{\circ}\text{C}$ | 42 |
| 11 | Cathodic Polarization of 7075 T6 Al Alloy in 3 wt.% NaCl Solution Without Stirring at 20°C + 2°C | 43 |
| 12 | Anodic Polariztion of 7075 T6 Al Alloy in Distilled Water Without Stirring at 20° C \pm 2° C | 45 |
| 13 | Anodic Polarization of 7075 T6 Al Alloy in Tap Water With Stirring at 20° C $\pm 2^{\circ}$ C | |
| 14 | Anodic Polarization of 7075 T6 Al Alloy in 1 wt.% NaCl and Inhibitor Without Stirring at 20°C + 2°C | |
| 15 | Anodic Polarization of 7075 T6 Al Alloy in 1 wt.% NaCl and Inhibitor Without Stirring at $20^{\circ}\text{C} \pm 2^{\circ}\text{C}$ | .49 |
| 16 | Anodic Polarization of 7075 T6 Al Alloy in 1 wt.% NaCl and Inhibitor Without Stirring at 20°C + 2°C | . 51 |

| Figure | | Page |
|--------|-------------------------------------------------------------------------------------------------------------------------------------------------|------------|
| 17 | Anodic Polarization of 7075 T6 Al Alloy in 1 wt.% NaCl and Inhibitor Without Stirring at $20^{\circ}C \pm 2^{\circ}C$ | 52 |
| 18 | Anodic Polarization of 7075 T6 Al Alloy in 1 wt.% NaCl, Inhibitor and Surfactant without Stirring at $20^{\circ}\text{C} \pm 2^{\circ}\text{C}$ | 55 |
| 19 | Cathodic Polarization of 7075 T6 Al Alloy in 1 wt.% NaCl and Inhibitor Without Stirring at 20° C \pm 2° C | 57 |
| 20 | Linear Polarization of 7075 T6 Al Alloy in 1 wt.% NaCl Under Various Condition Without Stirring at $20^{\circ}\text{C} \pm 2^{\circ}\text{C}$ | 59 |
| 21 | Linear Polarization of 7075 T6 Al Alloy in 1 wt.% NaCl Without Stirring at 20° C \pm 2° C | 6 9 |
| 22 | Linear Polarization of 7075 T6 Al Alloy in 1 wt.% NaCl Without Stirring at $20^{\circ}\text{C} \pm 2^{\circ}\text{C}$ | 61 |
| 23 | Anodic Polarization of 7075 T6 Al Alloy in 1 wt.% NaCl Under Stress Without Stirring at $20^{\circ}C \pm 2^{\circ}C$ | 62 |
| 24 | Anodic Polarization of 7075 T6 Alloy in Dilute NaCl Solution | 64 |
| 25 | Potential - pH Equilibrium Diagram for the System Aluminum - Water at 25°C | 66 |
| 26 | Cathodic Polarization of 7075 T6 Al Alloy in 1 wt.% NaCl Solution and Crevice Without Stirring at $20^{\circ}\text{C} \pm 2^{\circ}\text{C}$ | 67 |
| 27 | Cathodic Polarization of 7075 T6 Al Alloy in 3 wt.% NaCl Solution and Crevice Without Stirring at $20^{\circ}\text{C} \pm 2^{\circ}\text{C}$ | 68 |
| 28 | Steady - State Open - Circuit Potentials for Open and Crevice 7075 T6 Al Alloy in Dilute NaCl Solution With and Without Inhibitors | 69 |
| 29 | Steady - State Open - Circuit Potentials for Open and Crevice 7075 T6 Al Alloy in Dilute NaCl Solution | 72 |
| 30 | Anodic Polarization for Open and Crevice 7075 T6 Al Alloy in 1 wt.% NaCl Solution Without Stirring at 20°C + 2°C | 73 |

| Figure | | Page |
|--------|------------------------------------------------------------------------------------------------------------------------------------------------------------------------------|------|
| 31 | Anodic Polarization for Various Condition of Crevice in Dilute Solution Without Stirring at $20^{\circ}\text{C} \pm 2^{\circ}\text{C}$ | 74 |
| 32 | Steady - State Open - Circuit Potential for Open and Coupled Crevice 7075 T6 Al Alloy in 1 wt.% NaCl Solution Without Stirring at $20^{\circ}\text{C} \pm 2^{\circ}\text{C}$ | 77 |
| 33 | Steady - State Open - Circuit Potential Difference for Open and Coupled Crevice 7075 T6 A1 Alloy in 1 wt.% NaCl Solution | 78 |
| 34 | The Potential Difference for Open and Crevice 7075 T6 Al Alloy Under Active State in 1 wt.% NaCl Solution | 79 |
| 35 | Steady - State Open - Circuit Potential Under Stress in 1 wt.% NaCl Solution | 82 |
| 36 | Rate of Cracking Versus Stress Intensity for Dilute NaCl Solution | 84 |
| 37 | Schematic Representation of the Crack | 96 |
| 38 | Schematic Polarization Diagram of the Electrochemical Reactions Occurring at the Specimen Surface Showing the Influence of Potentiostatic Polarization | 97 |
| | Initidence of totalitostatic totalization | 21 |

I. INTRODUCTION

A. General Introduction

This thesis describes an experimental investigation of the electrochemical and mass transport behavior inside a crack, under both stressed and unstressed conditions, and in the presence of aqueous chloride ion. In order to investigate these corrosion processes, electrochemical corrosion methods have been found to be useful because these techniques accelerate the corrosion process and allow rate data to be obtained in a short time. Additionally, these techniques can be used to characterize the corrosion of alloys in specific environments. In this research, electrochemical potentiodynamic polarization techniques were used to determine (1) the electrochemical and mass transport mechanism of 7075 T6 Al alloys between the external environment and the crack tip; (2) the relation between micro-electrochemistry and an external environment controlled by an inhibitor; and (3) the relations between microchemistry at the crack tip and external chemistry in the presence of chloride ion.

Generally, the results show that crevice corrosion of the aluminum alloy depends on the width of the crack, the difference between the rate of the process in the crevice and on an open surface. The polarization behavior at the crack is different from the outer surface. Furthermore, intensive corrosion of aluminum alloys in a narrow crack is the result of a marked negative change of the potential. The value of the potential of aluminum inside the crack reaches a certain value which provides as well for the possible cause of the corrosion process because of the reaction of hydrogen evolution.

Crevice corrosion leads to the formation of localized cells where the solution may attain very high ionic concentration. During the very

initial stage of the formation of localized cells, the electric mass transport (migration) has been regarded as predominating over diffusion. The latter, on the contrary, mainly determines the concentration profile as soon as steady conditions of growth are reached. The transport number of the highly hydrated corrosion products is nearly zero and migration should play a secondary role. It will be shown that high ionic concentration and especially halide enrichment, ionic migration, acidity because of hydrolysis, ionic solvation, and low water-to-iron ratio allow a more realistic picture of the electrochemistry of the localized cells to be obtained.

A model is proposed for the combined effect of mass transfer, polarization on the current and potential profiles inside the crack. Furthermore, a mathematical model has been extended which links several parameters so that quantitative predictions can be made for crack corrosion behavior of 7075-T6 Al alloy in sodium chloride environments. Experimental work associated with providing selected input data for the model and also with providing verification of the model are described.

B. General Background And Resarch Objective

High strength aluminum alloys are notoriously susceptible to stress corrosion cracking in aqueous chloride solution. Several approaches have been used in efforts to overcome the problem, including variations in heat treatment, alloy composition, and thermomechanical processing. An attractive alternate approach is to modify the environment itself by the use of corrosion inhibiting substances. Inhibitors have been used successfully to prevent corrosion of aluminum alloys, and have been found to be somewhat effective in reducing stress corrosion cracking. (1), (2)

Inhibitors can function via either cathodic or anodic mechanisms. Mechanisms (3) whereby cathodic inhibitors (e.g., borax) function apparently are to provide an oxygen diffusion barrier at the metal surface, and, since the films also usually are poor electronic conductors, they are incapable of promoting oxygen reduction at the film-solution interface. On the other hand, anodic inhibitors (e.g., nitrite ion) react preferentially at electron sink sites, and promote the formation of protective In the case of nitrite ion, the film is formed by adsorpoxide films. tion of nitrite on the metal surface followed by a reaction to form ox-The reduction product of the nitrate inhibitor is soluble, hence ides. a protective film would be formed containing metal ion, oxygen and possibly hydrated oxide. The oxide layer which is formed by the combined action of nitrite and oxygen is continuous and adherent.

Several theoretical models have been proposed to describe electrochemical conditions in an unstressed crack. The earliest, by Evans (4), was based on a differential aeration mechanism. Differential aeration effects, resulting in oxygen concentration gradients, produce a cathodic reaction effect and also drive corrosion at locally variable rates under an electrolyte film of nonuniform thickness. If the local corrosion rate is limited by the oxygen flux, the attack would be most severe for thin films.

Rosenfeld (5) has proposed an alternate mechanism in which the metal within the crack suffers anodic attack as a result of restricted oxygen supply, and the external (aerated) surface forms a large cathode. Inside the crack, anodic dissolution, together with hydrolysis of the product metal ion, can cause an increase of hydrogen ion concentration. If the net corrosion reaction plus hydrolysis should lead to an increase of hydrogen ion concentration, the process would occur independently of any other process, and would accelerate with time to a steady state where diffusion out of the crack tip region would limit the buildup. corrosion reaction plus hydrolysis should lead to no net change in H concentration, merely an acid solution in a crack would be created. If the corroding solution contains some chloride ion, these transferred anions may be chloride ions, and acid formed inside the crack is hydro-Pourbaix (6) has claimed that this is one reason why chlorides are particularly harmful in promoting crevice corrosion and stress corrosion cracking.

McCafferty (7) adopts the systematic approach of Rosenfeld's (5) paper in order to investigate polarization kinetics aspects of a simple crevice system, and confirms the conclusion of Rosenfeld. According to McCafferty, in a crevice where the internal sample is not short-circuited to external metal, the anodic corrosion rate is determined by the limiting current for oxygen reduction. The limiting cathodic

current resulting from oxygen reduction was independent of pH and Cl concentration. Because the crevice height is comparable with the thickness of the oxygen diffusion layer, diffusion of oxygen into the crevice is impeded, hence the corrosion rate is reduced. This results from cathodic control.

Fontana (8) and Greene suggested another mechanism, based on electroneutrality, where chloride ions migrate into the crack to balance the otherwise increasingly positive charge resulting from metal ion concentration. This gives rise to an accumulation of aggressive anions at the crack tip. Alkire and Siitari (9),(10) offered a quantitative mathematical model, as well as experimental data, for a mass transfer control process according to Fontana's mechanism.

Another mechanism for the initiation of corrosion inside the crack was proposed by $\operatorname{Eklund}^{(11)}$, based on electron microscopic investigations of crack regions, which describes corrosion initiation at sulfide inclusions in the metal surface.

Models of corrosion with stress in a crack have been proposed for aluminum alloys (12),(13). These include active crack-path (14) mechanism, stress assisted dissolution by a mechanochemical mechanism, or by film rupture (15), brittle rupture (16), hydrogen embrittlement (16), and structurally-determined dissolution resulting from compositional differences in the grain boundary region. All of these mechanisms can be categorized generally for aluminum-base alloys under NaCl solution as involving (a) pre-existing active paths, (b) strain-generated active paths, or (c) specific adsorption at sub-critical stress sites.

Pre-existing reaction path models assume that localized dissolution occurs because the aluminum alloy contains locally active sites associated

with segregated impurities. Some aluminum alloys exhibit intergranular corrosion in the unstressed state partly because of the solubility of the corrosion products. If these are insoluble and relatively nonporous, one function of the imposed stress would be to rupture the protective film. Such mechanisms of strain-generated active paths have been proposed by several researchers (17),(18).

A dissolution-controlled mechanism assumes that dissolution follows a narrow path as a result of imposing a stress on a specimen. It arises from the interaction of elastically strained metal, produced by the stress, with the solution.

Several discussions (18),(19) have centered around the role of dislocations (one of the most important elements of this mechanism) which are considered to be reactive with respect to the matrix because of their movement or compositional differences arising from atomic rearrangements around stacking faults or regions of short range order. Several researchers (15),(18) showed that static dislocations in metals did not show evidence of chemical activity derived from the strain energy of their core, but the segregation of solution to dislocations in metals did not show evidence of chemical activity derived from the strain energy of their core, but the segregation of solution to dislocations can result in localized attack.

Another type of mechanism of strain-generated active path is a so-called film rupture mechanism (15). High strength aluminum alloys owe their electrochemical inactivity to a relatively inert aluminum oxide film, which forms on the exposed surface of aluminum and aluminum alloys, so that the active metal is separated from the corrosive environment. If the protective aluminum oxide film is mechanically

ruptured, the metal is exposed to chemical attack until such time as the protective film can reform, and thereafter further reaction is stifled until the film is again ruptured. Elastic strain in the underlying metal may be sufficient to bring the protective film to its fracture point, thus exposing metal. The active path along which the crack propagates is generated cyclically as disruptive strain and film buildup alternate with one another. Hoar (20) showed experimentally that currents associated with electrodes under stress may be much larger than those observed at static surfaces, a difference which suggests that the reaction rate upon straining is controlled by the rate of oxide rupture caused by slip-step emergence and by the subsequent passivation rate of the newly bared metal.

The mechanism of specific adsorption at subcritically stressed sites has been proposed. Where the local dissolution rate at the crack tip is under cathodic control, the ratio of hydrogen evolved to hydrogen adsorbed may play an important role in determining what proportion of a fracture is caused by dissolution and what proportion by hydrogen. Even when hydrogen embrittlement is the major cause of fracture, the minor role of the dissolution process will, under open-circuit condition, determine the rate of hydrogen ion discharge.

Each of these corrosion cracking models, with or without stress, in the presence of NaCl solution, has key features: (1) role of chloride and hydrogen ions; (2) cathodic reduction; hydrogen or oxygen reduction; (3) the potential gradient inside a crack; and (4) the potential effects of inhibitors.

A significant role of $C1^-$ ion inside the crack with and without stress has been demonstrated (6), (7), (9). Chloride ion is one of the

primary factors responsible for the proposed dissolution process related to the mechanism of a pre-existing active path and film rupture mechanism. Alkire, Hebert and Siitari (10),(21) also postulate the importance of Cl-inside the crack. If accumulation by migration of chloride ions within the crevice is significant, it is possible that the activation behavior would depend on Cl-concentrations. Pryor (23) believes that the manner in which Cl-promotes pitting is caused by a defect structure set up where Cl-ions exchange with 0-2 ions on the Al₂0₃ lattice, electrical neutrality being maintained by the passage of an appropriate number of Al³⁺ ions from the oxide into solution. The influence of Cl-concentration on pitting also has been studied by Bogar and Foley (22). At the higher Cl-concentration, the following reaction will take place.

$$A1 + 4 C1^{-} - A1C1_{4}^{-} + 3e^{-},$$

 $A1 + 4 C1^{-} + 3H^{+} - A1C1_{4}^{-} + 3/2 H_{2}.$

This action of Cl promotes pitting.

The importance of the cathodic reaction (hydrogen evolution reaction), as well as H⁺ ion on the side wall and external surface, has been investigated. Pickering and Frankenthal⁽²⁴⁾, Pickering and Ateya ⁽²⁵⁾, Seys and Brabers⁽²⁶⁾, Siitari and Alkire⁽²⁷⁾, observed hydrogen gas evolution from both real and artifical pits or crevices in aluminum during kinetics experiments. The gas extracted from the electrolyte was analyzed in a mass spectrometer and was found to be hydrogen gas. This evidence is important because it supports the mechanism of hydrogen embrittlement. Furthermore, Seys and Brabers⁽²⁶⁾ reported that hydrogen evolution is not an essential part of the pitting mechanism, but note that stress corrosion cracking commonly arises as a result of hydrogen gas formation. Evans and Edeleanu⁽²⁸⁾ proposed the mechanism of autocatalytic pit propagation resulting from the hydrogen evolution reaction

and a buildup of acidity.

Alkire and Siitari (29), showed quantitative mathematical models under mass transfer control and presented later a more developed model (21). It was demonstrated that cathodic processes can occur within the crack as well as on adjacent exterior surfaces and largely is influenced by the potential and concentration distribution inside the crack. and Frankenthal (24) showed that the large potential drops in solution are caused by formation of bubbles within regions of corrosion in the crack. The presence of gas bubbles on the electrode surface causes an increase of the electrolyte layer, adjacent to the electrode surface. The ohmic resistance increase is closely related to the bubble departure radius. The electrode-potential gradient between the crack and the external environment also is important as the driving force for mass transport between the crack tip and bulk environment. There are three forms of mass transport: migration, diffusion and convection. The transport of reactants and products in the crevice region is thus restricted so as to give rise to conditions different than those encountered by metal freely exposed to bulk electrolyte (29).

Although in a general way the corrosion mechanism of aluminum alloys is clear, individual aspects of the key features call for more clear elucidation. The activation mechanism of aluminum alloys in aqueous chloride solutions remains unclear: is there a gradual shift of the stationary potential to the negative side in the crevice because of acidification and transport of the metal from a passive to an active state? In this connection, it is highly important to ascertain more definitely the value of potentials or of other parameters at which localized corrosion develops.

Furthermore, the influence of geometrical factors on change in the composition of the medium and distribution of potentials and current, demand special study.

Consequently, an experimental program was conducted to provide information on the polarization kinetics, potential distribution in a crack, and other parameters under various conditions. The approach taken here is similar to that developed by McCafferty⁽⁷⁾ and others⁽⁵⁾.

II. THEORETICAL BACKGROUND

A. Electrode Kinetics.

The rate of a simple anodic electrochemical reaction where metal ions M^+ are produced from the solid metal phase M(s), may be written

$$M(s) \rightarrow M^+ + e^-$$

or as an anodic current density,

$$i_a = F \bar{K}_a, \qquad (1)$$

and, similarly, the rate of the reverse (cathodic) reaction also may be written as a current density,

$$i_{C} = -F \bar{K}_{C} C_{M}^{+}, \qquad (2)$$

where the quantities \overline{K}_a and \overline{K}_c are heterogeneous electrochemical rate constants which depend on the electrical potential, and C_M^+ is the concentration of M^+ . Anodic currents are taken to be positive and cathodic currents are negative. The potential dependence of each of the rate constants is defined to be

$$\bar{K}_a = K_a \exp\left(\frac{\mathbf{d}_a F}{R T} \emptyset\right),$$
 (3)

$$\bar{K}_{c} = K_{c} \exp \left(-\frac{c \cdot F}{R \cdot T} \emptyset\right),$$
 (4)

where the potential \emptyset is taken with respect to a reference electrode, e.g., hydrogen or saturated calomel electrode. The constants K_a and K_c are the fundamental heterogeneous rate constants and are independent of potential. The constants F and R are the Faraday constant and gas constant, respectively, and T is the absolute temperature. The parameters d_a and d_c are intrinsic kinetic parameters of the system, and usually have the value of 1/2 for elementary one electron transfer reactions. With these definitions, the anodic and cathodic

reactions may be written

$$i_a = F K_a \exp \left(\frac{d_a F}{R T} \emptyset\right),$$
 (5)

and

$$i_{C} = -F (K C_{M} +) \exp \left(-\frac{d_{C} F}{R T} \emptyset\right). \tag{6}$$

(For the above reaction, the cathodic reaction is first order in M⁺ and the cathodic rate is a linear function of the concentration of M⁺. The anodic process also could be considered first order with respect to M, but the metal concentration does not change during the reaction and is absorbed in the rate constant for convenience.)

The net current density for the reaction will be

$$i = i_a + i_c , \qquad (7)$$

or

$$\frac{1}{F} = K_a \exp\left(\frac{\partial_a F}{RT} \emptyset\right) - \left(K_c C_M^+\right) \exp\left(-\frac{\partial_c F}{RT} \emptyset\right). \quad (8)$$

At steady state, the net current is zero so that

$$K_a \exp \left(\frac{A_a F}{R T} \emptyset^o\right) = K_c C_M + \exp \left(-\frac{A_c F}{R T} \emptyset^o\right),$$
 (9)

and the equilibrium potential ϕ^{O} therefore is

$$\emptyset^{\circ} = \frac{R}{F} \frac{T}{(d_a + d_c)} \ln \frac{K_c C_M^+}{K_a}. \tag{10}$$

Defining a quantity called the exchange current density,

$$i_0 = F K_a \left(\frac{K_c C_M^+}{K_a} \right) d_a / (d_a + d_c),$$
 (11)

the net current density may be written

$$i = i_0 [\exp [\frac{d_0 F}{R T} (\emptyset - \emptyset^0)] - \exp [-\frac{d_0 F}{R T} (\emptyset - \emptyset^0)]].$$
 (12)

One may further define the surface overpotential,

$$\gamma_{s} = \emptyset - \emptyset^{o}, \tag{13}$$

and obtain

$$i = i_0 \left[\exp \left(\frac{d_a F}{R T} \gamma_s \right) - \exp \left(-\frac{d_c F}{R T} \gamma_s \right) \right]. \tag{14}$$

Equation (14) is known as the Butler - Volmer expression for the electrode - kinetics of the single step. Expressing the net rate of an electrode reaction in terms of the exchange current density and overpotential is equivalent to expressing it in terms of the heterogeneous rate constants and the potential. (32),(33),(34)

B. Corrosion Reaction

The general relationship for current balance at the corrosion potential is

$$\sum I_{\mathbf{a}} = -\sum I_{\mathbf{c}} . \tag{15}$$

A heterogeneous surface will satisfy the overall current balance expressed in equation (15) although it is not obeyed locally. If the heterogeneous surface is a collection of locally homogeneous areas A on which the current density is uniform, the current balance equation is

$$\sum_{i_k} \mathbf{i}_k = -\sum_{j} \mathbf{i}_j \mathbf{A}_j . \tag{16}$$

Attention will be given to homogeneous surfaces which satisfy the current density balance at each point on the surface, i.e., the current equation is

$$\sum i_k = -\sum i_j . \tag{17}$$

For the special case of a single metal dissolution reaction coupled with a single cathodic reaction,

$$i_a = -i_c = i_{corr}, \qquad (18)$$

and the last relationship identifies the corrosion current. Substituting the Butler-Volmer equation for each reaction,

$$i_{oa}[\exp \left[\frac{d_{aa}F}{RT}(\phi^* - \phi_a^o)\right] - \exp \left[-\frac{d_{ac}F}{RT}(\phi^* - \phi_a^o)\right] =$$

$$\left[\begin{array}{c} \frac{d_{ca}F}{RT} \left(\begin{array}{cc} \phi^{*} - \phi^{o}_{c} \end{array}\right) \right] - \exp\left[-\frac{d_{cc}F}{RT} \left(\begin{array}{cc} \phi^{*} - \phi_{c} \end{array}\right) \right], \tag{19}$$

where the potential, \emptyset , is the corrosion potential, and it lies between \emptyset_a^o and \emptyset_c^o . Given the values of i_{oa} , i_{oc} , and \emptyset_a^o , \emptyset_c^o one can compute the corrosion potential.

A closed form solution for equation (19) can be found when the

values are all equivalent,

$$d_{aa} = d_{cc} = d_{ac} = d_{ca}. \tag{20}$$

Additionally, if all the α values are equal to 1/2, equation (19) may be rearranged to give the corrosion potential ϕ^* ,

$$\phi^* = \frac{R T}{F} \ln \frac{i_{oa} \exp (F/2RT) \phi_a^0 + i_{oc} \exp (F/2RT) \phi_c}{i_{oa} \exp (-F/2RT) \phi_a^0 + i_{oc} \exp (-F/2RT) \phi_c}.$$
 (21)

When the equilibrium potentials for the two reactions are widely separated, the reverse reaction for either or both reactions may be negligible. Stern and Geary (35) first treated this superposition for metal dissolution and hydrogen evolution, and obtained

$$i_{corr} = i_{oa} \exp \left(\frac{d_{aa}F}{RT}\right) \left(\phi^* - \phi_a^o\right) = i_{oc} \exp \left(-\frac{d_{cc}F}{RT}\right) \left(\phi^* - \phi_c^o\right).$$
 (22)

The corrosion potential can be calculated from equation(22)

$$(\alpha_{aa} + \alpha_{cc}) \phi^* = \frac{RT}{F} \ln \left(\frac{1_{oc}}{1_{oa}}\right) + \alpha_{cc} \phi^o_c + \alpha_{aa} \phi^o_a. \tag{23}$$

Introducing the definition for the current density [Eq. (22)] and corrosion potential [Eq. (23)], the total current density is given by $(cf. Stern^{(36),(37),(38)})$

$$i = i_a + i_c = i_{corr} [exp (\frac{d_{aa}F}{RT}) (\phi - \phi^*) - exp (-\frac{d_{cc}F}{RT} (\phi - \phi^*))].$$
(24)

This equation resembles the Bulter-Volmer equation for a single reaction, where the corrosion potential and corrosion current density have replaced the equilibrium potential and exchange current density.

Neglect of the reverse reaction is valid for large positive potential (with respect to the equilibrium potential) for the anodic reaction.

Neglect of the oxide reaction is valid for large negative potentials (with

respect to the equilibrium potential) for the cathodic reaction. At the corrosion potential, both conditions are assumed to be fulfilled simultaneously for the Stern treatment and each reaction is said to be under the Tafel condition. The teatment is illustrated in Figure 1, i.e., if $i_a > i_c$, the current i is

$$i = i_{corr} \exp \left(\frac{d_{Ra}F}{RT} \right) \left(\phi - \phi^* \right), \tag{25}$$

and if $i_c > i_a$, it is

$$i = -i_{corr} \exp \left(-\frac{d_{cc}F}{RT} \left(\emptyset - \emptyset^* \right) \right). \tag{26}$$

Equation (25) can be rewritten as

$$\phi - \phi^* = \frac{RT}{d_{aa}} F \ln \frac{1}{i_{corr}}$$
, (27)

or

$$\phi - \phi^* = A + \frac{RT}{\phi_{aa} F} \ln i, \qquad (28)$$

Figure 1 shows a schematic plot of Eq. 28 as $\phi - \phi^*$ vs i .

The value of the anodic Tafel slope is

$$\frac{d \left(\phi - \phi^* \right)}{d \log i} = \frac{2.303 \text{ RT}}{c \zeta_{aa} \text{ F}}$$
 (27)

Extrapolation of Tafel branches to their interaction at the corrosion potential gives the corrosion current density, i corr, and is shown by the solid-dashed line, and the deviation from the extrapolated curves indicates the increased importance of the other, superposed, reaction as the corrosion potential is approached from either Tafel extreme. The Tafel extrapolation technique for measurement of corrosion kinetic parameters may be used to determine the anodic and cathodic Tafel slopes as well as the corrosion current density. This technique has been used widely for the investigation of corrosion kinetics, with the most

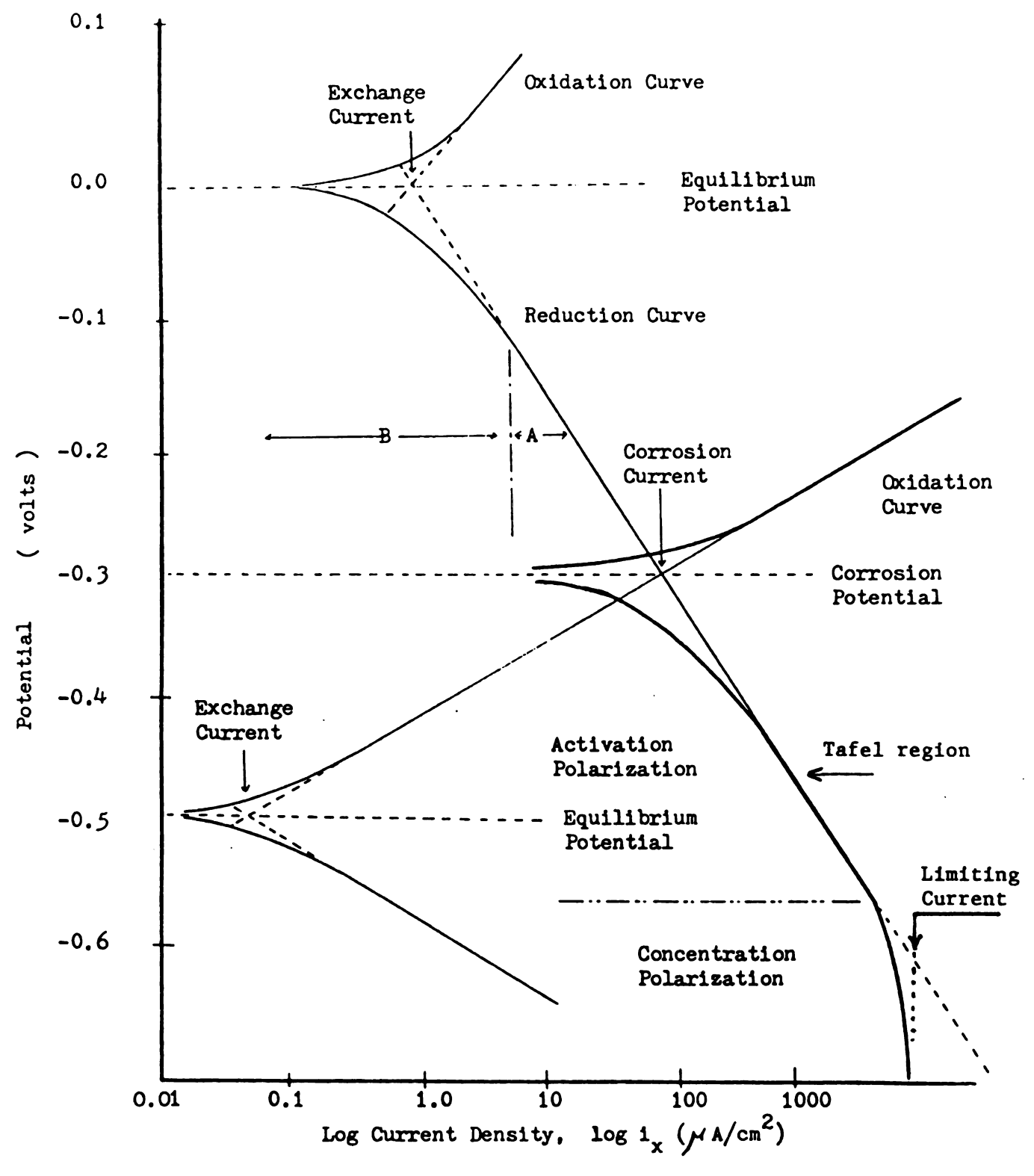


FIGURE 1 THEORETICAL ELECTROCHEMICAL SYSTEM WITH TWO OXIDATION - REDUCTION REACTIONS

success in acidic solutions and other systems in which there are soluble reaction products. Aside from limitations caused by the precipitation of insulating and protective films, the Tafel technique has limitations caused by ohmic and mass transfer effects.

(1) Ohmic Effects

Ohmic resistance between the reference electrode and the polarized electrode contributes to total overvoltage measured. The resistance is a function of solution conductivity, distance between the reference electrode and the sample, and the geometry of the system. Barnatt (39) has presented an analysis of the magnitude of the IR drop expected as a function of both the current density and the solution conductivity. According to Barnatt (39), the resistance is a linear function of current and can be expressed as

$$\delta = \frac{\lambda_{aa} F L}{K R T} i_{ave}, \qquad (29)$$

where L is a characteristic dimension for the system, and K is the electrolyte conductivity. The magnitude of § depends on the level of current and reflects the increased importance of ohmic effects at high current density in Tafel polarization measurements.

(2) Concentration Polarization

At high overvoltages, the measurement of activation overvoltage
may be complicated by an interfering phenomena called concentration
polarization. Concentration polarization occurs when the reaction rate
or the applied external current is so large that the species being

oxidized or reduced cannot reach the surface at a sufficiently rapid rate. The solution adjacent to the electrode surface becomes depleted of the reacting ions and the rate then is controlled by the rate at which the reacting species can diffuse to the surface. Analytically, it is given by Uhlig (58) as follows:

$$\phi - \phi^* = \frac{R T}{z F} \ln (1 - \frac{1}{1_L}),$$
 (30)

where i_L is the limiting current density for a cathodic process and i is the applied current density. As i approaches i_L , $\emptyset - \emptyset^*$ approaches infinity. This is shown by the plot of $\emptyset - \emptyset^*$ versus i in Fig. 1.

The limiting current density can be evaluated from the expression

$$i_{L} = \frac{z + D c}{r}, \qquad (31)$$

where D is the diffusion constant for the ion being reduced, z is the number of unit charges transported per ion in the diffusion process,

I is the thickness of the stagnant layer of electrolyte next to the electrode surface, and c is the concentration of diffusion ion in moles/liter.

C. Mass Transfer

The simplest electrode reactions are those in which the kinetics of all electron transfer and associated chemical reactions are very rapid compared with those of the mass transfer process. Under these conditions, the chemical reactions can usually be treated in a particulary simple way. If, for example, an electrode process involves only fast heterogeneous charge transfer kinetics and mobile, reversible homogeneous reactions, one finds that (a) the homogeneous reactions may be regarded as being at equilibrium and (b) the surface concentrations of species involved in the faradaic process are related to the electrode potential by an equation of the Nernst form.

Mass transfer results either from differences in electrical or chemical potential, or from movement of a volume element of solution. The modes of mass transfer (40) are

- 1. Migration, movement of a charged body under the influence of an electric field (electrical potential gradient).
- 2. Diffusion, movement of a species under the influence of a chemical potential gradient (concentration gradient).
- 3. Convection, stirring or hydrodynamic transport. Generally fluid flow occurs because of natural convection (convection caused by a thermal or density gradient), or forced convection, and ,may be characterized by laminar flow and turbulent flow. The modelling of diffusion, migration, and convection in solution is described by the four relationship:
- 1. The flux equation for charged species,

$$N_{i} = -\frac{Z_{i}D_{i}C_{i}F}{RT} \nabla \phi - D_{i}\nabla C_{i} + C_{i}V.$$
 (32)

2. The current equation in solution,

$$i = F \sum_{i} Z_{i} N_{i} . \tag{33}$$

3. The material balance,

$$\frac{\partial C_{i}}{\partial t} = -\nabla \cdot N_{i} + R_{i} . \tag{34}$$

4. The equation of electroneutrality,

$$\sum_{i} Z_{i} C_{i} = 0. \tag{35}$$

In equation (32), N_i is the flux of species i (mole sec⁻¹ cm⁻²) at distance x from the surface, D_i is the diffusion coefficient (cm²/sec), ∇^C_i , or , in one dimension, $\frac{\partial^C_i}{\partial x_i}$, is the concentration gradient at distance x, \emptyset is the potential, C_i and C_i are the charge and concentration of species i, respectively, and v is the velocity (cm/sec) with which a volume element in solution moves along the x axis. The quantity C_i is a certain function of concentrations of the components participating in the reaction. The three terms on the right-hand side represent migration, diffusion and convection respectively to the flux.

In equation (34), this equation can be written as

$$\frac{\partial C_{i}}{\partial t} + v \nabla C_{i} = D_{i} \nabla^{2} C_{i} + \frac{Z_{i}}{RT} F D_{i} \nabla (C \nabla \emptyset) + R_{i}.$$
 (36)

C. 2. Equation of Motion of Electrolyte ions in Crack

Suppose two metal surfaces form a narrow slit filled with an electrolyte solution. Let S denote a middle surface, equidistant from the side walls of the slit. The slit width is assumed small compared with the radius of curvature of S at any point. Let u, v be fixed orthogonal Gaussian coordinates of a point on the surface S. The solution contains ions of n species, the concentration of each species being equal to C_1 . Let h denote the part of the slit width outside the double layer in which \emptyset , as well as true concentrations, may be considered constant along the normal to the surface S. This situation is shown in Fig. 2.

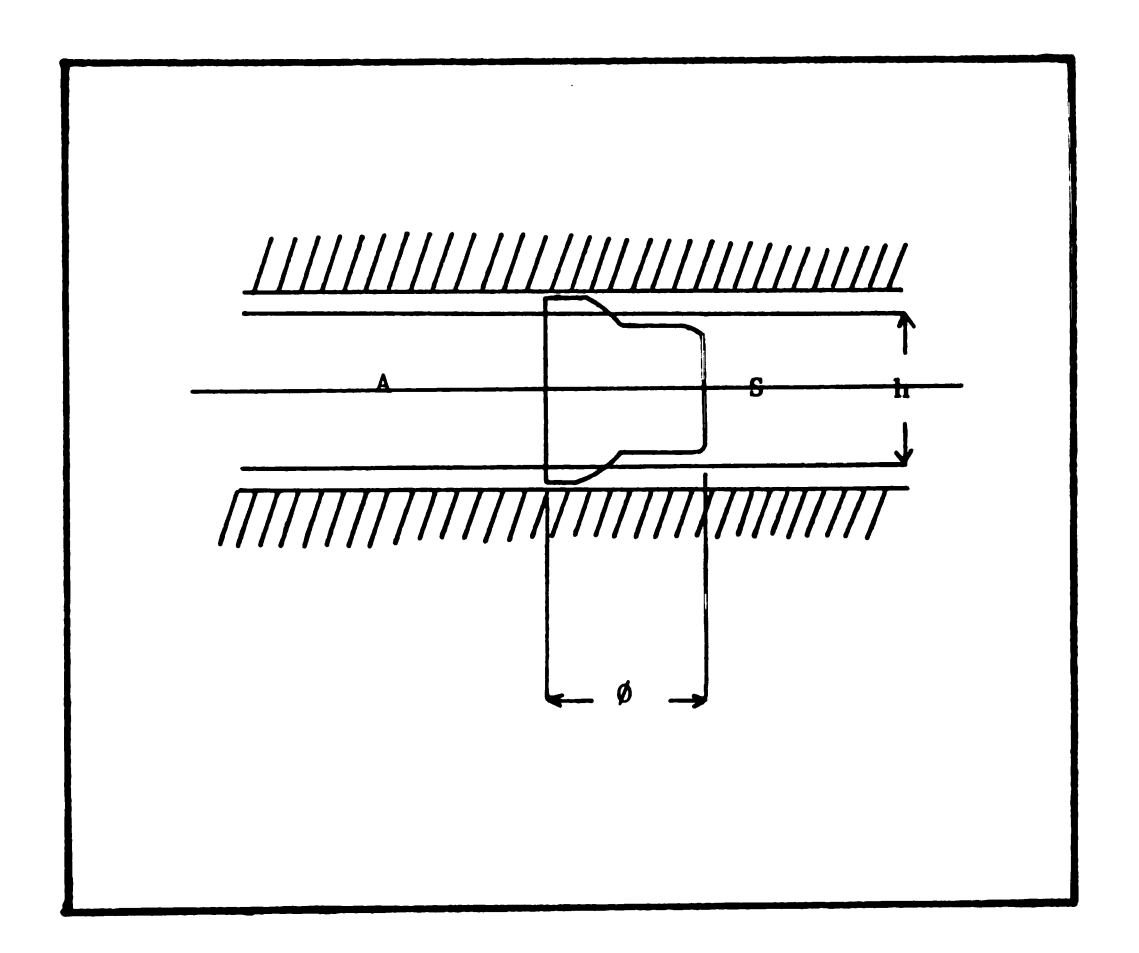


Figure 2 . Structure of elastic potential in a narrow crevice filled up with electrolyte.

The value of the liqid flow velocity v is assumed to be zero, and the double-layer thickness negligibly small compared with h. Chemical reaction occurs in the thin-layer metal-electrolyte between the boundaries of the layer A and the slit, therefore on the boundaries of the layer A, there exists a flow of ions (or, hence electric current) in the direction of the normal to the surface S.

The law of mass conservation in the layer A may be expressed by the following equations on the surface S:

$$\frac{\partial C_{i}}{\partial t} + v \nabla C_{i} = D_{i} \nabla^{2} C_{i} + \frac{Z_{i}}{R T} F D_{i} \nabla (C \nabla \emptyset) - \frac{1}{h} N_{i} (\emptyset, C_{i}), (37)$$

where N_1 (\emptyset , C_1) is the number of ions of the i-th species passing over into the double layer from a layer A per unit time per unit area of the the middle surface; vector operations being carried out along the surface S. The functions N_1 (\emptyset , C_1) are determined by the polarization curves which depend on the kinetics of chemical reactions and phase transitions in the double layer.

Equation (37) is obtained from rigorous three-dimensional equations of the electrolyte motion in the following way. In the first place, Eq. (36) lies In the orthogonal curvilinear system of coordinates (u, v, w) so that the surface S should coincide with the surface w = 0. Then we introduce the following two assumptions: (i) vector v at any point of the layer A is independent of w, its component along the normal to the surface S being equal to zero; (ii) the derivatives $\partial \phi/\partial u$ and $\partial \phi/\partial v$ at any point of the layer A are independent of w. Taking these assumptions into account, the exact equations are integrated with respect to w within the layer A from -h/2 to h/2, and average concentrations over the layer

thickness are introduced. The quantities N_i (\emptyset , C_i) are equal to

$$N_{i} = D_{i} \left(\frac{z_{i} F}{R T} C_{i} \frac{\partial \phi}{\partial w} + \frac{\partial C_{i}}{\partial w} \right) \begin{vmatrix} h/2 \\ -h/2 \end{vmatrix} . \tag{38}$$

They represent the flows of the corresponding chemical reagents into the double layer. The solution in the layer A is electrically neutral.

Equations (35) and (37) represent a closed system with respect to the required functions $C_1(u, v)$ and $\emptyset(u, v)$. The system should be supplemented with initial and boundary conditions.

At any moment the following equations of electrochemical kinetics are to be obeyed at the crack front:

$$D_{i} \frac{\partial C_{i}}{\partial n} + \frac{D_{i} z_{i} F}{R T} C_{i} \frac{\partial \emptyset}{\partial n} = F_{i} (C_{i}, \emptyset), \qquad (39)$$

and

$$F_1 = Z_1 F \left[K_a \exp \left(\frac{d_x F}{R T} \phi \right) - \left(K_c C_M + \right) \exp \left(- \frac{d_c F}{R T} \right) \right]. (40)$$

Equation (40) is the same as Eq. (8).

The crack growth rate V may be found from the mass conservation law

$$V = \frac{M D_{M}}{\mathcal{E}} \left(\frac{\partial C_{M}}{\partial n} + \frac{Z_{M} F}{R T} C_{M} \frac{\partial \emptyset}{\partial n} \right) . \tag{41}$$

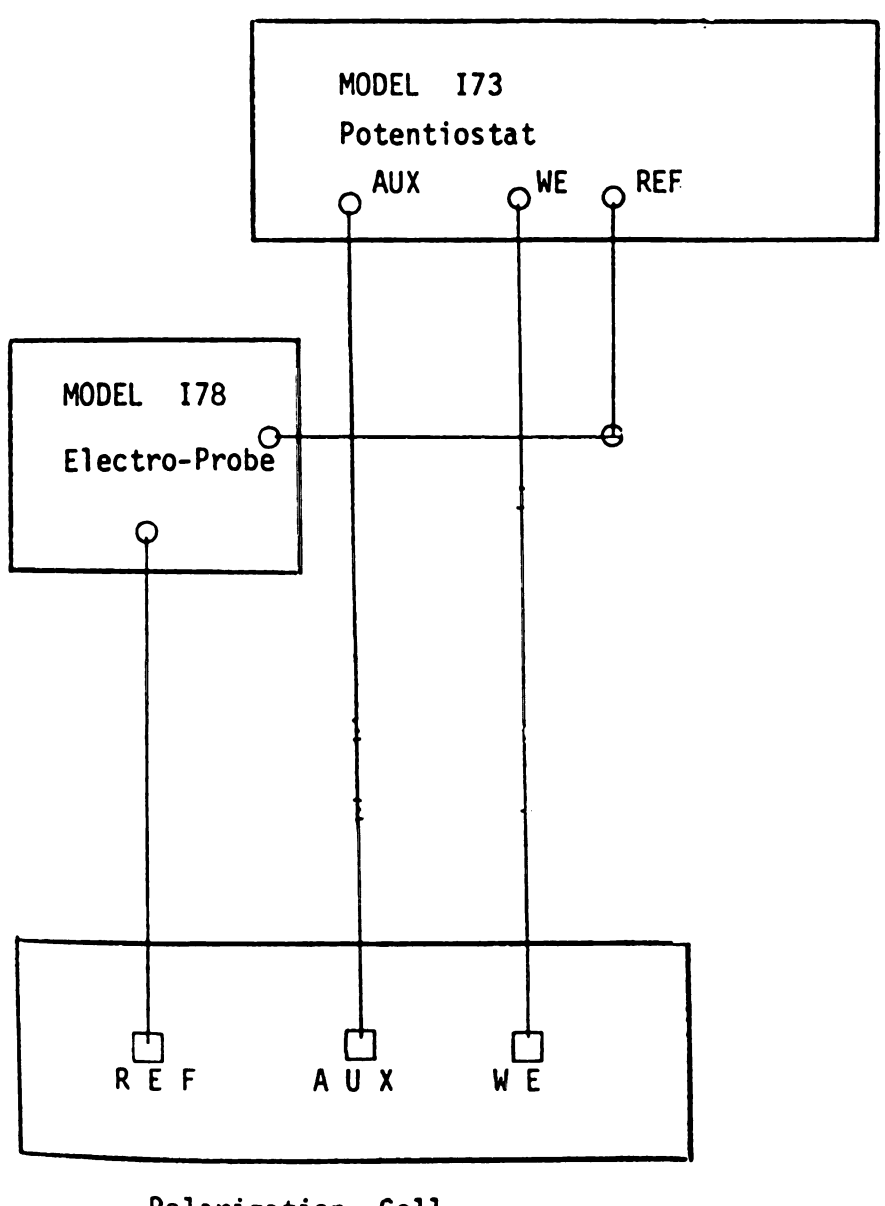
The following symbols are used: D_M , C_M , Z_M , and M are the corresponding quantities referring to the ions of the metal being dissolved, n the direction of the normal to the crack front on the surface S, and \mathcal{E} the volume fraction of the metal anodic component being dissolved owing to the anode reaction at the crack root.

III. EXPERIMENTAL TEST PROCEDURE AND APPARATUS

Electrochemical techniques often are employed to evaluate crevice corrosion. Critical potential values such as the crevice corrosion potential (61), and a crevice protection potential (62), have been proposed to indicate crevice corrosion tendency. From a practical point of view, it is useful to know the corrosion kinetic behavior within crevices. The polarization method, widely used in order to study the kinetic behavior, shows good accuracy for general corrosion. In the case of crevice corrosion, however, the reliability of this method seems to be poor in corrosion kinetic behavior of metal in neutral solution because of an instability of polarization potential during measurement. This instability is considered to be because of an existence of thick oxide film on the surface of In the case of aluminum, however, the corroding surface is metal. exposed to the solution with reduced pH and enriched ion concentration and consequently, is expected to have little film on it. This gives rise to a stability of polarization potential. Therefore, the polarization method is expected to be applicable.

A polarization cell is shown in <u>Figure 3</u> and is arranged in the system circuit shown in Figure 3. The function of the circuit is to develop sequentially increasing or decreasing potentials on a test electrode and to measure the corresponding current associated with the potential.

This results in a polarization curve of the potential versus current which is a "foot print " of the corrosion behavior of the material-environment combination. The relative positions of the curves can be used to compare corrosion behavior of various materials and environments. Additionally, the potentio-dynamic polarization technique is useful to determine the



Polarization Cell

FIGURE 3 SIMPLIFIED EXPERIMENTAL SYSTEM

effect of inhibitor, corrosion rates, and kinetics behaviors without resorting to more tedious and less accurate weight change methods.

Three types of crevices were investigated for the NaCl solution:

(1) An "isolated "artificial crevice, where the crevice metal was not coupled to the open external metal; (2) a "coupled" artificial crevice, where crevice metal was coupled to the external metal; and (3) a real crack with stress. The first configuration allowed study of local cell activity within a crevice, the second simulated the more practical case, and the third studied the real crack. The kinetics behaviors, polarization behaviors and pH of solution were studied for the first and second types of crevices. The corrosion potential inside the real crack with stress was studied for the third case.

A. Experimental System

The experimental system was divided into the following basic units; (1) Potentiostat (2), Corrosion Cell, (3) Electrometer Probe.

The simplified experimental system is also shown in Figure 3.

(1) Potentiostat

The potentiostat was a Princeton Applied Research Model 173. The instrument features a current capability of one ampere, with compliance voltages as high as 100 V in either polarity, and a slew rate of 10 V per microsecond. It incorporates two independently built-in potential/current sources, each adjustable to any voltage in the range of \pm 4.999 V as well as logic and switching circuity for controlling the sources from the front panel or by externally derived trigger.

(2) Corrosion Cell

(a) Working Electrode

The working electrode , shown in Figure 6 & 7, was fabricated in the local machine shop.

(b) Reference Electrodes

A standard calomel electrode (SCE) was used as the reference electrode to give a reduction potential of 0.24 V. Such an electrode is not easily poisoned or contaminated, and it is insensitive to electrolyte composition because of its design. To avoid mutual contamination of the test solution and the reference electrode, the two usually are isolated by means of a salt bridge or liquid junction.

(c) Auxiliary Electrode.

Platinum can be used in almost any solution over a wide range of temperature without special precautions, and its rate of polarization is very low, hence it was used as an auxiliary electrode to supply current.

(3) Heat Source

Since solution temperature was a variable, some means of controlling this parameter was needed. The cell was placed on top of a variable control Thermolyne electric heater and was manually controlled to about $+10^{\circ}$ C. The heater was also equipped with a magnetic stirrer.

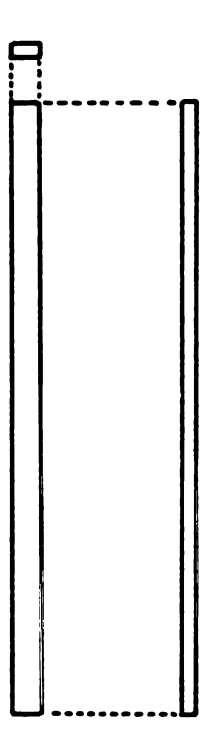


Figure 4 A rectanglular specimen for bare surface test

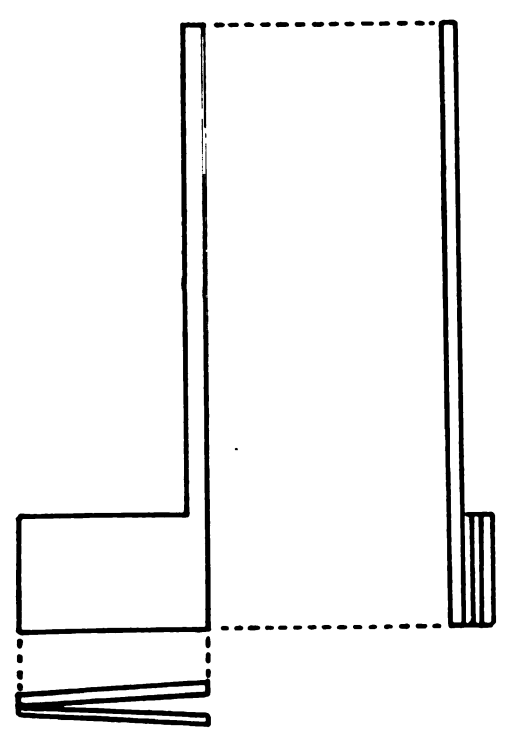


Figure 5. A modified artificial crevice

(4) Electrometer Probe

A PAR model 178 Electrometer Probe was supplied with the Potentiostat so that the potential at high-impedance (Reference Electrode) could be monitored. After placing the probe at the end of a cable it could be positioned very near the monitored potential. As a result, stray capacitance loading was minimized with a subsequent optimization of stability.

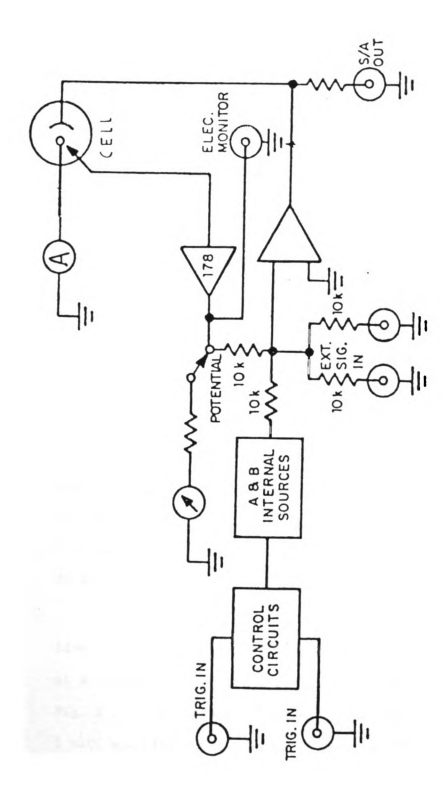
B. System Assembly

(1) Corrosion Cell

The polarization cell and its components were cleaned in laboratory detergent solution followed by rinsing in distilled water. The solution and a stirring magnet were placed in the large beaker, and the working electrode and standard calomel electrode were inserted. With the SCE in place, the working and auxiliary electrodes and thermometer were positioned with respect to an imaginary horizontal plane established by the tip of the SCE. Vertical alignment of the electrodes and thermometer were maintained by the specimen-holding unit because they had enough depth to provide the support needed to prevent lateral movement of these items. The specimen-holding unit was designed in order to maintain an equal distance between all three electrodes.

(2) Control System

Figure 4 is a simplified diagram of the test system consisting of the Princeton Applied Research Model 173 potentiostat, the Model 178 probe and an electrochemical cell. The potentiostat was furnished with two special interconnecting cables to interface the electrochemical cell. One interconnecting cable also has three different colored cables:



BLOCK DIAGRAM OF SIMPLIFIED EXPERIMENTAL SYSTEM IN CONTROL E (POTENTIOSTATIC) OPERATION FIGURE

- (1) a red cable clip, connected to the Counter Electrode of the electrochemical cell;
- (2) a green cable clip, connected to the Working Electrode; and
- (3) a black clip which is not connected or connected to the ground.

 Another cable from the Model 178 Electrometer Probe must be connected in Control E operation. The Electrometer Probe Connector on the front panel provides ± 24 volts and also carries the probe output signal back to the potentiostat. For proper operation in the Control E mode (Selector switch set to Ext Cell in the front panel) the probe must be connected to the Reference Electrode at the cell.

C. Equilibration

Specimen preparation was conducted during the time the solution was being stirred. After stirring was terminated, the assembled working electrode was placed in the corrosion cell and properly positioned. In order to find the time to come to equilibrium, the open circuit corrosion potential was measured as a function of time. In the case of the bare surface electrode, after the electrode was placed in solution (1 wt. % NaCl), there was a little increase in open circuit potential from -0.755 to -0.730 V. Electrode potential slightly increased with

time. After 3.5 hr (the induction time), the potential remained at a constant value, about -0.710 V (vs SCE). This is shown in Fig. 5. Therefore, 7075 T6 Al alloy specimen was held in the 1 wt. % NaCl solution for 3.5 hours in order to allow it to come to equilibrium before any data were taken. During this time, the electrodes were electrically disconnected from the control system.

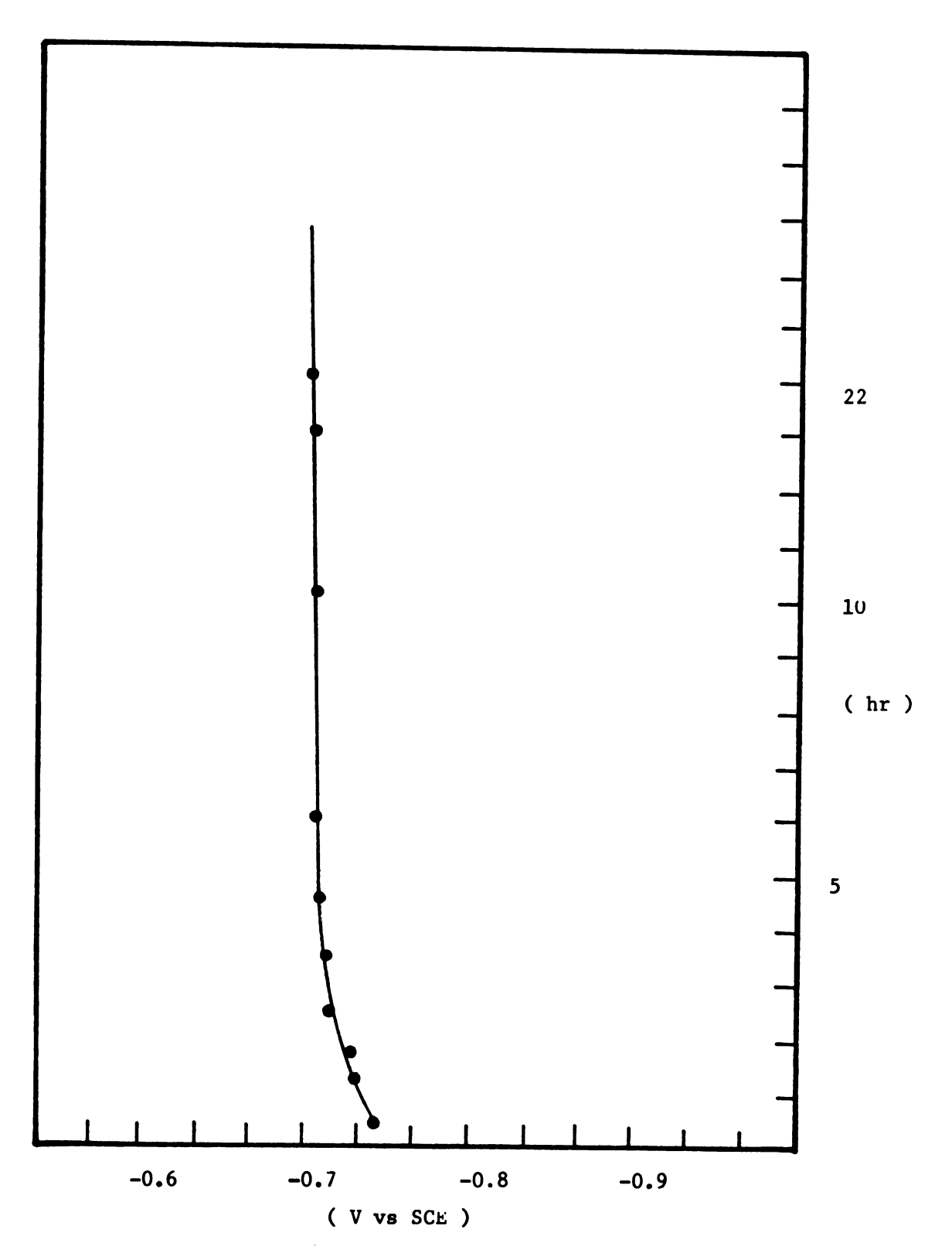


Figure 7 STEADY-STATE OPEN-CIRCUIT POTENTIAL FOR 7075 T6
Al alloy in 1.0 wt.% NaCl SOLUTION

D. System Operation.

(1) Initial Stage

It was necessary to allow the system to stabilize thermally for several hours before data were taken. This warm-up period coincide with the equilibration period for the corrosion cell.

(2) Second Stage

In the three-electrode configuration, Control E operation automatically compensates for the system internal resistance.

(3) Measurement of Corrosion Potential

The equipment was set up and connected to the system as shown in Figure 3. Whenever the potentiostat was connected to the cell, the potential of the Working electrode vs. the Reference electrode was automatically displaced. In order to measure the corrosion potential, the Cell Select switch was set to Ext. Cell., and the meter should deflect to the left. The A Channel polarity switch was set to correspond to the meter reading. The operating Modal switch is set to Null and Channel A Applied Potential/Current controls are adjusted as required to obtained a zero meter induction. The setting of the Channel A Applied Potential Current control will then correspond to the corrosion potential.

(4) Operation

Control E operation of potentiostat was always used. After the cell connection was made, the cable connects to the Model 258 digital Multimeter. When ready to start, the Selector switch was set to EXT CELL. The Counter electrode was driven to whatever potential was required to establish the Working electrode.

E. Test Material

(1) Chemical Analysis.

Commercial aviation-grade 7075-T6 aluminum alloy was used for the study. This was from the same lot used in an earlier PACER LIME test program. (75) No further information is available beyond the nominal chemical analysis, Table 1.

Table

7075-T6 A1 Alloys

| Element | Zn | Mg | Cu | Cr | Mn |
|---------|------|------|------|------|----|
| % | 5.52 | 2.76 | 1.41 | 0.23 | 0 |

(2) Mechanical Analysis.

In order to analyze the mechanical properties of Commercial 7075-T6 aluminum alloy, mechanical tests were performed. Tensile strength and yield strength were measured with an Instron tensile test machine. Table 2 shows the mechanical properties for this material.

Table 2

Mechanical Properties of 7075-T6 Al Alloys

| | Tensile Strength | Yield Strength | Hardness | |
|---------------|------------------|----------------|--------------|--|
| | (psi) | (psi) | (Rockwell) | |
| Specimen | 72,000 | 66,000 | в 76 | |
| Handbook (74) | 83,000 | 73,000 | в 85 | |

(3) Specimen Preparation

(a) Polarization Kinetic Test.

Rectangular specimen, for bare surface test and a modified artificial crevice specimen, as shown in Figure 6 and 7, respectively,

first were ground with 240 grit paper and then polished with 600 grit paper. Oxide scale and surface defects were removed during the grinding operation. The specimens were measured to the nearest 0.001 cm., and the surface area was calculated. The samples were cleaned thoroughly in acetone and alcohol, and finally degreased with petroleum ether (32).

(b) Stress Corrosion Test.

Modified WOL-type, constant deflection specimens were used. (41), (42) (43), (44) (44) (44) (44) (44) (44) (44) (44) (44) (44) (44) (44) (44) (44) (44) (44) (44) (44) (44) (44) (44) (44) (44) (44) (44) (44) (44) (44) (44) (44) (44) (44) (44) (44) (44) (44) (44) (44) (44) (44) (44) (44) (44) (44) (44) (44) (44) (44) (44) (44) (44) (44) (44) (44) (44) (44) (44) (44) (44) (44) (44) (44) (44) (44) (44) (44) (44) (44) (44) (44) (44) (44) (44) (44) (44) (44) (44) (44) (44) (44) (44) (44) (44) (44) (44) (44) (44) (44) (44) (44) (44) (44) (44) (44) (44) (44) (44) (44) (44) (44) (44) (44) (44) (44) (44) (44) (44) (44) (44) (44) (44) (44) (44) (44) (44) (44) (44) (44) (44) (44) (44) (44) (44) (44) (44) (44) (44) (44) (44) (44) (44) (44) (44) (44) (44) (44) (44) (44) (44) (44) (44) (44) (44) (44) (44) (44) (44) (44) (44) (44) (44) (44) (44) (44) (44) (44) (44) (44) (44) (44) (44) (44) (44) (44) (44) (44) (44) (44) (44) (44) (44) (44) (44) (44) (44) (44) (44) (44) (44) (44) (44) (44) (44) (44) (44) (44) (44) (44) (44) (44) (44) (44) (44) (44) (44) (44) (44) (44) (44) (44) (44) (44) (44) (44) (44) (44) (44) (44) (44) (44) (44) (44) (44) (44) (44) (44) (44) (44) (44) (44) (44) (44) (44) (44) (44) (44) (44) (44) (44) (44) (44) (44) (44) (44) (44) (44) (44) (44) (44) (44) (44) (44) (44) (44) (44) (44) (44) (44) (44) (44) (44) (44) (44) (44) (44) (44) (44) (44) (44) (44) (44) (44) (44) (44) (44) (44) (44) (44) (44) (44) (44) (44) (44) (44) (44) (44) (44) (44) (44) (44) (

$$K_{I} = \frac{V E}{W^{1/2}} \frac{F}{C} , \qquad (42)$$

where W (= 2.55 B) is the width of the specimen, E is Young's modulus, V is the initial displacement; F is a function of a/w (a is crack length),

$$F \left(\frac{a}{w}\right) = (30.96 - 195.8 \left(\frac{a}{w}\right) + 730.6 \left(\frac{a}{w}\right)^{1/2} - 1186 \left(\frac{a}{w}\right)^{3} + 254.6 \left(\frac{a}{w}\right)^{4}\right), \tag{43}$$

and C is the compliance.

F. Test Solution

(1) Material used.

Each specimen was tested in a series of solutions of various concentrations of sodium chloride with and without inhibitors, and

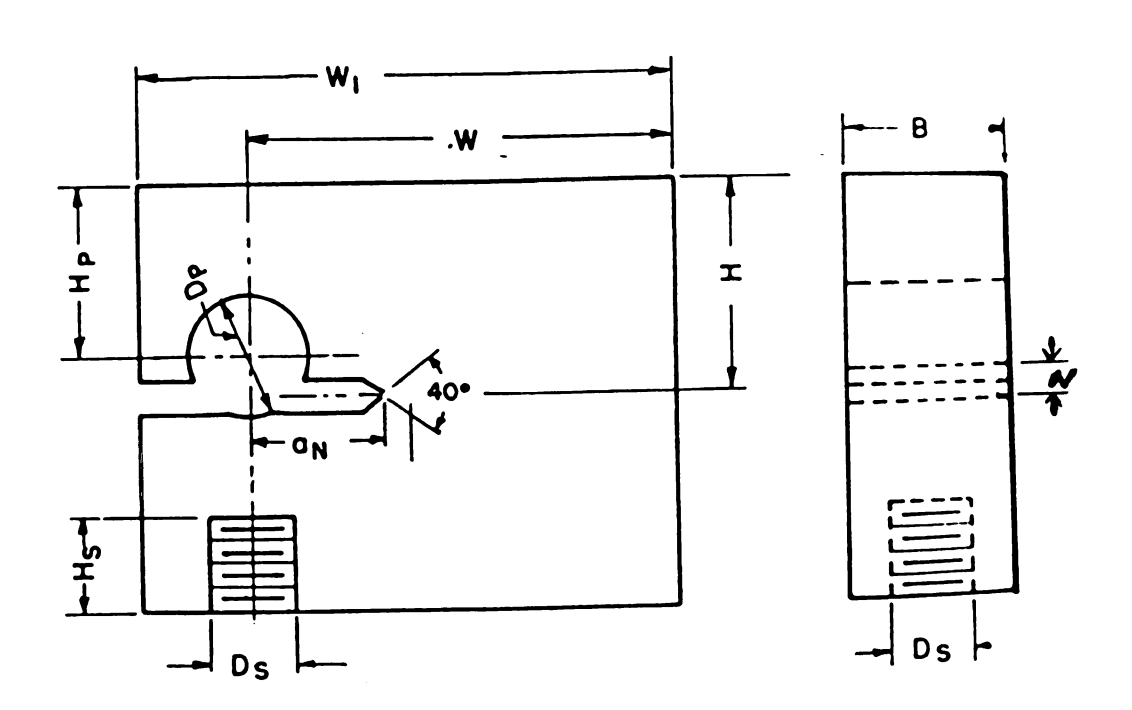


FIG.8 -WOL fracture specimen.

with one of several surface-active agents. The inhibitors and surface-active agents are listed in Table 3.

Table 3

The inhibitors and surfactant

Type Inhibitor Surfactant

Type I NaNO₂, NaSCN. 2-Amino-2-Methyl

Type II CH_3COON , $(COONa)_2$ Type III $Na_2B_4O_7$

(2) Preparation:

Solutions were prepared fresh just prior to testing. Concentrations were in weight percent solute, based on the total weight of the solution.

G. pH Test

In order to analyze the small amount of corrodent present without chemical changes, alkacid paper was used for measurement of pH within the crack. The pH paper tests permitted accurate estimates of the acidity inside the crack.

IV. EXPERIMENTAL RESULTS

A. Effect of Cl concentration.

In <u>Figure 9</u>, anodic profiles at the bare surface are presented for concentrations between 0.1 wt.% and 3 wt.% NaCl at room temperature without stress and inhibitors. The figure shows that the corrosion potential of corroding 7075-T6 Al alloy depends strongly on the solution concentration, i.e., increasing corrosion potentials correspond to decreasing C1 concentration. Furthermore, increasing corrosion current corresponds to increasing C1 concentration, i.e., the current density is dependent upon the C1 concentrations. All profiles in Figure 9 were continuous, but were not adaptable to Tafel analysis because of a short linear region. During the course of the experiment, formation of a very thin dark gray adherent film on the surface of the specimen was visually observed at the beginning of the experiment.

In Figures 10 and 11, cathodic profiles at the bare surface are shown for concentrations 1 % and 3 % NaCl at room temperature without stress and inhibitors. These figures show that the current density of corroding 7075-T6 Al alloy is independent of the solution concentration. All profiles in Figures 10 and 11, show the limiting current density resulting from the oxygen reduction or oxide passivation. As the potential is decreased, no deposit continues to accumulate at the surface of the specimen, and no gas evolution nor bubble formation were observed at the specimen surface. According to these results, the anodic profiles in Figure 9, showed that the current density depends upon the C1 concentration. Cathodic profiles in Figures 10 and 11,

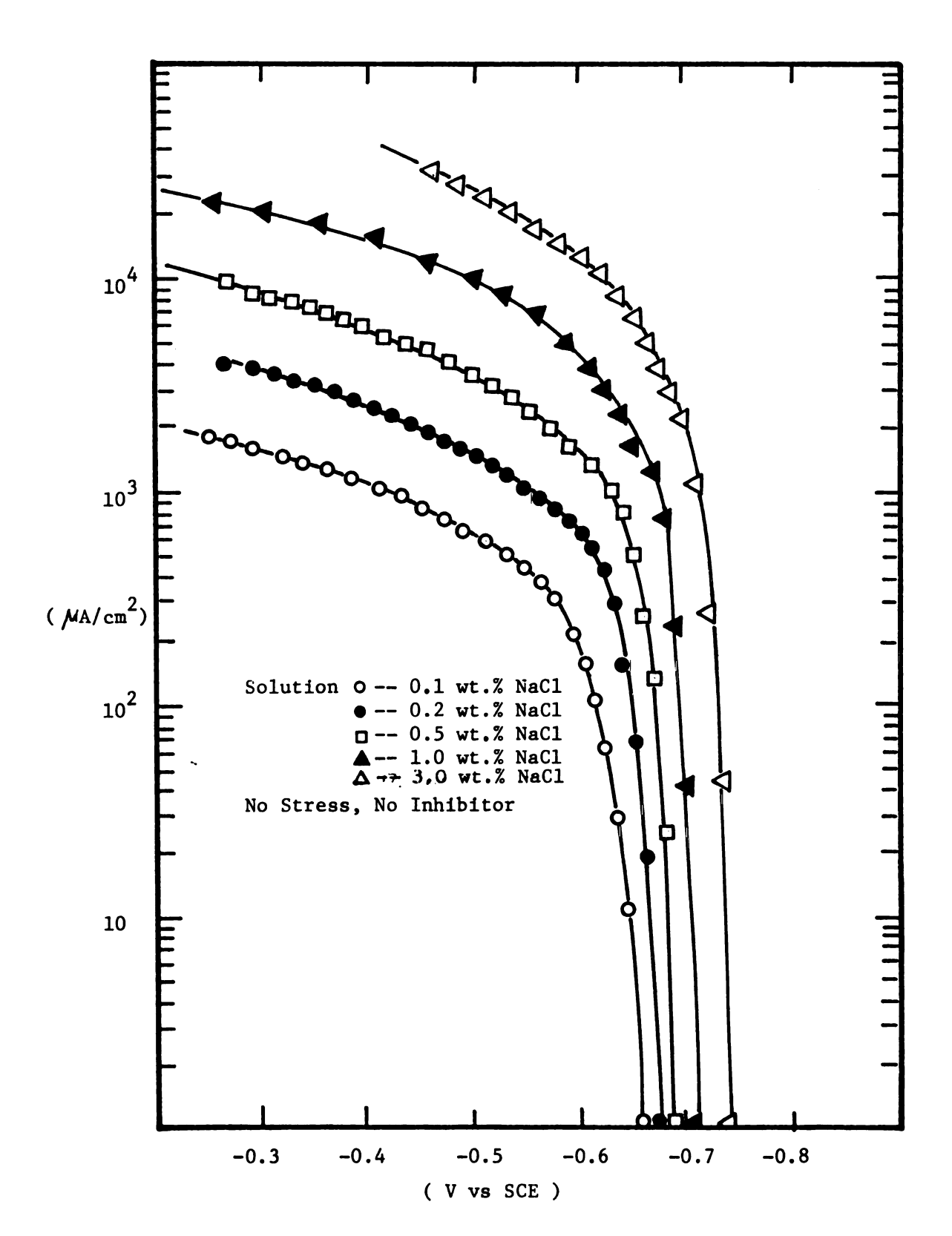


FIGURE 9 ANODIC POLARIZATION OF 7075 T6 A1 ALLOY IN DILUTE SODIUM CHLORIDE SOLUTION WITHOUT STIRRING AT 20°C + 2°C

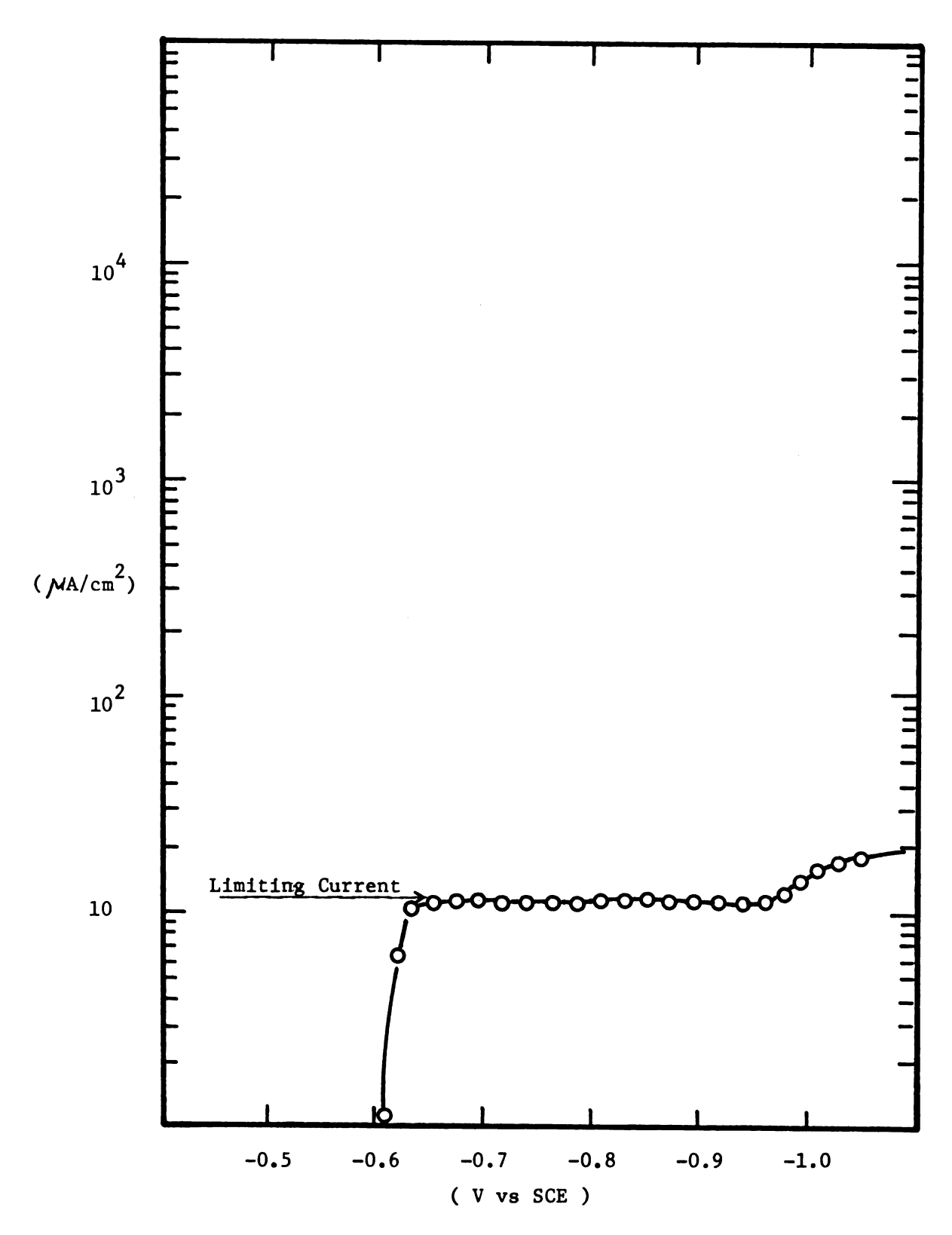


FIGURE 10 CATHODIC POLARIZATION OF 7075 T6 A1 ALLOY IN 1 wt.% NaCl Solution without Stirring at $20^{\circ}\text{C} \pm 2^{\circ}\text{C}$

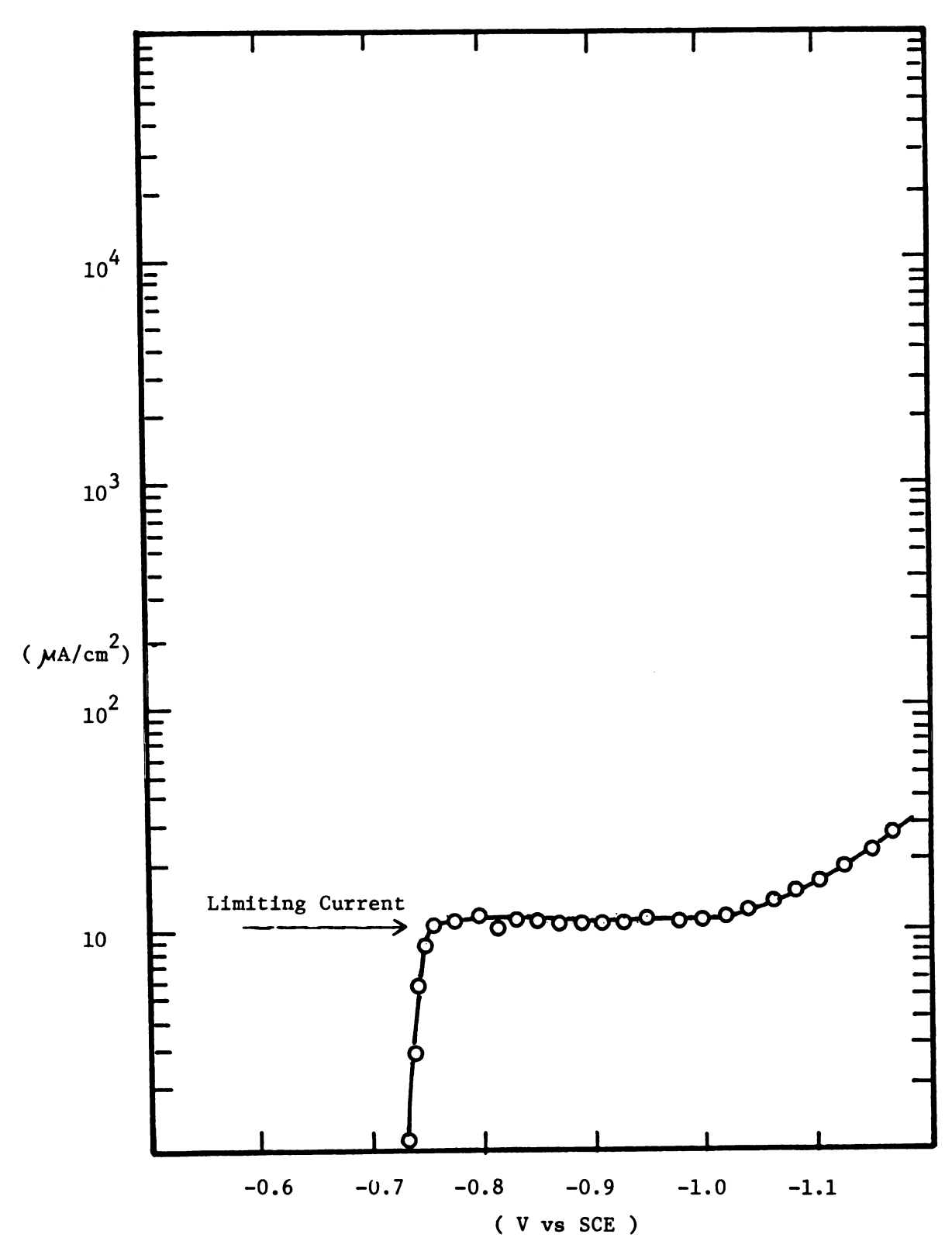


FIGURE 11 CATHODIC POLARIZATION OF 7075 T6 A1 ALLOY IN 3 wt.% NaCl Solution Without Stirring at $20^{\circ}\text{C} \pm 2^{\circ}\text{C}$

however, show that the current density is independent of the Cl concentration.

In <u>Figures 12 and 13</u>, Anodic profiles are shown for distilled water and tap water, respectively, at room temperature without stress, stirring, or inhibitors. <u>Table 4</u> shows the chemical composition of tap water (72). The figures show that the corrosion potential of tap water for corroding 7075-T6 Al alloy is lower than the corrosion potential of distilled water because of chemical elements effects as shown in Table 4.

The profile in Figure 12 was continuous with no discontinuites and may be adaptable to Tafel analysis and the corrosion current density can be found. However, the profile in Figure 13 was not adaptable to Tafel analysis because of a short linear region. By means of the Figure 12 and Tafel methods, the corrosion current density, about 30 MA/cm² can be found.

A. 2. Effect of Inhibitors

Figures 14 and 15 show the anodic polarization behavior of 7075-T6 Al alloy in the inhibitor solutions such as $NaNO_2 + Na_2B_4O_7$ (0.1 wt. %) and 0.1 wt.% NaSCN, respectively, with 1 wt.% NaCl. The anodic polarization curves contained no discontinuities, which normally are associated with film formation, and no passivation. The corrosion potential of the corroding Al alloys was independent of the addition of the inhibitors to the solution.

It is known $^{(47),(48)}$ that these inhibitors, NaNO₂,NaNO₂ + Na₂B₄O₇ combined, and NaSCN increase passivation against chloride attack. The nitrite ion affects the potential, that is , those salts whose anions have high redox potentials. For example,

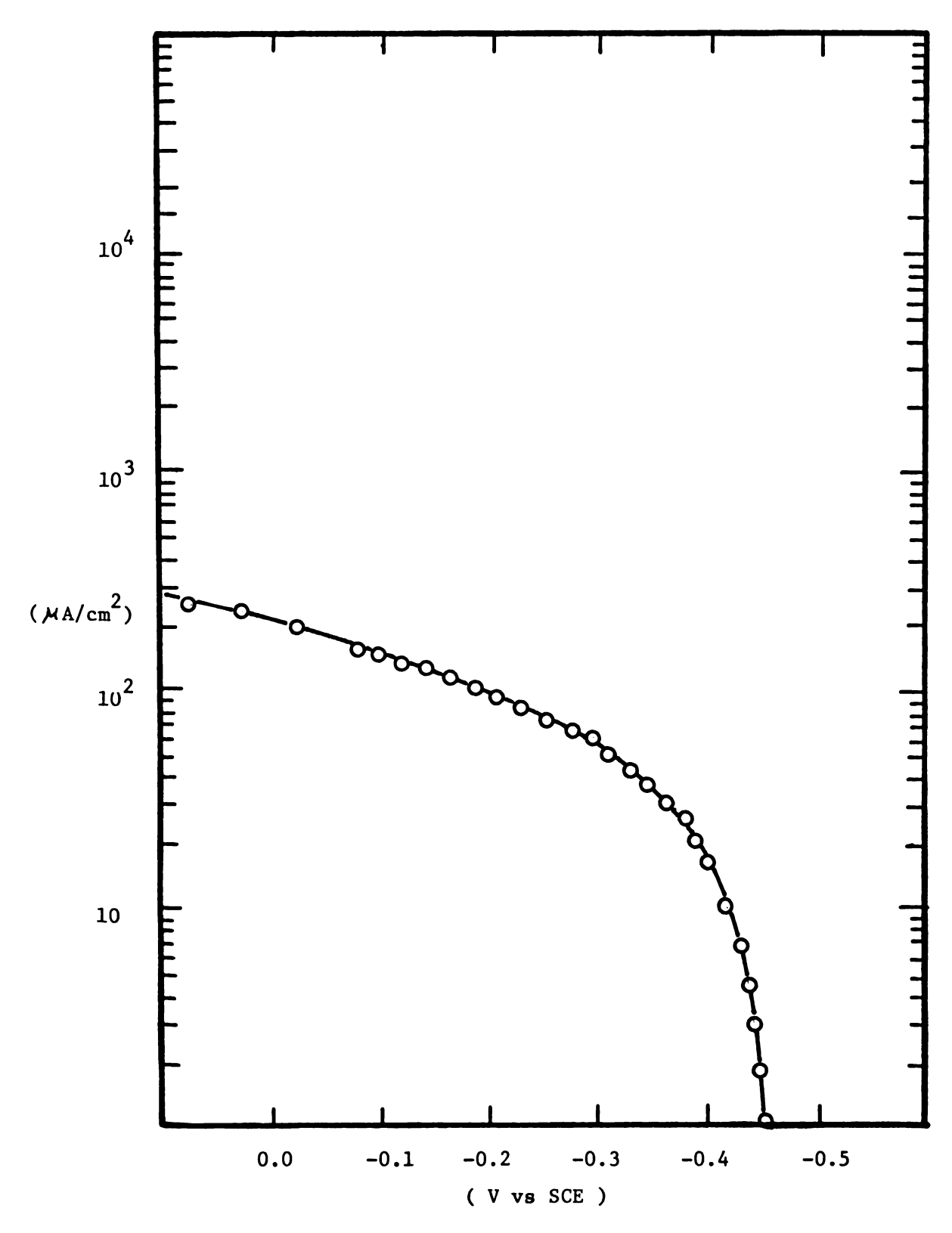


FIGURE 12 ANODIC POLARIZATION OF 7075 T6 A1 ALLOY IN DISTILLED WATER WITHOUT STIRRING AT $20^{\circ}\text{C} \pm 2^{\circ}\text{C}$

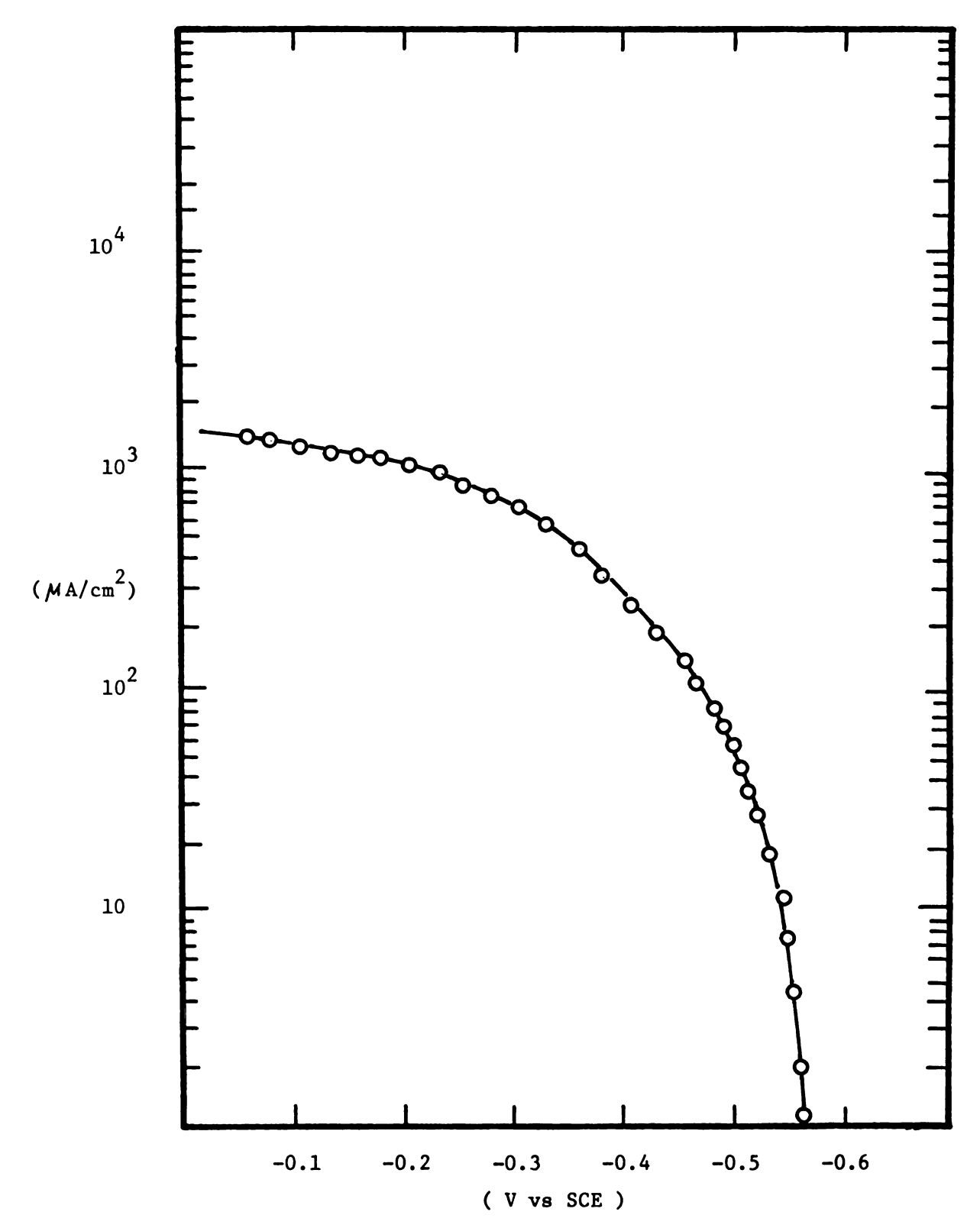


FIGURE 13 ANODIC POLARIZATION OF 7075 T6 A1 ALLOY IN TAP WATER WITHOUT STIRRING AT $20^{\circ}\text{C} \pm 2^{\circ}\text{C}$

Table 4

The Chemical Composition of Tap Water

| Element | | Concentration ($mg/1$) |
|-----------|---------------------|-------------------------------|
| Magnesium | (Mg) | less than $0.1 \text{ mg/}1$ |
| Chlorides | (C1) | 8 mg/1 |
| Sulfates | (SO ₄) | 0.3 mg/1 |
| Nitrates | (NO ₃) | less than $0.01 \text{ mg/}1$ |
| Nitrites | (NO ₂) | 0.03 mg/1 |
| Ammonia | (NH ₄) | less than $0.1 \text{ mg/}1$ |
| Zinc | (Zn) | 0.025 mg/1 |
| Copper | (Cu) | less than $0.11 \text{ mg/}1$ |
| Nickel | (Ni) | 0.2 mg/1 |
| Iron | (Fe) | 0.5 mg/1 |
| Aluminum | (A1) | 0.332 mg/1 |

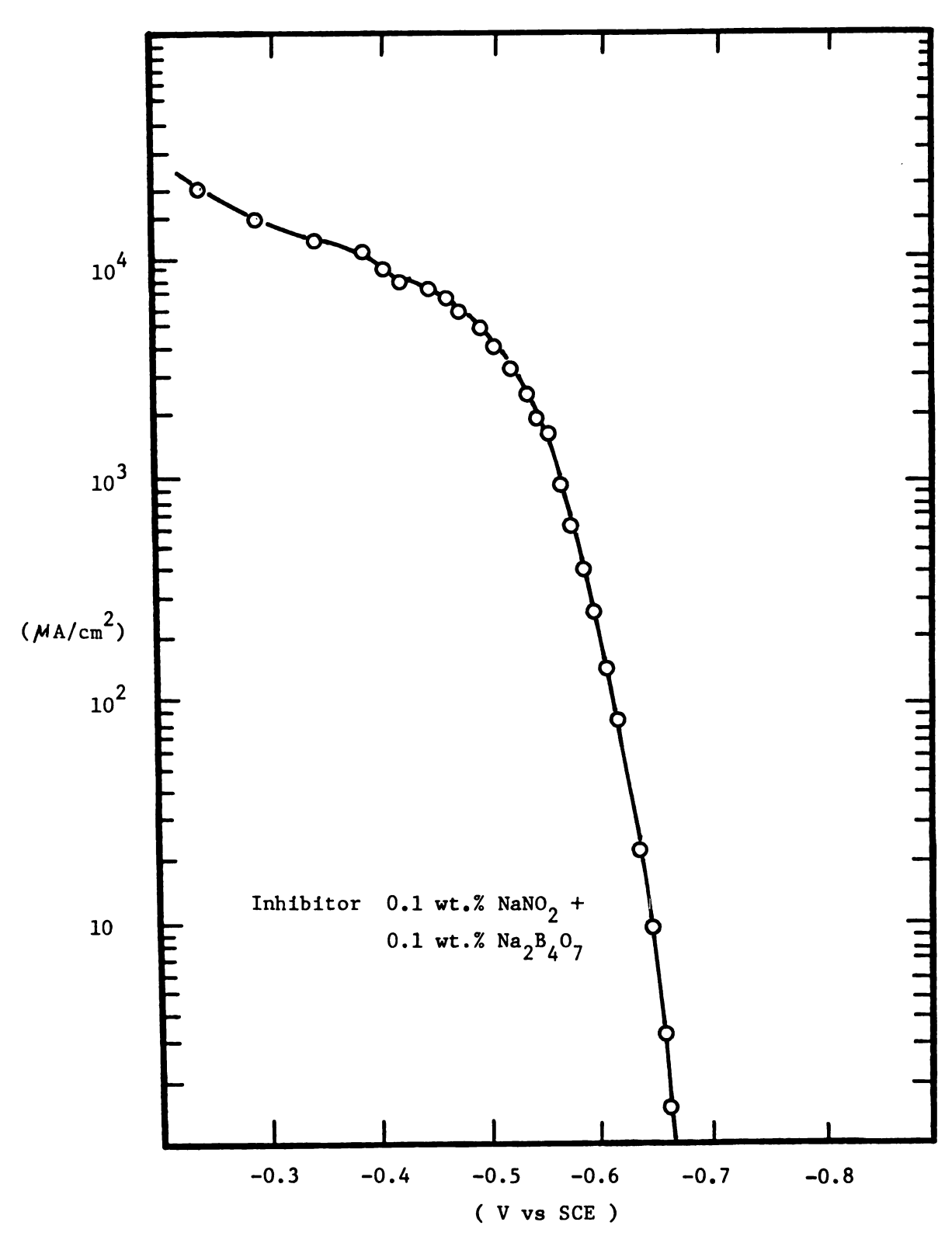


FIGURE 14 ANODIC POLARIZATION OF 7075 T6 A1 ALLOY IN 1 wt.% NaCl AND INHIBITOR WITHOUT STIRRING AT 20° C \pm 2° C

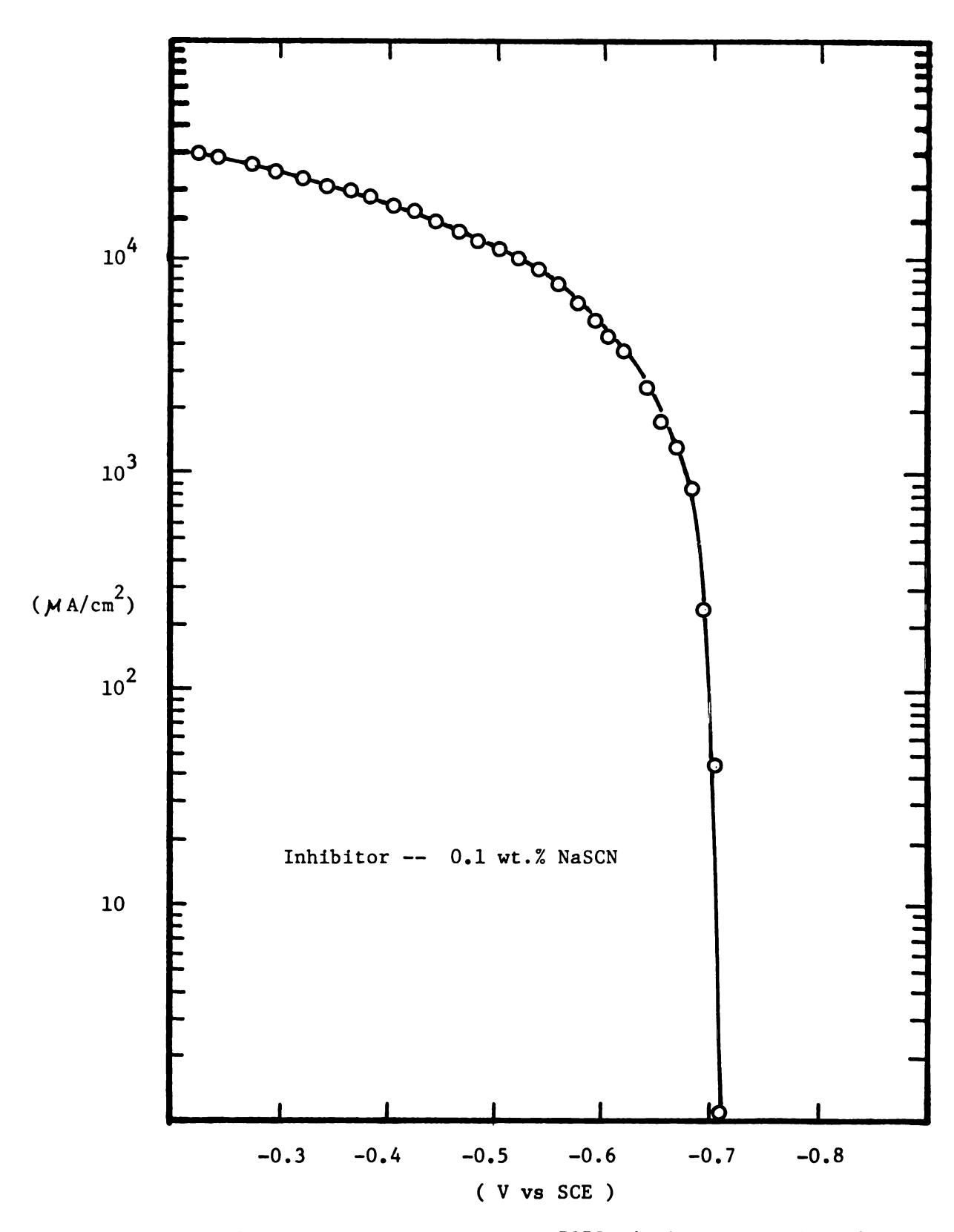


FIGURE 15 ANODIC POLARIZATION OF 7075 T6 A1 ALLOY IN 1 wt.% NaCl and inhibitor without stirring at $20^{\circ}\text{C} \pm 2^{\circ}\text{C}$

$$NO_{2}^{-} + 8 H^{+} + 6e \stackrel{>}{<} NH_{4}^{+} + 2H_{2}O$$

$$E = + 0.90 V. SHE$$

The anodic profile in Figure 14 shows a small effect of NaNO₂ and Na₂B₄O₇ inhibitors upon the polarization behavior of 7075-T6 Al alloy, but Figure 15 shows no effects of inhibition.

It may be suggested that the passive film formed by NaNO₂ in this range of inhibitor concentration still is weak and ineffective against chloride attack when chloride ion is present in high concentration without a high concentration of inhibitors. It also is known that oxidizing inhibitors, such as NaNO₂, raise the corrosion potential and can have adverse results if they are present at insufficient concentration.

Oxidising inhibitors or passivators, by providing an additional cathodic reactant, effectively reduce cathodic polarization, so that the corrosion current will be increased. Therefore, if added in insufficient quantity, oxidising inhibitors can have disastrous consequences. If no passivation results, as in these experimental results, anodic dissolution increases or the passive film is weak.

Figures 16 and 17 show the anodic polarization behavior of 7075-T6

Al alloy in the inhibitor solutions, CH₃COONa and (COONa)₂, respectively, with 1 wt.% NaCl. Acetate and oxalate ions are chelating agents, ions or molecular species with two or more atoms with unshared pairs of electrons. The chelating agent can donate the unshared electron pair to a metal atom to form a stable 5- or 6-member ring resembling a "claw", with the result that the metal atom is held in a stable configuration and the chelate produced usually does not exhibit the properties of the metal atom or the chelating agent. In the case of aluminum

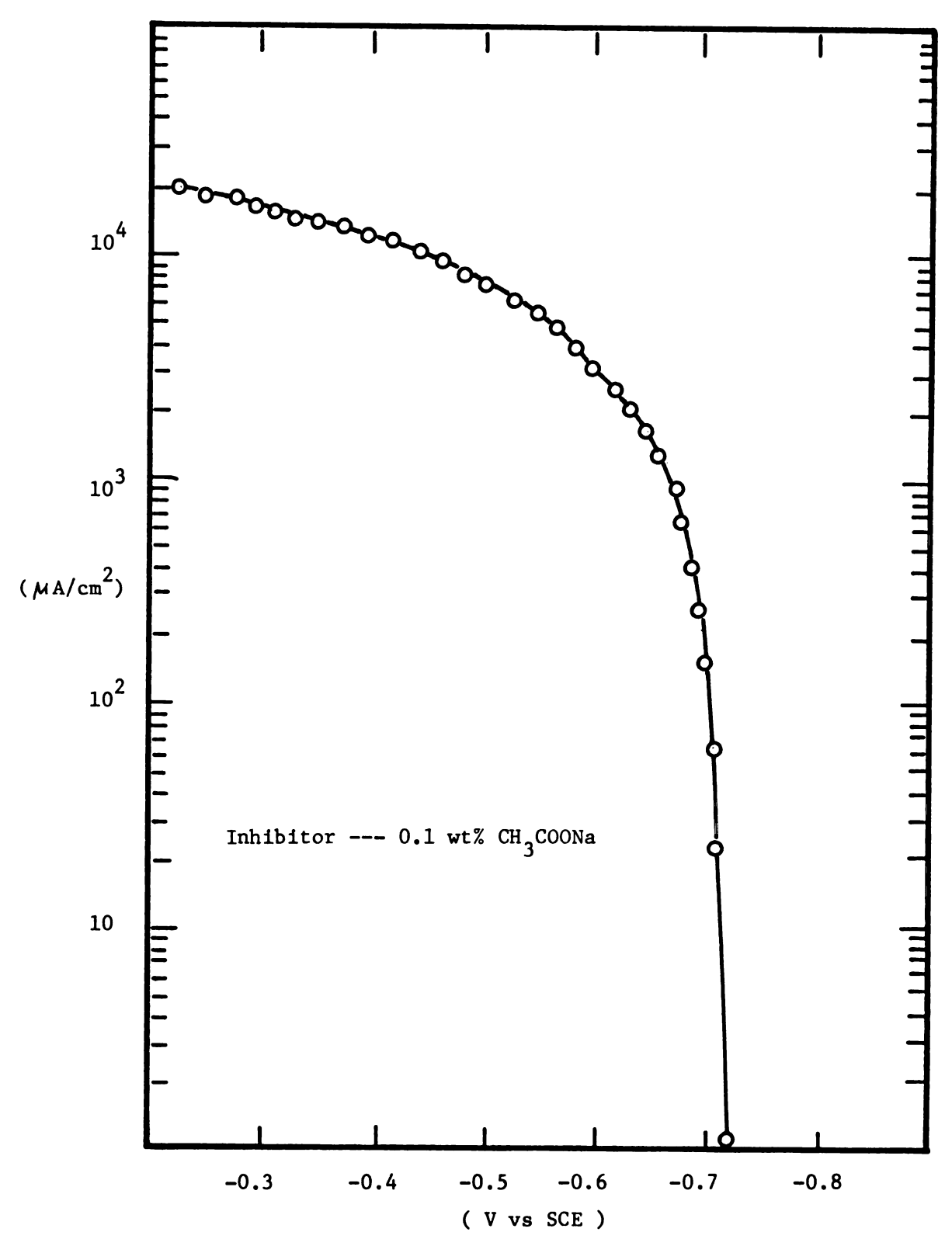


FIGURE 16 ANODIC POLARIZATION OF 7075 T7 A1 ALLOY IN 1 wt.% NaCl AND INHIBITOR WITHOUT STIRRING AT $20^{\circ}\text{C} \pm 2^{\circ}\text{C}$

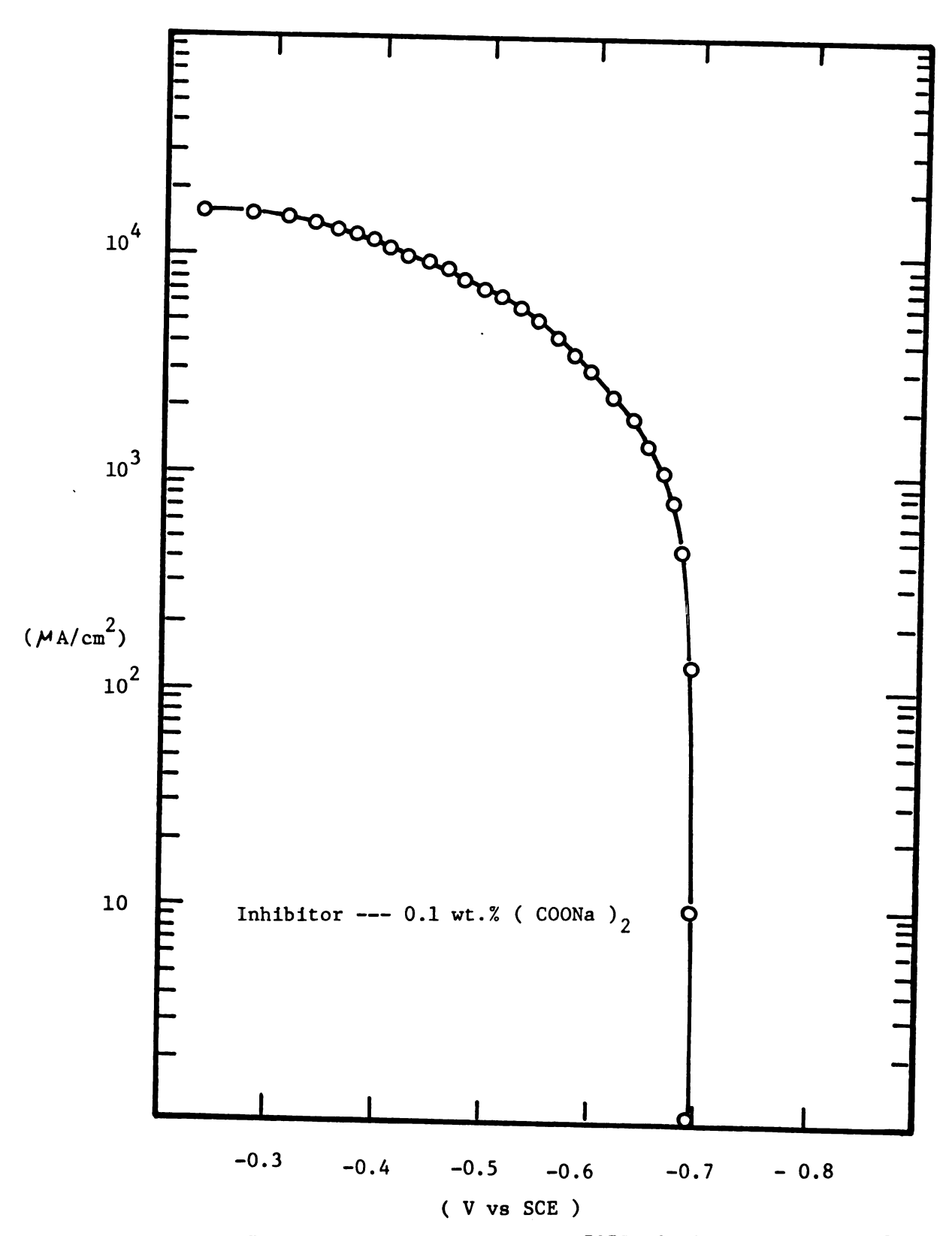


FIGURE 17 ANODIC POLARIZATION OF 7075 T6 A1 ALLOY IN 1 wt.% NaCl AND INHIBITOR WITHOUT STIRRING AT 20° C \pm 2° C

alloys, the chelating agent can react with the aluminum cation in the oxide film. Depending on the chelating agent, the resulting compound may be stable and insoluble, or it may be a stable, soluble, complex ion with a solubilizing function on the oxide.

In these experiments, there was no change essentially in corrosion potential as well as anodic polarization curves when sodium acetate and sodium oxalate were added to 1 % NaCl. Metallographic examination of the samples showed a general corrosion on the surface. It is known that a chelating agent, as an inhibitor, reacts with aluminum to form an insoluble aluminum oxalate or acetate compound, and prevents aluminum corrosion by a precipitation type effect.

In chloride solutions, the possibility of inhibition should be viewed from the point of interfering with the reaction

$$A1^{3+} + 2 C1^{-} + 2OH^{-} \stackrel{=-}{\leftarrow} A1 (OH)_{2} C1_{2}^{-}$$
,

by which the oxide film is thinned. A species may form a complex ion which may be stable and soluble,

$$A1^{3+} + nR^{-} \stackrel{--}{\longleftarrow} A1R^{3-n}$$

and accelerate corrosion. On the other hand, the species may react as

$$A1^{3+}$$
 + $3 R^{-} \stackrel{\longrightarrow}{\longleftarrow} A1 R_3$,

wherein the species Al $\rm R_3$ is stable, uncharged and very slightly ionized and resides at or near the aluminum surface. Although these precipitation type of inhibitors are known to prevent aluminum corrosion in the presence of chloride, Figures 16 and 17 show no effect of these type of inhibitors upon the polarization behavior of 7075-T6 Al alloy .

Figure 18 shows the anodic polarization behavior of 7075-T6 Al alloy

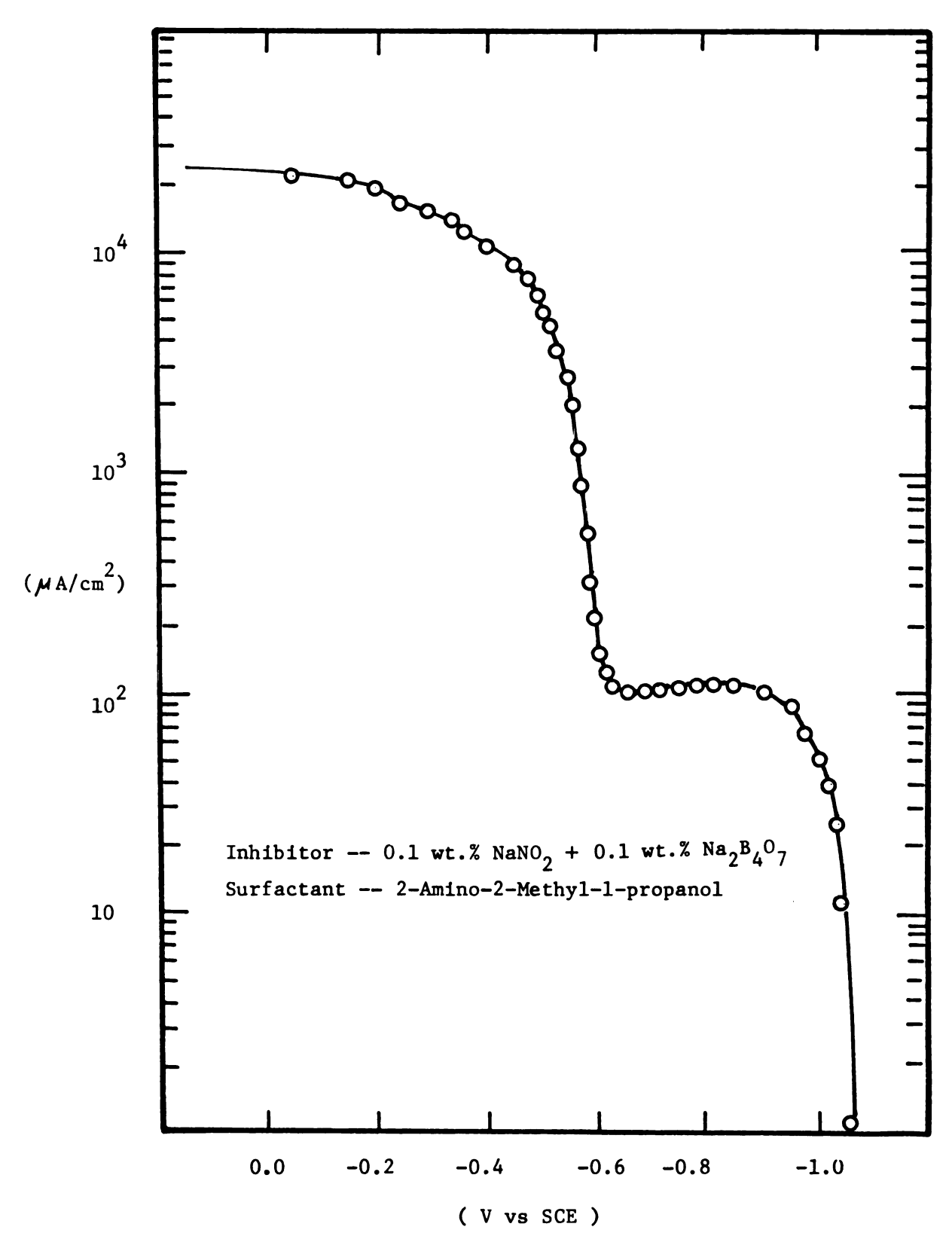


FIGURE 18 ANODIC POLARIZATION OF 7075 T6 A1 ALLOY IN 1 wt.% NaCl, INHIBITOR AND SURFACTANT WITHOUT STIRRING AT $20^{\circ}\text{C} \pm 2^{\circ}\text{C}$

in the presence of borate-nitrite (0.1% $NaNO_2 + Na_2B_4O_7$) inhibitor, with small additions of surfactant, such as 2-Amino-2-Methyl-1-propanol, to the 1% NaCl solution. According to Khobaib, Quakenbush and Lynch's research (50) small additions of some surfactants improve the inhibition of borate-nitrite systems and, these mixtures provide good protection to aluminum alloys in high chloride-containing solutions. Figure 18 shows that the corrosion potential has been moved in the active direction by the addition of surfactant, from -0.710 V (vs SCE) to -1.049 V. The corrosion potential was greatly altered by 2-Amino-2-Methyl-1-propanol. During the equilibration, a very thick black oxide films formed. With the potential increasing to -0.630 V, the current density remains constant because of oxide formation on the specimen surface. At a potential of -0.550 volt (vs SCE), the oxide slightly breaks down and the anodic current density increases because of the occurrence of gas or bubble formation at the surface. As the potential is increased, the oxide film continues to form at the surface of the specimen.

According to Figure 18, a small, addition of surfactant, 2-Amino-2-Methyl-1-propanol very much affects the anodic polarization curve, and it may be suggested that this surfactant provides good protection to Al alloys in the present of chloride solution. It is suggested that the small additions of surface active compounds, such as Amino-Methyl-propanol interferes with the dissolution reaction by interacting with the passive film already provided by the inhibitor formation which results in the development of a stronger and possibly thicker adsobed protective film.

Potentiodynamic cathodic polarization curves at room temperature and at 1 wt.% NaCl and 1 wt.% NaCl + 0.1 wt. % NaNO $_2$ are shown in

Figures 10 and 19, respectively. The cathodic polarization curve of Figure 10 indicated the limiting current density because of the hydrogen evolution reaction occurring from -1.08 V (vs SCE) to -0.715 (vs SCE). The limiting current density is about 11.5 (μ A/cm²). the experiment, a small amount of bubble formation and gas evolution on the surface was observed. As the potential is decreased, the gas evolution is increased. In Figure 19, the anodic polarization curve also indicated the limiting current density resulting from oxygen reduction or hydrogen evolution reaction between -0.910 (vs SCE) and -0.715 The limiting current density is about 15.5 (μ A/cm²). (vs SCE). The inhibitor, NaNO, effects a raising of the potential. It is also known that NaNO, has good ability for increased passivation against chloride attack. Although nitrite is known to prevent aluminum corrosion in the presence of chloride-containing solutions, Figure 19 shows that NaNO, either reduces cathodic polarization or induces the limiting current density. In view of these results, it may be suggested that nitrite, a passivator in the range of concentrations ($0.1 \text{ wt.}\% \text{ NaNO}_2$), may be ineffective against chloride attack because of the reducing cathodic polarization.

The linear polarization technique appeared to be the most suitable approach for determination of corrosion rates. Instead of imposing a very large change in voltage, typical of the Tafel method, the linear polarization method involves only 10-30 mV swings positive or negative from the corrosion potential, in increments of about 1 mV. A direct plot of current vs. potential yields a straight line according to the Stern-Geary (35) equation,

$$(\Delta E/\Delta I)_{E-O} = R_{D} = B/i_{corr},$$
 (44)

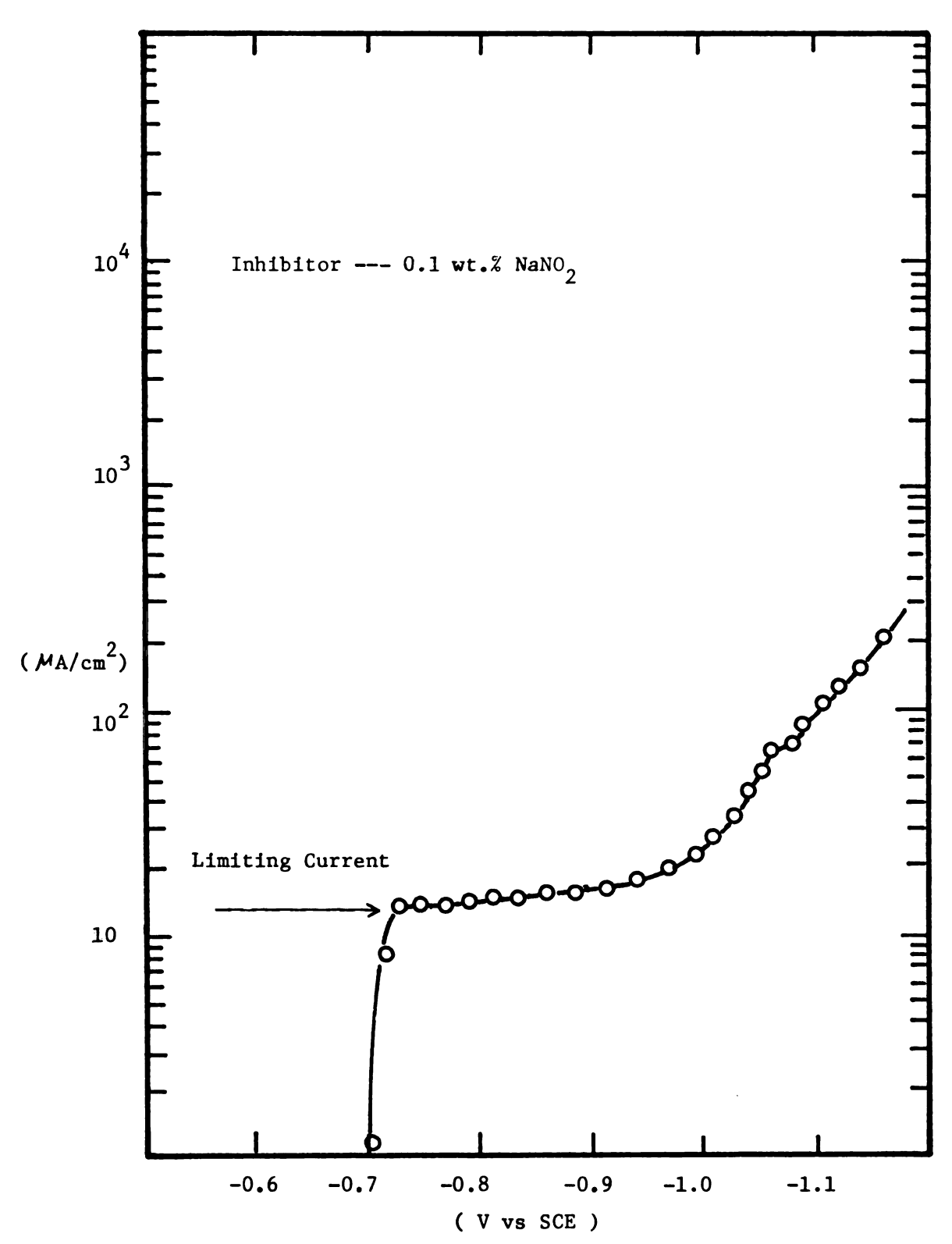


FIGURE 19 CATHODIC POLARIZATION OF 7075 T6 A1 ALLOY IN 1 wt.%
NaCl AND INHIBITOR WITHOUT STIRRING AT 20°C + 2°C

where R_{p} is polarization resistance, and i_{corr} is the corrosion current density.

In Figure 20, polarization measurements on these specimens of 7075-T6 Al alloys, without inhibitor and surfactant, with only surfactant, with surfactant and inhibitor are shown. Values of R are taken from the initial slopes of the curves and are tabulated with corresponding corrosion potentials in Figures. In Figures 21 and 22, polarization measurements on 7075-T6 Al alloy with inhibitors only (1 wt.% NaCl solution) are shown. According to these results, the inhibitor may be effective on a bare surface specimen and in the presence of chloride ions. If, however the surfactant is added to the inhibitors, the combination will prevent chloride from attacking Al alloys.

B. Effect of Stress

In <u>Figure 23</u>, the anodic profile is presented for the concentration 1 wt.% NaCl at room temperature with stress, but no inhibitors. The figure shows that the corrosion potential of corroding 7075-T6 Al alloy moved 15 mV in the active direction as a result of applied stress.

Furthermore, applied stress affects the increasing current density. The profile in Figure 23 is continuous, but is not adaptable to Tafel analysis because of a short linear region. Throughout the experiment, formation of a thin white adherent film on the surface of the specimen was observed. As the potential is increased, a deposit continued to accumulate at the surface of the specimen and, simultaneously, gas evolution on the specimen surface was observed. In view these observations, it can be concluded that the applied stress affects the polarization behavior of 7075-T6 Al alloy and raises the current density.

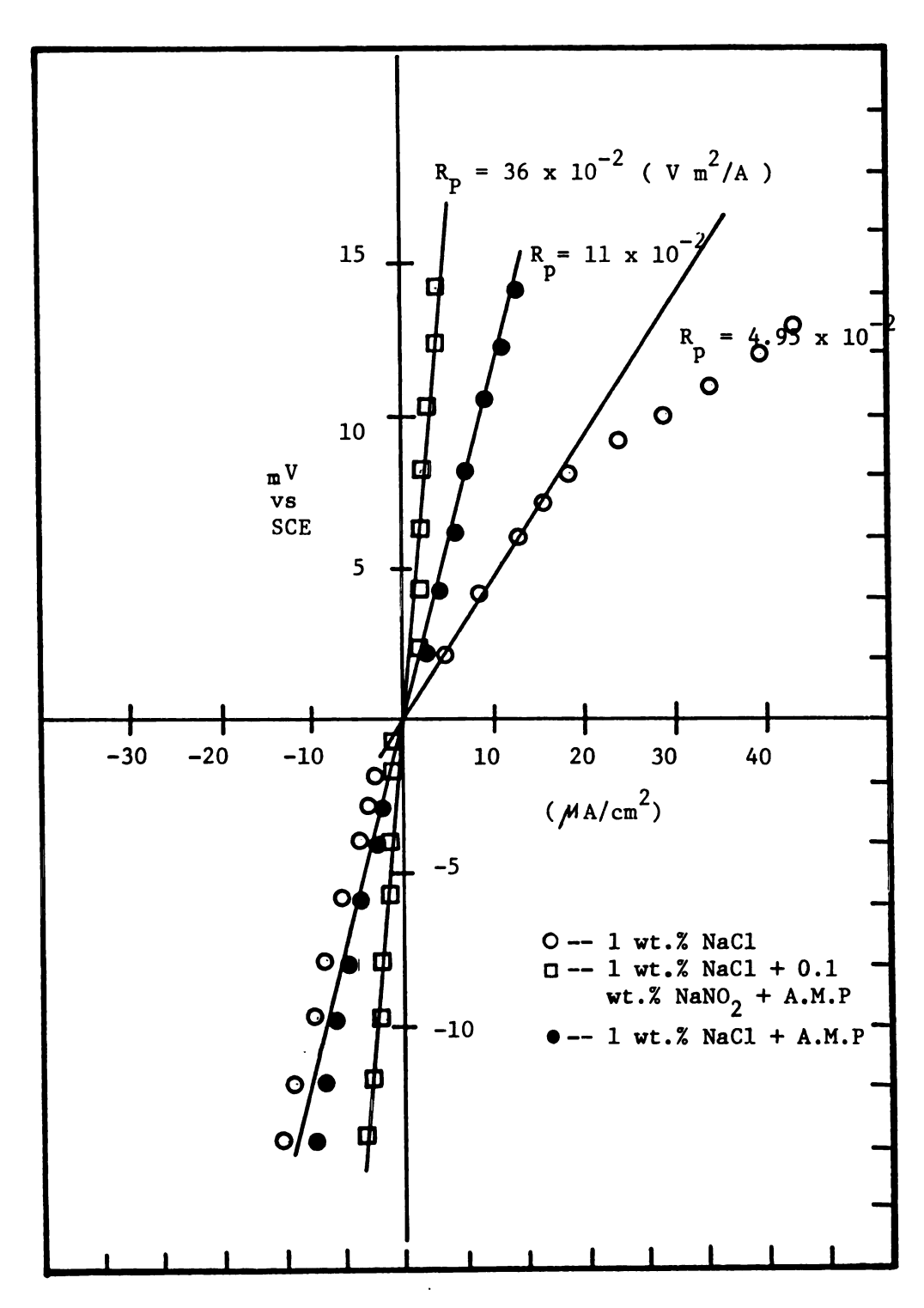


FIGURE 20 LINEAR POLARIZATION OF 7075 T6 A1 ALLOY IN 1 wt.% NaC1 UNDER VARIOUS CONDITIONS WITHOUT STIRRING AT 20°C \pm 2°C

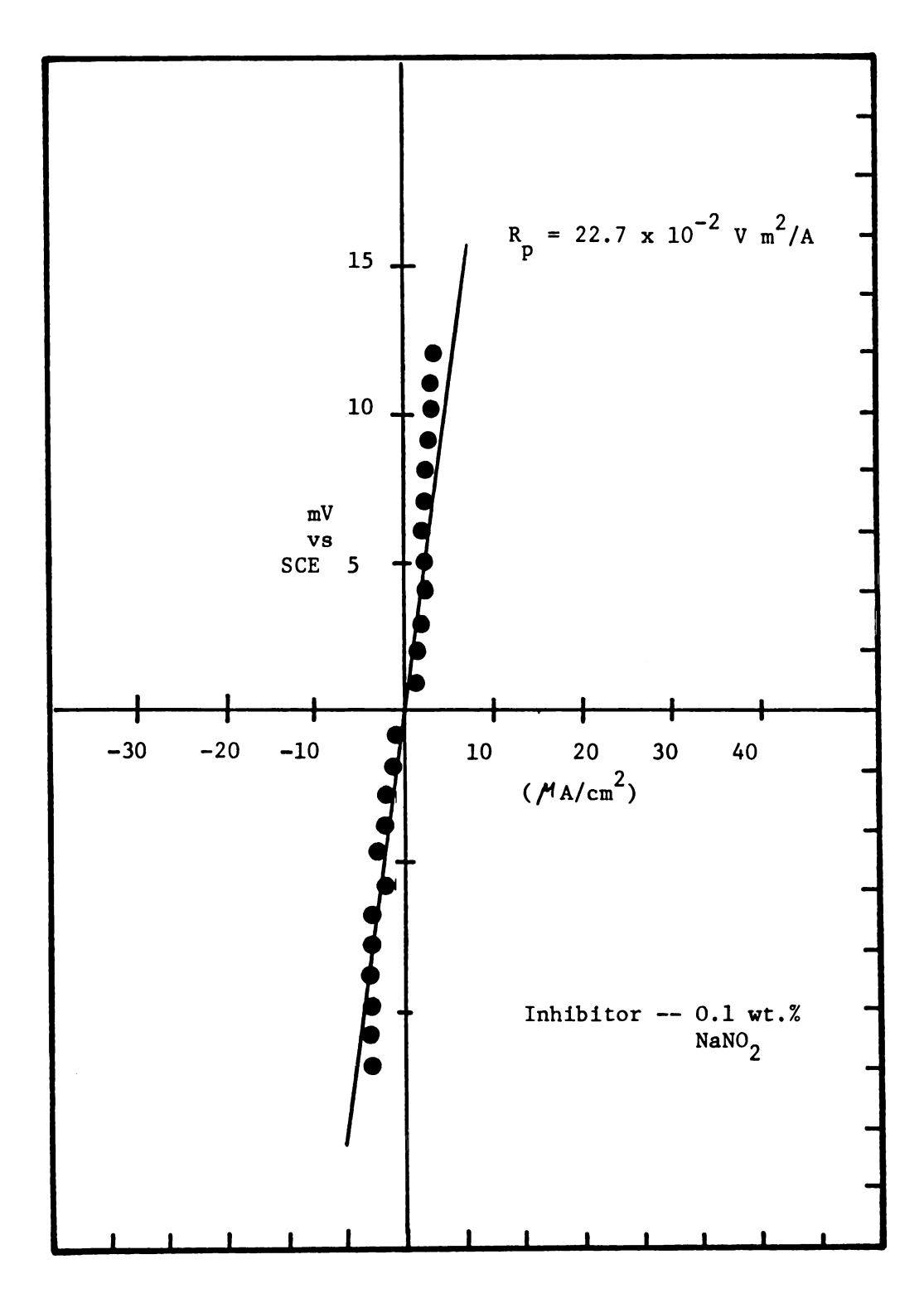


FIGURE 21 LINEAR POLARIZATION OF 7075 T6 A1 ALLOY IN 1 wt.% NaC1 WITHOUT STIRRING AT $20^{\circ}\text{C} \pm 2^{\circ}\text{C}$

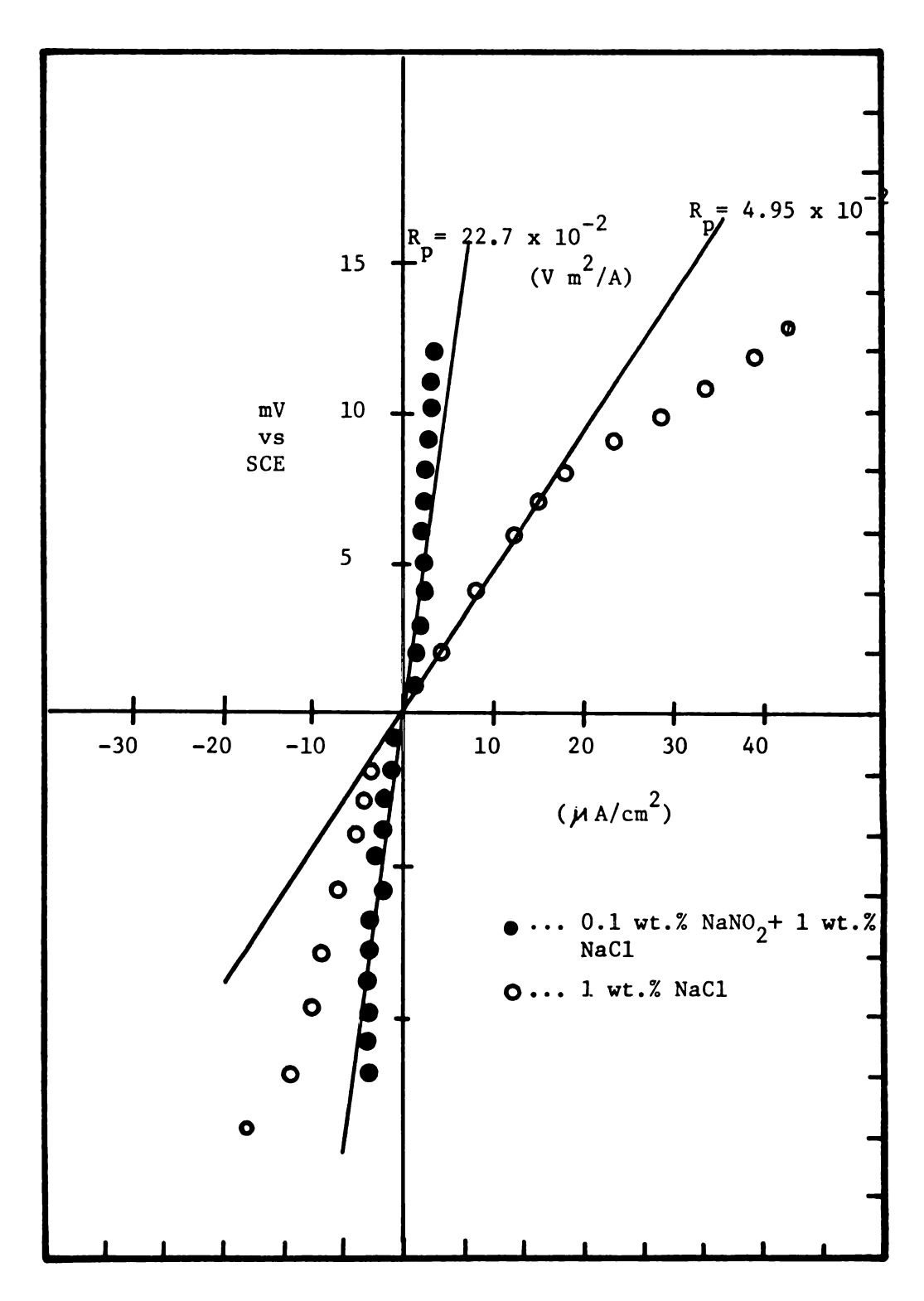
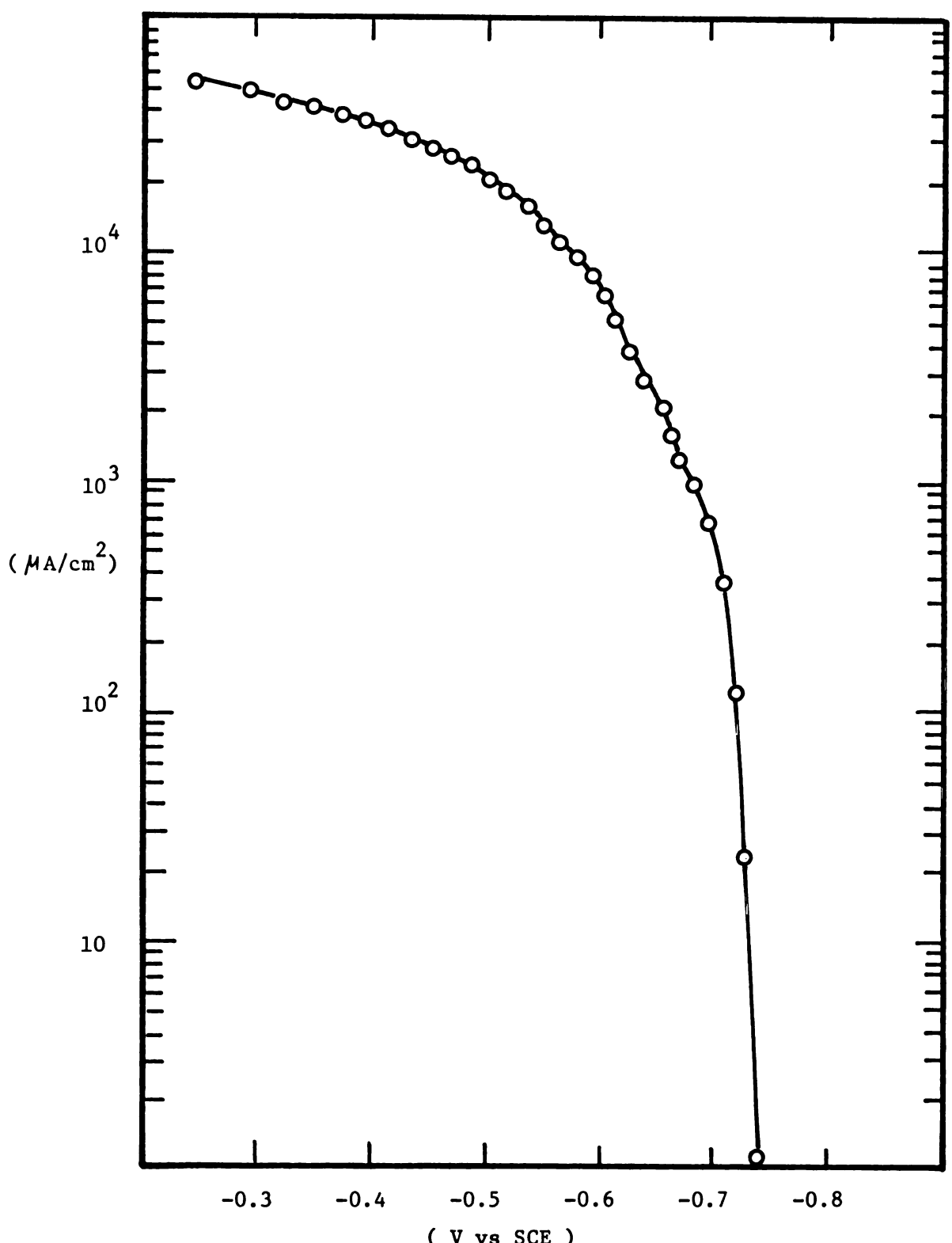


FIGURE 22 LINEAR POLARIZATION OF 7075 T6 A1 ALLOY IN 1 wt.% NaC1 WITHOUT STIRRING AT $20^{\circ}\text{C} \pm 2^{\circ}\text{C}$



(V vs SCE)

FIGURE 23 ANODIC POLARIZATION OF 7075 T6 A1 ALLOY IN 1 wt.%

NaC1 UNDER STRESS WITHOUT STIRRING AT 20°C + 2°C

Furthermore, stress affects the type of oxide film formation at the surface of specimen.

C. Crack Electrochemistry.

Experiments on crack or crevice corrosion were carried out on 7075-T6 Al alloy in 1 wt.% NaCl solution with and without inhibitors at ambient temperature. Additionally, the effect of applied stress has been analysed. When artificial cracks are immersed in an aqueous chloride solution, rapid corrosion or accelerated crack electrochemistry may occur. This accelerated dissolution arises because the crevice restricts mass transport of dissolved corrosion products away from the metal surface. Consequently, the chemical system of the crack electrolyte may change, and species which are aggressive to the metal surface may accumulate there.

Several mechanisms have been proposed for corrosion inside the crack, all of which involve three basic components, alone, or in combination: differential aeration, localized acidification, and migration of chloride ions into the crack. The type of cracks have been analysed for NaCl solution without inhibitors: (1) an "isolated "crevice, where the crevice metal was not coupled to the open external metal; and (2) a "coupled" crevice, where crevice metal was coupled to the open external metal.

D. Isolated Crevices.

In <u>Figure 24</u>, anodic profiles are presented for 0.5, 1 and 3 wt.%

NaCl concentrations at bare surfaces and in isolated cracks. According

to the anodic polarization curve for the isolated crack in Figure 24,

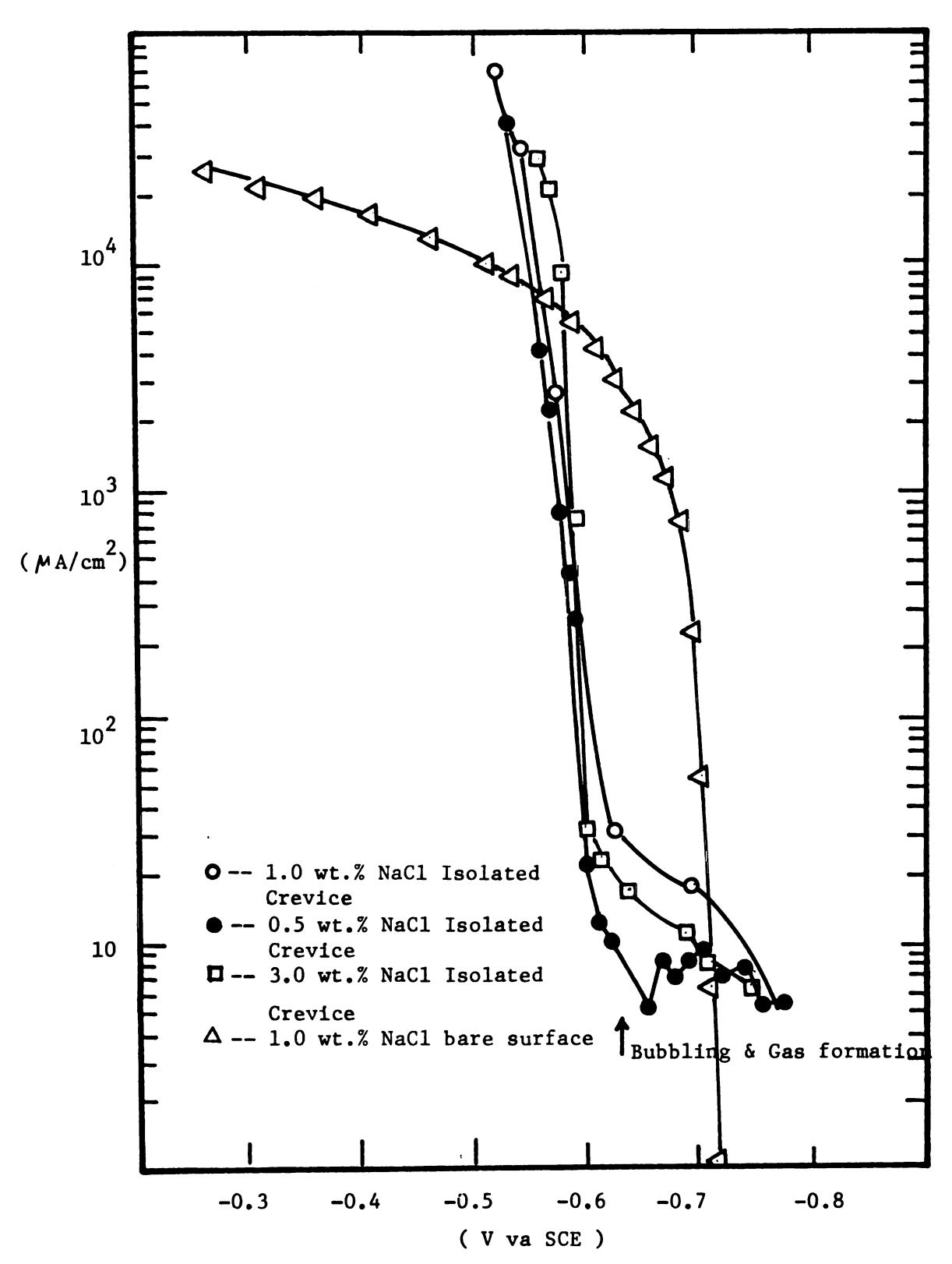


FIGURE 24 ANODIC POLARIZATION OF 7075 T6 A1 ALLOY IN DILUTE NaC1 SOLUTION

gas bubbles were visually observed in the potential range between -0.850 V to -0.600 V. Also negative current has been observed. Above this potential, the curves are linear with smooth slopes. Anodic profiles for isolated crevices show that anodic dissolution inside the isolated crevice is independent of the concentration of NaCl. Anodic dissolution inside the crevice, however is much higher than at the bare surface. The experimental data show that , in the potential range between -0.850 to -0.600 V, the hydrogen evolution reaction may take place, i.e.,

$$H_2O + e^- \longrightarrow \frac{1}{2} H_2 + OH^-,$$

because negative current under anodic condition and profuse bubble formation could be observed. The gas extracted from electrolyte was analysed in chemical flame test. The gas was hydrogen.

According to Figure 25, this reaction can take place thermodynamically.

This hydrogen reduction reaction proceeded slowly in neutral aqueous media.

In Figure 26 and 27, cathodic profiles are presented for concentrations of 1 and 3 wt.% NaCl inside the isolated crack. According to the cathodic polarization curve for the isolated crack in Figures 26 and 27, gas bubbles were observed in the entire range of potentials.

Cathodic profiles for isolated crevices show the limiting current.

Also it is shown that cathodic polarization curves are dependent of the concentration of NaCl. With increasing NaCl concentration, the current density increased.

The open circuit corrosion potential was measured as a function of time. An isolated artificial crack is immersed in various concentrations of NaCl with and without inhibitors. Figure 28 shows the results for several conditions. The solution (1.0 wt.% NaCl with and without

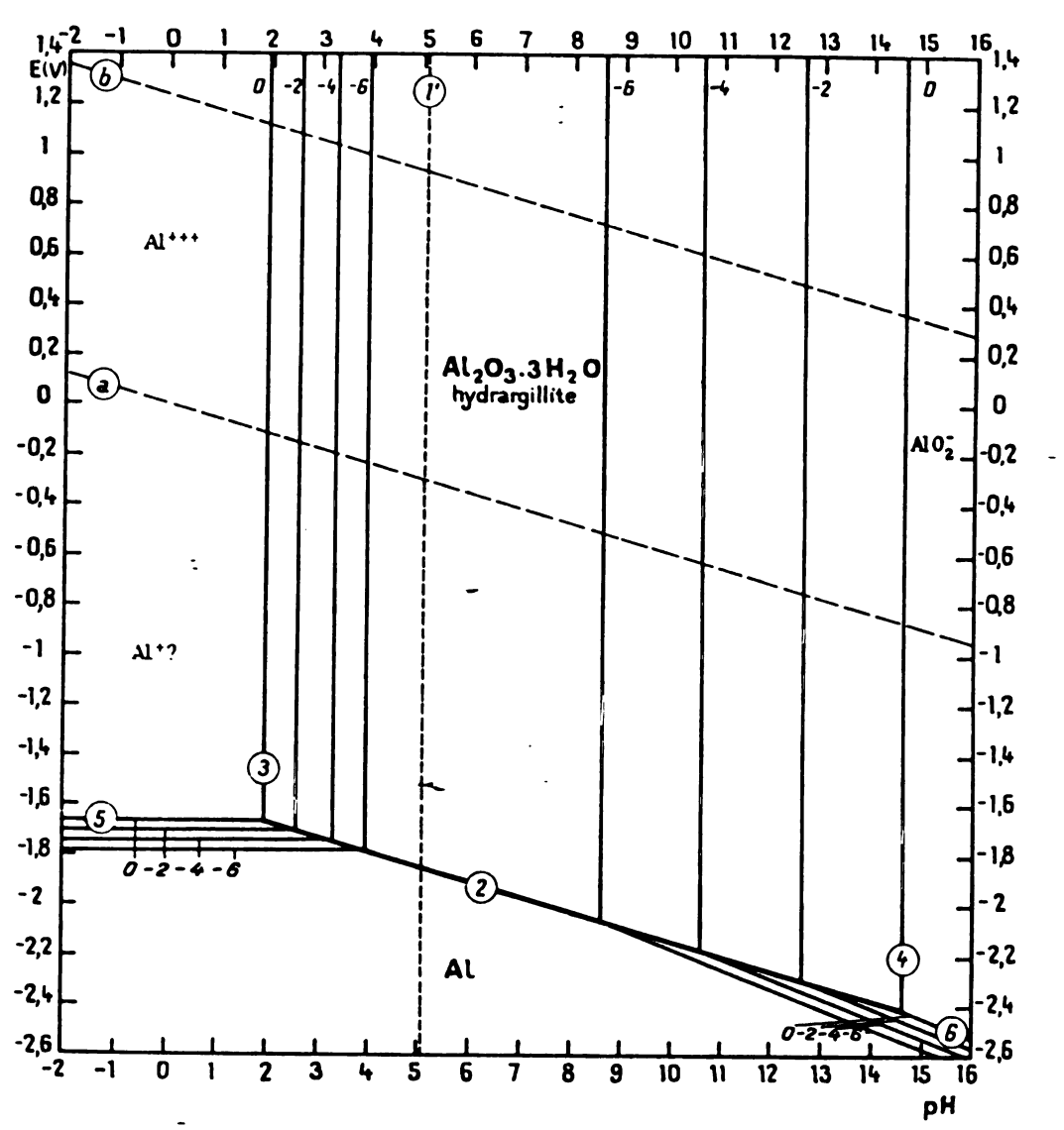


Fig. 25 Potential-pH Equilibrium diagram for the System Aluminum-Water, at 25° C. (77)

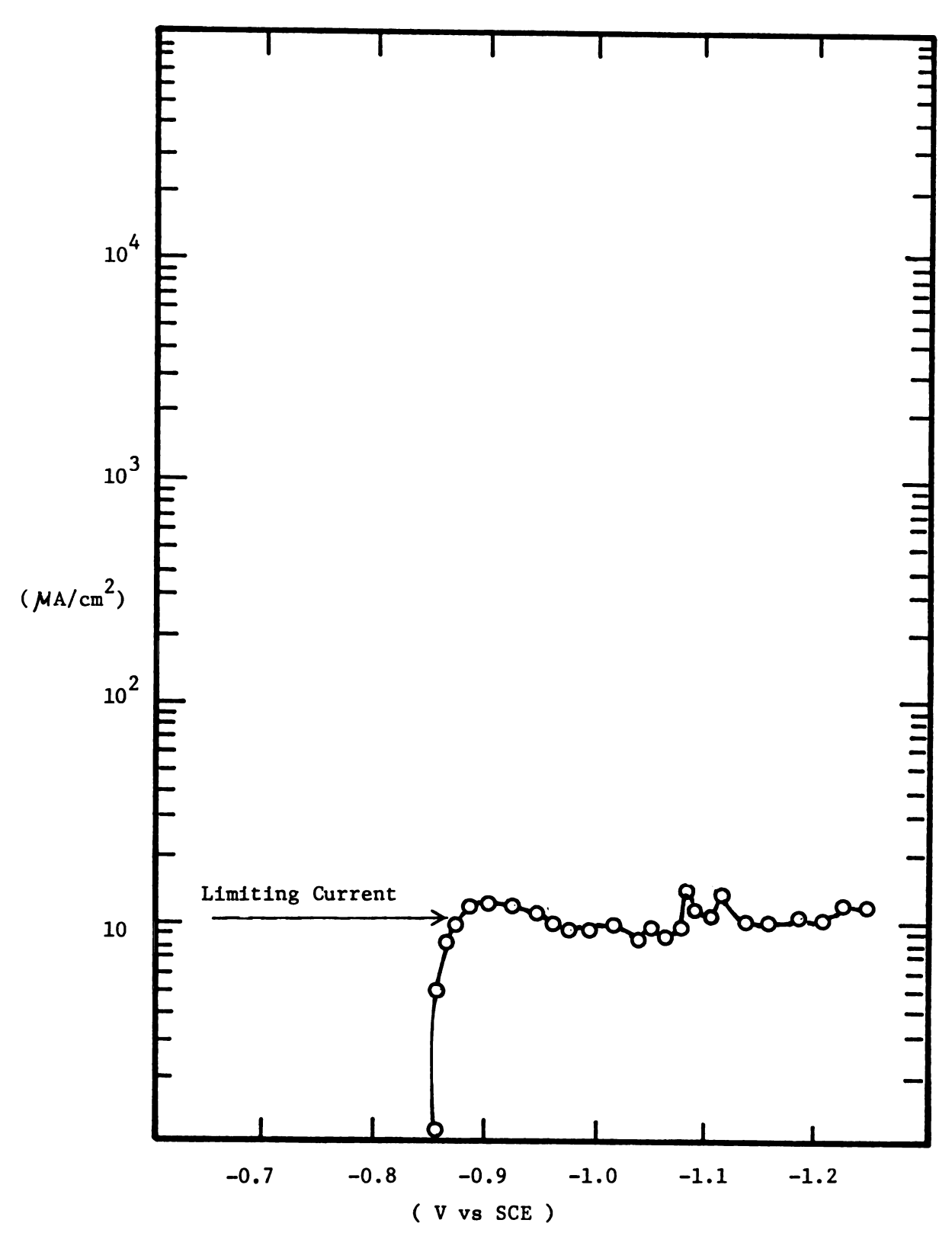


FIGURE 26 CATHODIC POLARIZATION OF 7075 T6 A1 ALLOY IN 1 wt.%

NaCl Solution And CREVICE WITHOUT STIRRING AT 20°C

+ 2°C

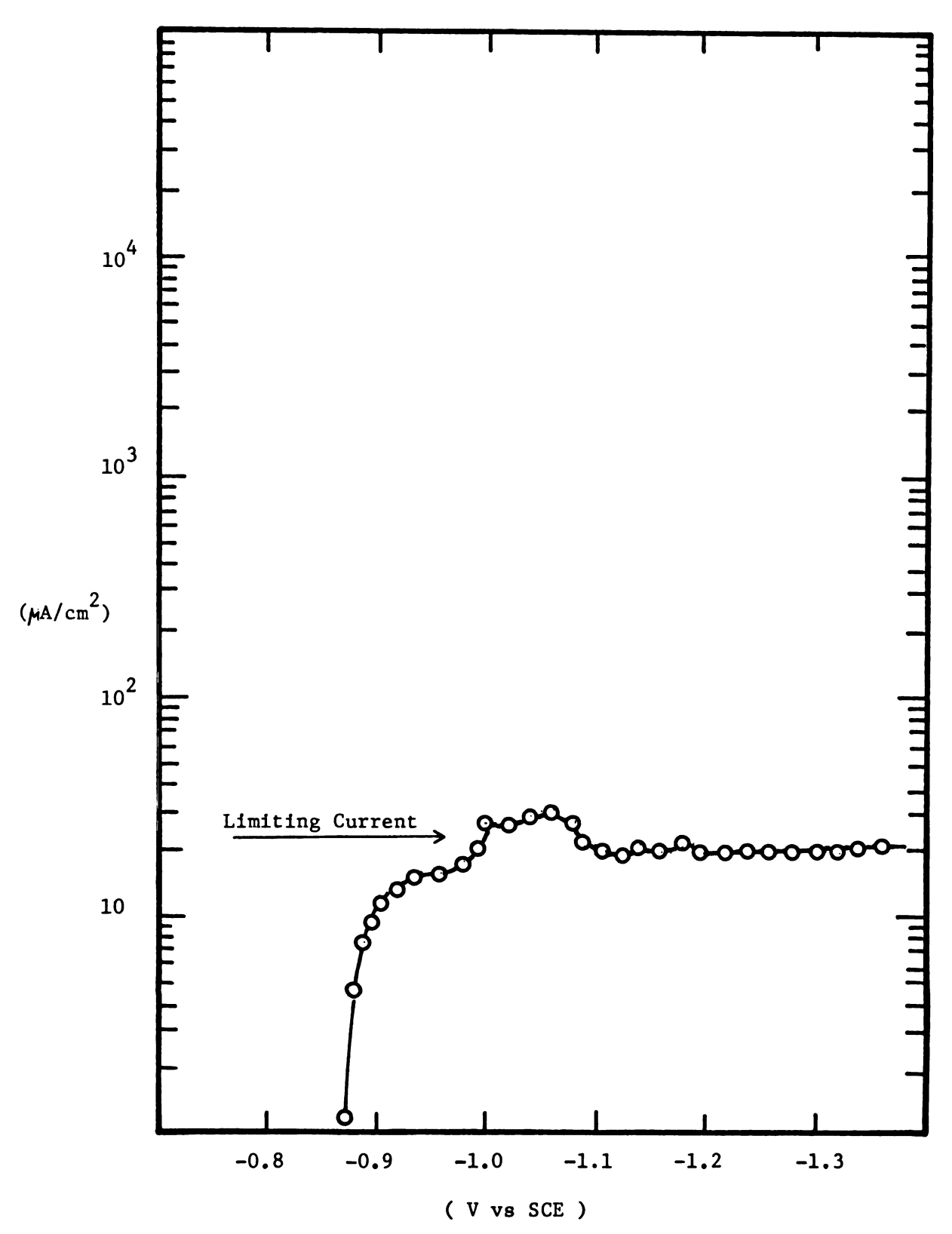
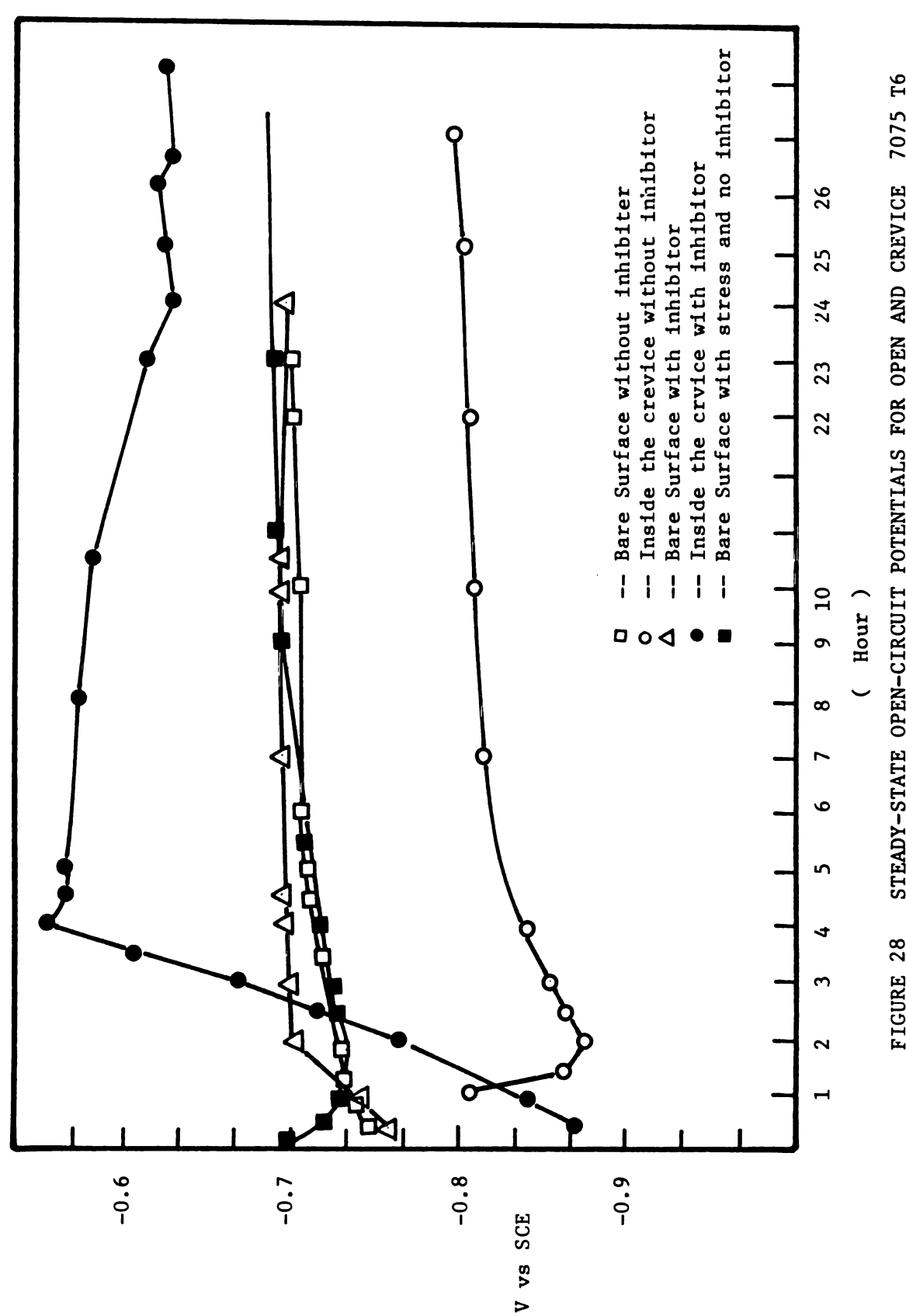


FIGURE 27 CATHODIC POLARIZATION OF 7075 T6 A1 ALLOY IN 3 wt.% NaCl Solution and CREVICE WITHOUT STIRRING AT 20° C \pm 2° C



STEADY-STATE OPEN-CIRCUIT POTENTIALS FOR OPEN AND CREVICE 7075 T6 T6 A1 ALLOY IN DILUTE NaCl SOLUTION WITH AND WITHOUT INHIBITORS FIGURE 28

0.1 wt.% NaNO_2 + 0.1 wt.% $\mathrm{Na}_2\mathrm{B}_4\mathrm{O}_7$) was aerated and without stirring during the experiment. In the case of the bare surface electrode (no connection to crack), after the electrode was placed in solution (1 wt.% NaCl without inhibitor), there was a little increase in open circuit potential from -0.755 to -0.730 V vs SCE. Electrode potential slightly increased with time. After 3.5 hr. (the induction time), the potential remained at a constant value, about -0.710 V vs SCE. On the other hand, after the electrode was placed in solution (1 wt.% NaCl + 0.1 wt.% NaNO $_2$ + 0.1 wt.% $\mathrm{Na}_2\mathrm{B}_4\mathrm{O}_7$), there was a rapid increase in potential from -1.016 to -0.924 V. After 2 hr, the potential remained at a constant value, about -0.710 V, which was the same as the potential at a bare surface electrode.

In the case of an isolated crack electrode, after the electrode was placed in solution (1 wt.% NaCl without inhibitor), the corrosion potential moved toward the active direction, and the potential attained a value of about -0.880 V. After 7 hr, the potential remained at a constant value of about -0.810 V, which is much less than the value obtained with the bare surface electrode (no connection to crack electrode).

After the artificial crevice electrode was place in solution (1 wt.% NaCl with 0.1 wt.% NaNO $_2$ + 0.1 wt.% Na $_2$ B $_4$ O $_7$), the corrosion potential moved very rapidly in the noble direction from -0.890 to -0.820 V. As time passes, the electrode potential consistantly increased. After, 4 hr. the corrosion potential attained a value about -0.550 V which is much different from the other conditions. After 20 hr, the potential remained at a constant value, about -0.630 V which was higher than the bare surface electrode, with and without inhibitor, and the cracked electrode (isolated) without inhibitor.

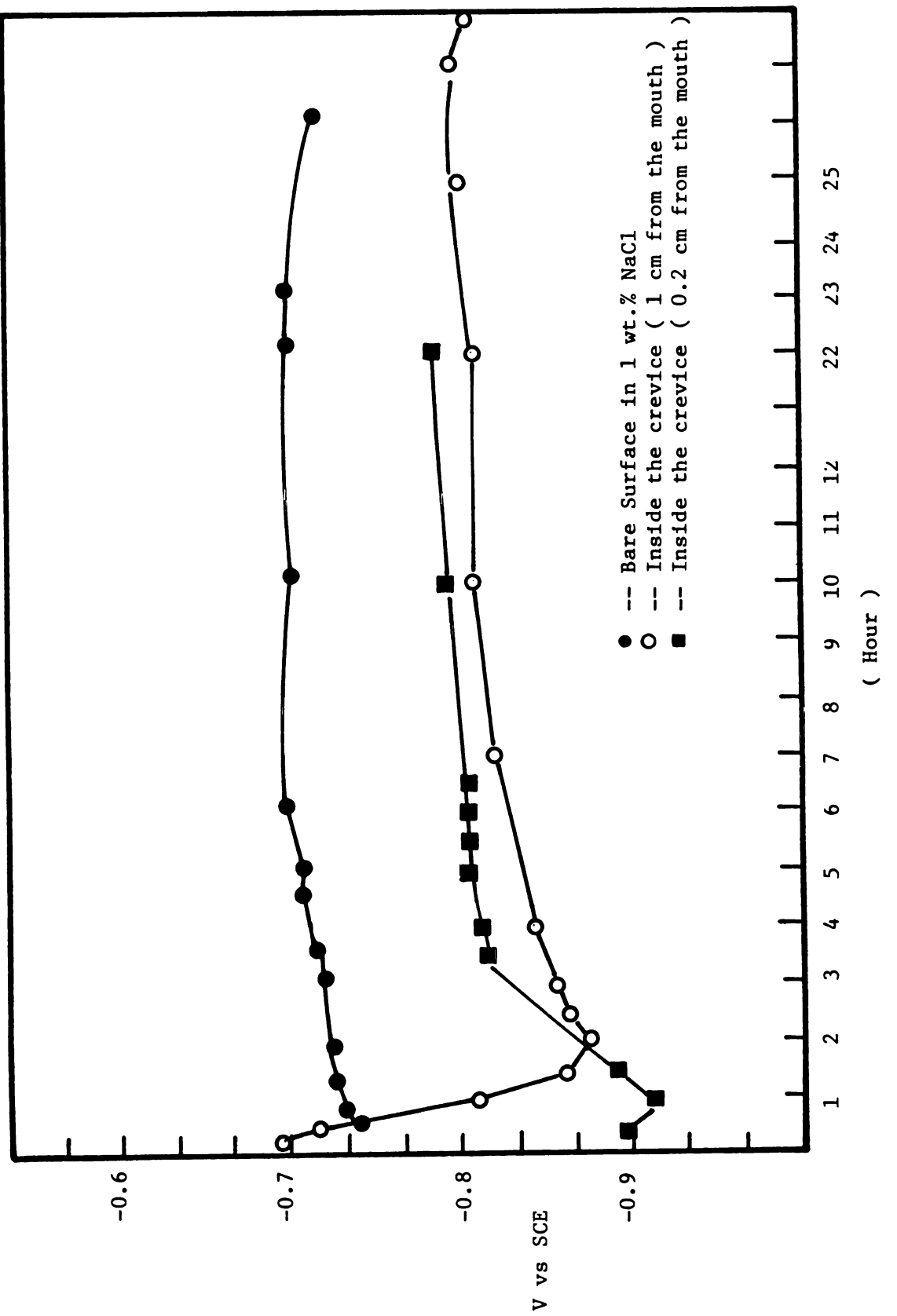
Figure 29 shows the open circuit corrosion potential at the different position of inside the crack as a function of time. The solution (1.0 wt.% NaCl without inhibitors) was aerated with no stirring during the experiment. The results show a small potential drop inside the crack (isolated crack).

E. Coupled Crack.

We have confined ourselves to a consideration of electrochemical and corrosion behavior of Al alloys inside the crack alone. In reality, for existing structures, the crevice always is in contact with Al alloy outside the crack. In this experiment, the polarization behavior of a " coupled " crevice, where crevice metal was coupled to the open external metal was studied. In Figure 30, anodic profiles are presented for 1 wt. % NaCl on a bare surface, not coupled to the any other metal and a coupled crack. According to the anodic polarization curve for a coupled crack in Figure 30, gas bubbles were observed in the potential range between -0.850 V to -0.700 V both on the bare surface and inside the crack, and current oscillation was observed. Above this potential, the curves are linear with smooth slopes. The anodic profiles for a coupled crevice shows that anodic dissolution inside the crack is much higher than is the case for a bare surface.

Some references (54), (55) show that the cathodic reaction (oxygen reduction) continues outside the crack after the oxygen within the crack has been consumed, and anodic reaction is confined to the crack.

Figure 31 also compares the current densities for the isolated (uncoupled) crack to that for Al alloy couples under various concentrations. According to the polarization curves for the coupled crack, in solutions



STEADY-STATE OPEN-CIRCUIT POTENTIALS FOR OPEN AND CREVICE 7075 T6 A1 ALLOY IN DILUTE NAC1 SOLUTION FIGURE 29

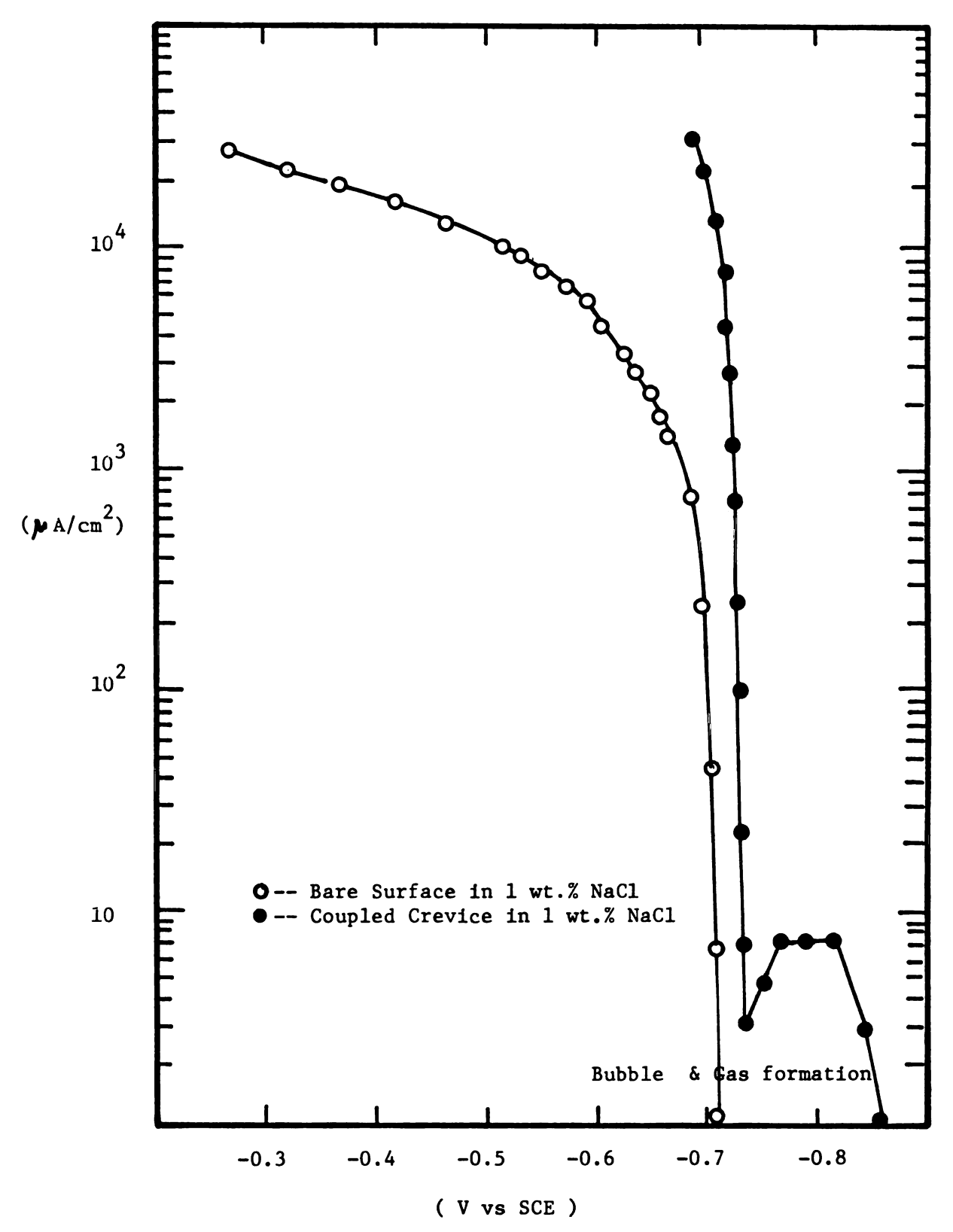


FIGURE 30 ANODIC POLARIZATION FOR OPEN AND CREVICE 7075 T6 A1 ALLOY IN 1 wt.% NaCl Solution WITHOUT STIRRING AT $20^{\circ}\text{C} \pm 2^{\circ}\text{C}$

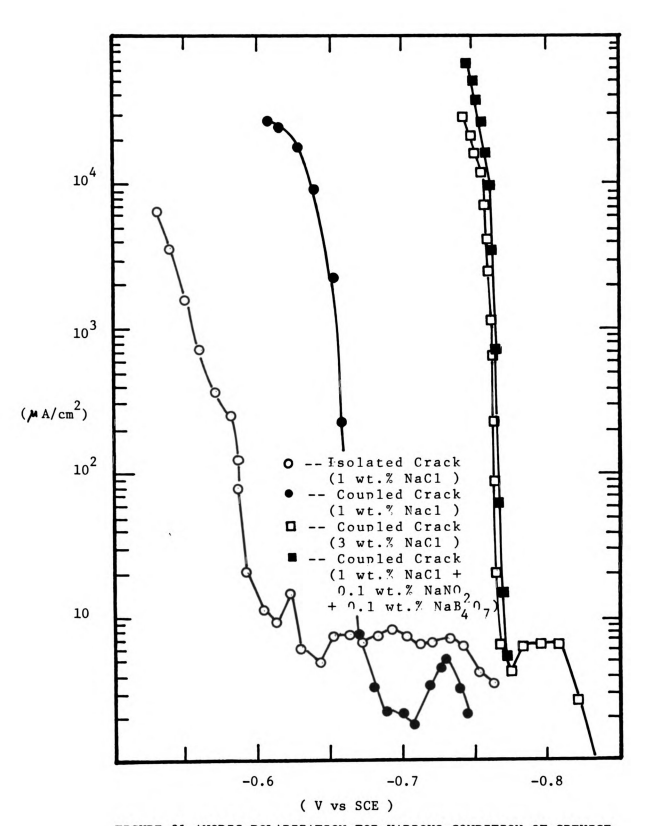


Figure 31 anodic polarization for various condition of crevice 7075 T6 A1 alloy in dilute solution without stirring at $20^{0}\text{C} \pm 2^{0}\text{C}$

(3 wt.% NaCl and 1 wt.% NaCl), Figure 31, gas formation as well as bubbling were observed in the potential range between -0.800 V to -0.730 V at bare surface as well as inside the crack. The rate of gas formation as well as bubbling inside the crack were less than at the bare surface. Above this potential, the curves are linear with smooth slopes. The anodic profile for 3 wt.% NaCl solution shows that anodic dissolution inside the crack is higher than for 1 wt.% NaCl solution. At higher Cl ion concentration, gas formation and bubble formation are less than at the low Cl ion concentration inside the crack.

In Figure 31, anodic profile is presented for a coupled crack at 1 wt.% NaCl + 0.1 wt.% NaNO₂ + 0.1 wt.% Na₂B₄O₇ inhibitive solution. According to the anodic polarization curve for a coupled crack, Figure 31, gas bubbling was observed in the potential range between -0.85 V to -0.710 V at both bare the surface and inside the crack, and oscillations in current were observed. In the potential range between -0.850 V to -0.710 V, the profile shows discontinuities because of cathodic reduction, gas bubbling, and depolarization.

At the bare surface (external surface), formation of a very thick black adherent film on the specimen surface was observed. Above the potential, -0.710 V, the curve is linear. Inside the crack, no gas bubble formation was observed. Figure 31, compares the anodic polarization curve for a coupled crack in the non-inhibitive solution with that for a coupled crack in an inhibitive solution. In the former case, the breakdown anodic dissolution potential is a little higher than that in the non-inhibitive solution. The nitrite ion effects a raising of the potential, that is.

$$NO_{2}^{-}$$
 + 8 H⁺ + 6e⁻ $\stackrel{--}{\leftarrow}$ NH₄⁺ + 2H₂O,

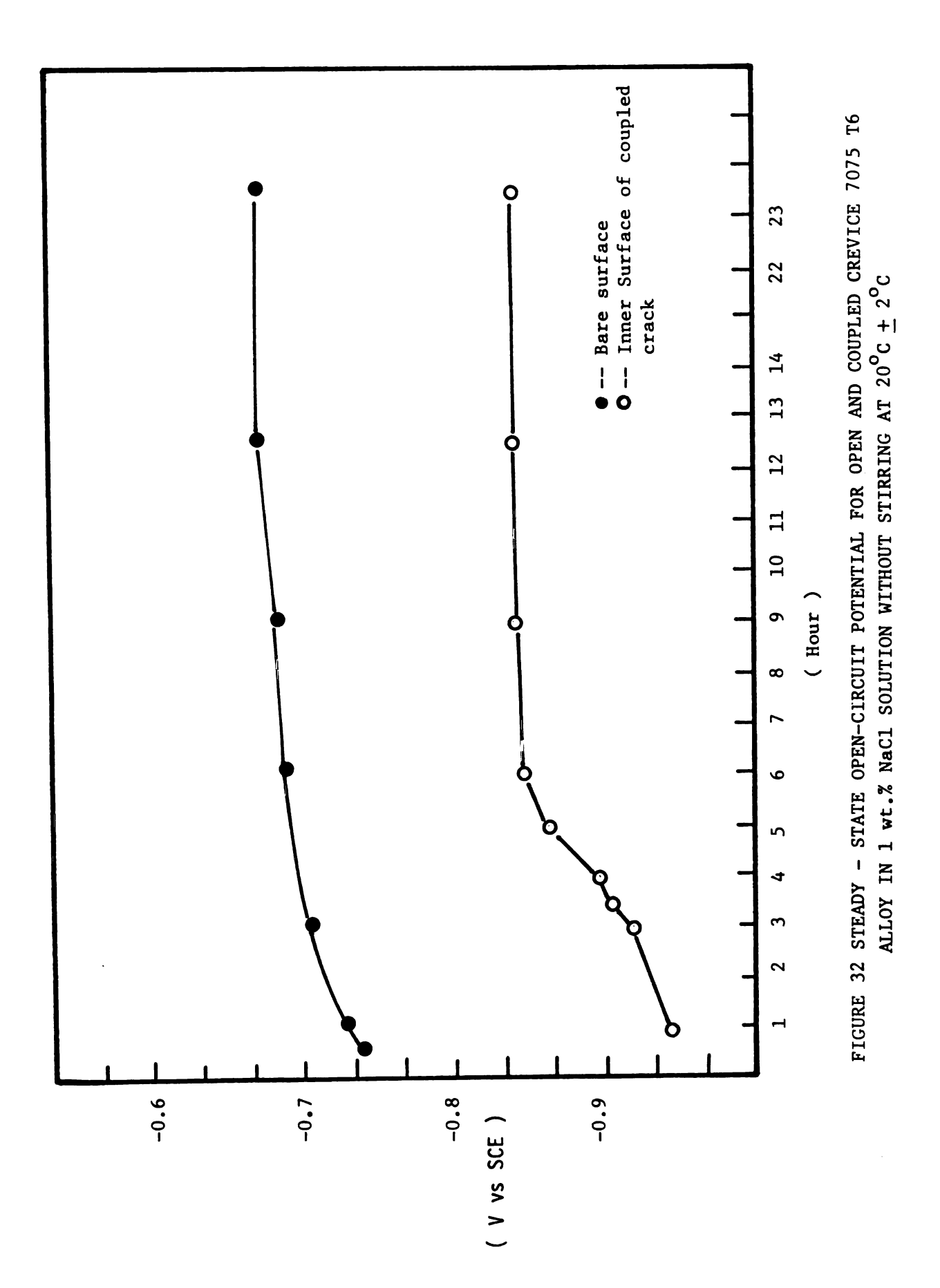
E = + 0.90 V SHE.

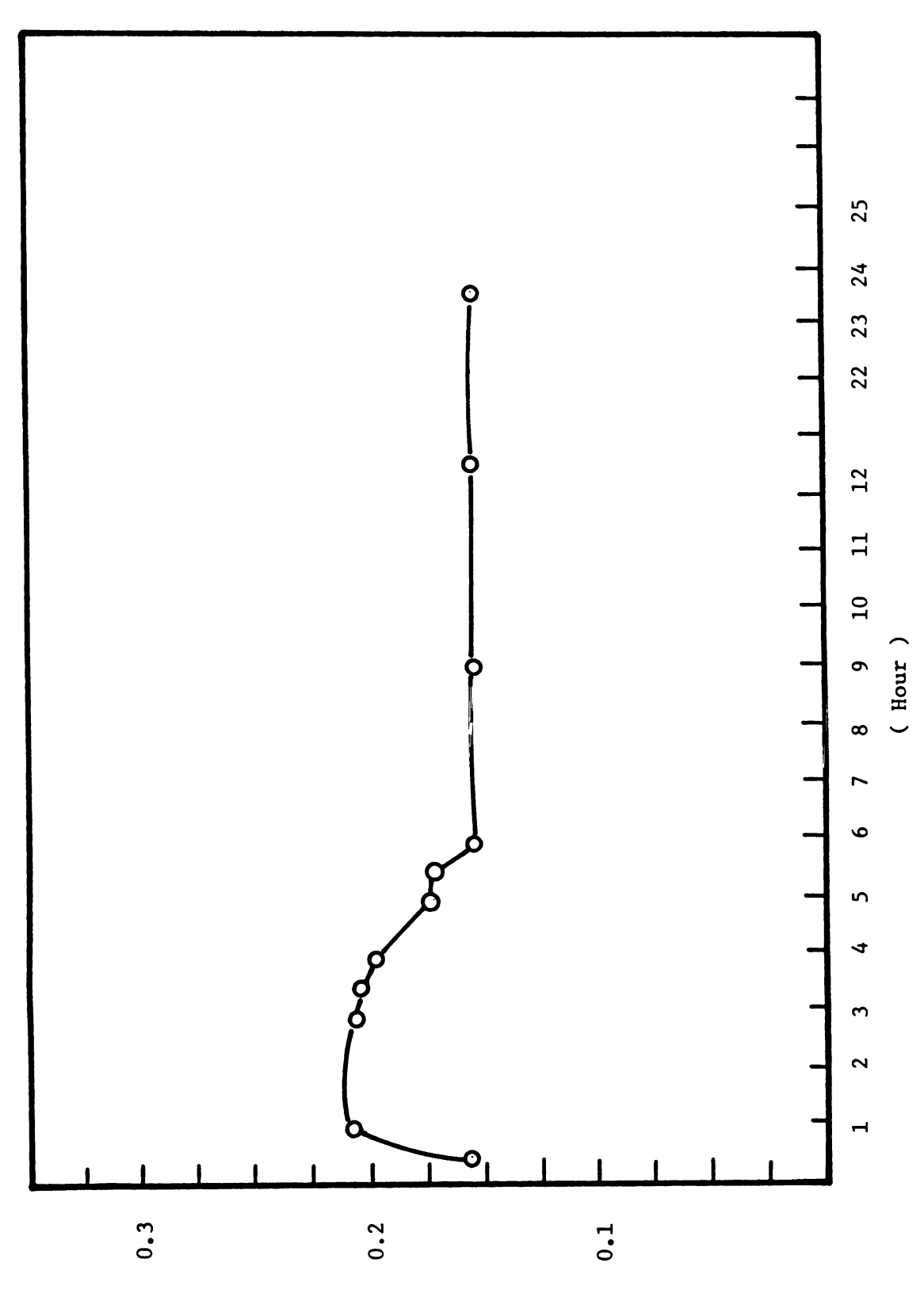
However, the current density is almost the same for both cases. From the experimental results, these concentrations of inhibitors may be a little more effective inside the crack, but, the inhibitive action is weak.

The open circuit corrosion potential was measured as a function A coupled artificial crack was immersed in 1 wt.% NaCl of time. without inhibitor, (Figure 32). The solution (1 wt.% NaCl) was aerated and not stirred during the experiment. In all cases (open circuit corrosion potential, anodic polarization and cathodic polarization), the measurements were made at the same position inside the crack. The cracked specimen of 7075-T6 Al alloys and the external Al alloy were coupled for a few minutes. Upon coupling, the corrosion potential of the external specimen shifted to the more noble direction, compared with the bare surface specimen (uncoupled to other electrode), whereas the corrosion potential of the cracked specimen shifted to the more active direction compared with the isolated specimen. After 6 hr, a steady-state condition was attained, at a potential difference of about 150 mV, which corresponds to Rosenfeld's data. Since this value is not small, an IR drop between the crack interior and outer electrode must be large.

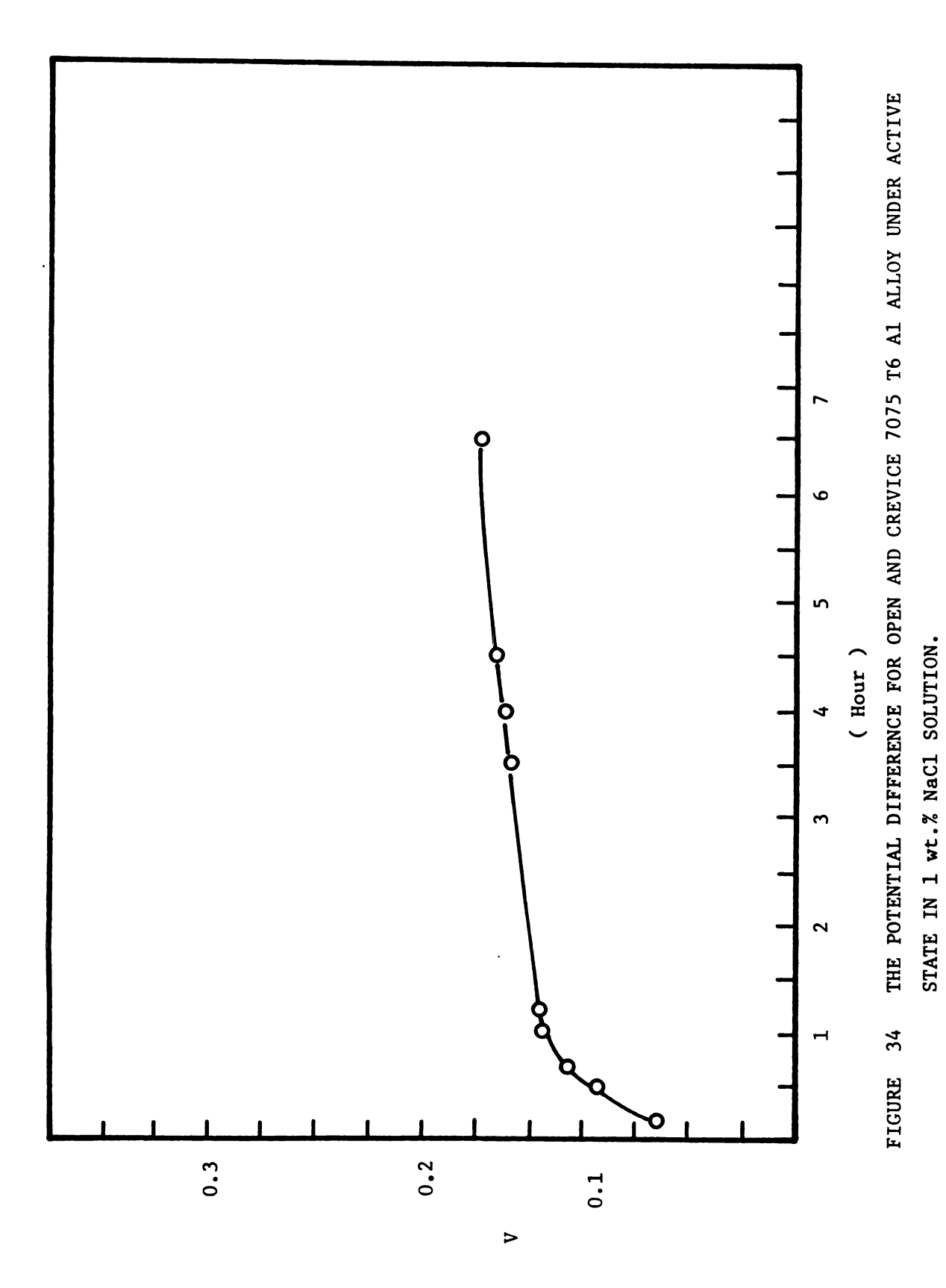
Figure 33 shows the potential difference between the crack interior and outer electrode as function of time. After 6 hr, steady-state was attained. The electrode potential was measured as a function of time under the active state. After several hours, the potential differences were attained at a steady state condition of about 150 mV, i.e., the same value as that under the nonsteady-state conditions.

Figure 34 shows the results, i.e., the potential difference between the external specimen and the cracked specimen under the active state.





STEADY-STATE OPEN-CIRCUIT POTENTIAL DIFFERENCE FOR OPEN AND COUPLED CREVICE 7075 T6 A1 ALLOY IN 1 wt.% NaCl SOLUTION FIGURE 33



According to Rosenfeld's paper, the electrode potential of the crack under active state was more negative than that of the open specimen because of a restricted oxygen supply to the crevices. This experimental data may show or prove Rosenfeld's experimental model.

In McCaffertys (7) paper and others (56), the concept that there is a large potential difference between the inner crack and the external metal is based upon potential measurements of uncoupled, unpolarized components in solutions of differing oxygen content. Futhermore, the potential difference between the inner and outer surface is much larger before coupling than after. This experiment shows different evidence, that is, the potential difference between the inner and outer surface is much larger after coupling than before.

These experimental data show that the potential drop changes slowly with distance from the crack tip, but to the mouth of the crack, the rate of change increases, i.e., inside the crack, the potential drop is very small. On the other hand, the potential drop between inside the crack and outside the crack is very large. Thus, the outside surface must support a cathodic reaction and it must be supported at a potential which is positive with respect to the potential of the anodic reaction in the crack. This evidence suggests that metal inside the crack is isolated from the external surface reactions, i.e., the separation of the anodic and cathodic regions. According to this potential difference, the electrochemical driving force is not small and this becomes more favorable for the development of corrosion inside On the other hand, a small potential difference inside the the crack. crack may cause a large concentration change and a correspondingly large increase in current density at a given applied potential. (57)

Under the open circuit condition, the cathodic reaction on the outer surface would occur naturally if dissolved oxygen were the primary bulk oxidant. Coupling this with a net anodic reaction inside the crack region for an overall current balance would lead to a steady state crevice corrosion. Then, applying a small positive or negative potential (under active state), bubble formation both inside and on the outer surface of the sample, because of hydrogen evolution reaction, has been observed in this experiment. Near the corrosion potential region of the outer surface of sample as well as inside, it is quite possible thermodynamically to take place.

C. Real Crack.

The open circuit corrosion potential was measured as a function of time. A real crack was immersed in 1 wt.% NaCl solution with stress and without inhibitors. In order to measure the potential inside the crack, a special microcapillary tube was used. In all cases, the measurements were made at the same position inside the crack.

Figure 33 shows the results for this condition. The solution (1.0 wt.% NaCl) was aerated and not stirred during the experiment. Corrosion potentials of both the external surface and inside the crack shifted to the more active direction because of the stress. After 20 hr, a steady-state condition was attained at a potential difference of about 35-45 mV. Since this value is small, an IR drop between the crack interior and outer surface must be small.

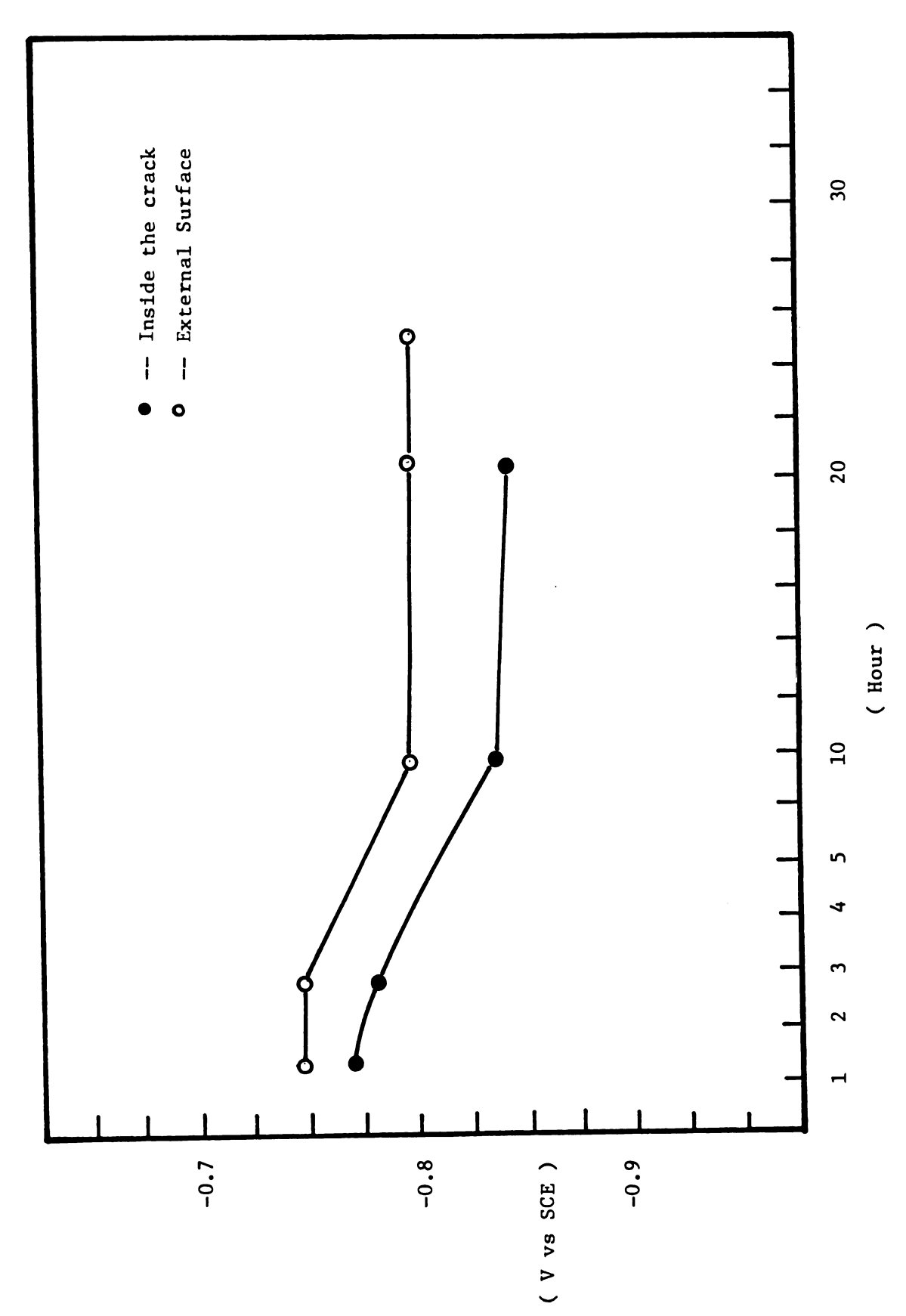


FIGURE 35 STEADY-STATE OPEN-CIRCUIT POTENTIAL UNDER STRESS IN 1 wt.% NaC1 SOLUTION.

A schematic representation of crack velocities of aluminum alloys as a function of stress intensity typically yields a curve with three distinctive regions (48). These regions are as follows: Region I, where crack growth is initially observed and changes rapidly with stress intensity; Region II, the "plateau" region which may be nearly parallel to the stress intensity axis; and a sharply increasing crack growth rate region (Region III) just prior to failure.

In our experiments, a stress intensity factor $(K_1 = 12 \text{ Mpa}, \overline{m})$, corresponding to Region II was used for SCC because in this region crack growth appears to be mainly environmentally controlled, and independent of K. Figure 36 shows the experimental result together with reference values $^{(78)}$. During crack propagation, the length of the crack can be measured in an optical microscope whenever necessary, then data for the da/dt vs. K_1 plot can be obtained. The specimen of configuration shown in Figure 8 was loaded using a torque wrench to a torque of 12.7 (N-m), with the equilibrium relationship expressed mathematically,

$$T = G D P^{(79)}$$
 (44)

where, T is Torque (N-m), D is the Nominal bolt diameter (m), P is the induced force or clamp load (N), and is G an empirical constant, which takes into account friction and the variable diameter under the head and in the threads where friction is acting. The P in Equation 1 (Novak and Rolfe $^{(41)}$) and Equation 42 yielded $K_T = 12 \text{ MPa}\sqrt{m}$.

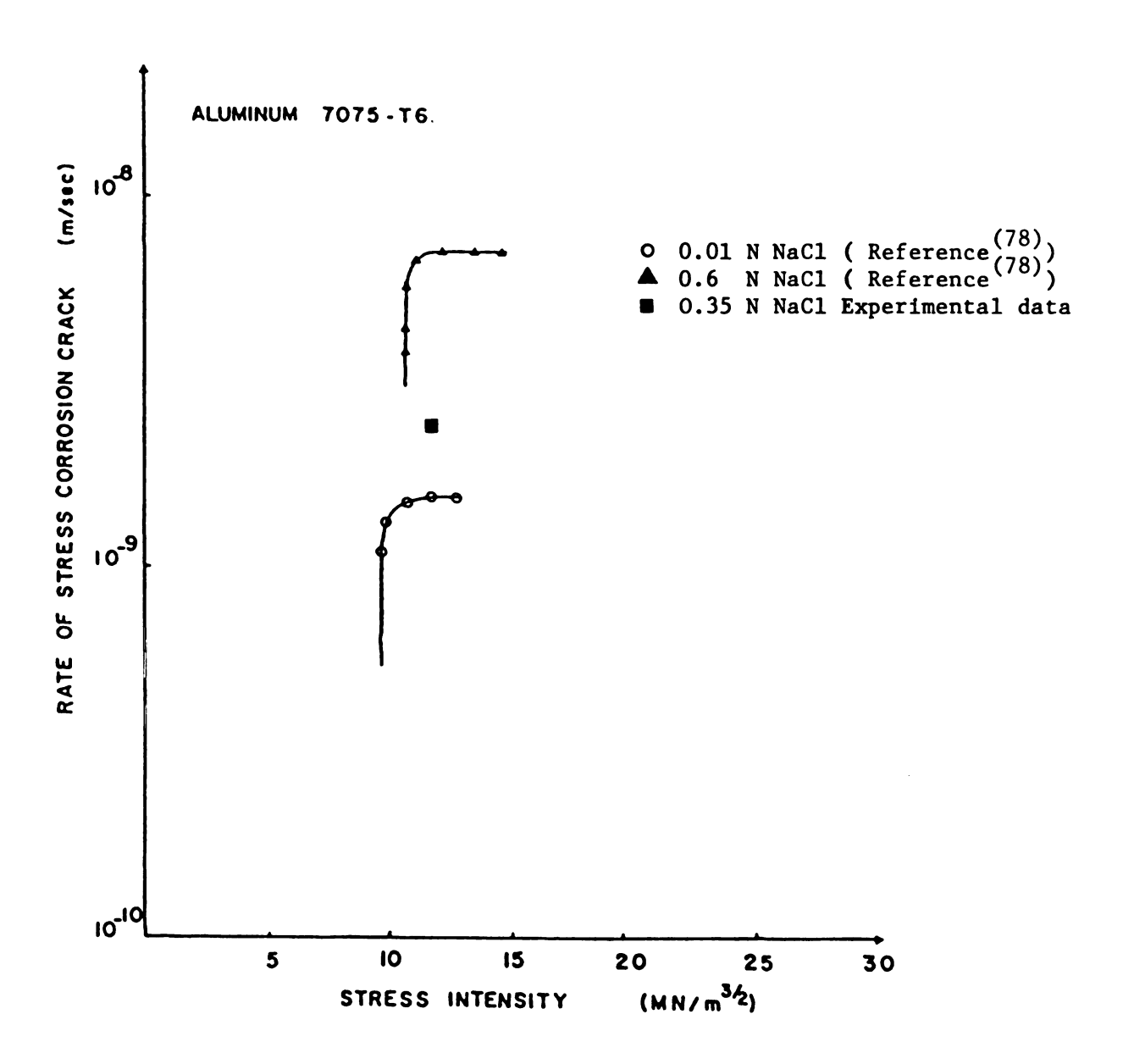


FIGURE 36 RATE OF CRACKING VERSUS STRESS INTENSITY FOR DILUTE NaCl SOLUTION

V. DISCUSSION

A. Bare Surface Corrosion.

Polarization profiles in Figure 9 show that since the bare surface dissolution rate is dependent on chloride content, the reaction involves complexes of chloride anion. Corrosion of Al and 7075-T6 Al alloy at the bare surface, in solutions containing dilute NaCl, is accompanied by the consumption of hydrogen, oxide, chloride, and sodium ions.

The most probable reactions mechanism accompanying the initial stage of the corrosion process of 7075 T6 Al alloys in NaCl is as follows (45):

$$A1 \stackrel{=}{\leftarrow} A1^{3+} + 3e^{-},$$
 (a)

$$A1 + H_2O \stackrel{->}{\leftarrow} H^+ + A10H^{2+},$$
 (b)

$$A1^{3+} + C1^{-} \stackrel{=}{\leftarrow} A1C1^{2+},$$
 (c)

$$A10H^{2+} + 2H_2O \stackrel{>}{\leftarrow} A1(OH)_2C1 + 2H^+,$$
 (c)

$$A1C1^{2+} + 2H_2O \stackrel{=}{\leftarrow} A1(OH)_2C1 + 2H^+, (d)$$

$$A1(OH)C1^{+} + H_{2}O \stackrel{-}{\leftarrow} A1(OH)_{2}C1 + H_{1}^{+}$$
 (f)

$$A1(OH)_2C1 + H_2O \stackrel{=}{\leftarrow} A1(OH)_3 + H^+ + C1^-.$$
 (g)

It is believed ^{(45),(46)}, that the hydrated aluminum ion, Al(H₂0)⁺³, is formed rapidly (about 1 sec). The hydrated Al³⁺ ion also undergoes a very fast hydrolysis reaction written as Equation (b). Later, both the Al³⁺ and Al(OH)²⁺ ion can react with Cl⁻ ions, i.e., Equations (c) and (e). Reaction (e) is faster, however, than reaction (d). From these experimental results, it may be suggested that both reactions (c) and (e) may take place as an anodic dissolution

mechanism.

On the other hand, the over-all cathodic reaction in nearly neutral solutions, based on the experimental results, is oxygen reduction,

$$o_2 + 2 H_2 O + 4e^- --- > 4 OH^-.$$
 (h)

From Figures 10 and 11, the limiting current density (i_L) is $10\,\mu\text{A/cm}^2$ for both concentrations (1 wt.% and 3 wt.% NaCl). Oxygen is relatively insoluble in NaCl solution at room temperature. According to Eq. (29), this low solubility in turn means that there is a small limiting current density for the cathodic reduction of oxygen.

In Figure 25, the applied stress affects the polarization behavior of Al 7075-T6 and raises the current density.

Stress corrosion cracking of the 7075-T6 aluminum alloys in chloride ion environments is because of the formation and growth of cracks of an almost brittle nature, which propagate along the grain boundaries. A number of mechanisms have been proposed (51),(52),(53) to account for the phenomenon. Three of the proposed mechanisms which have received wide attention are the film rupture (15),(16) model, the pre-existing active path model (14), and the hydrogen embrittlement mechanism (51),(52).

In the pre-existing path model, emphasis is placed on the microstructural and electrochemical parameters. Chemical inhomogeneities
in the material are regarded as being the key factor. An example often
quoted is the segregation of alloying elements in the form of precipitates
at grain boundaries in 7075 T6 aluminum alloy, creating a precipitatefree zone, in the adjacent material. In a corrosive environment a
highly localized electrochemical reaction can be established between the

precipitates and the adjacent material. Although this is an adequate explanation for intergranular corrosion, it does not account for the important role of tensile stresses in producing SCC (stress corrosion cracking).

According to the film rupture model, the role of the tensile stress is to rupture the protective or passivating oxide film. This exposes highly localized regions of fresh metal surfaces with electrochemical potentials quite different from the surrounding areas still protected by the oxide film. Thus corrosion is envisaged to occur at these sites until a new passivating oxide film can reform. This fresh film will in turn be ruptured and the corrosion and repassivation processes repeated, thereby generating an active path for SCC. In this mechanism, the rate of repassivation is the key factor. If repassivation is very rapid, insufficient corrosion will occur to promote SCC.

The mechanism of hydrogen embrittlement involves diffusion of water molecules or hydrogen ions down the crack, reduction of these species to adsorbed hydrogen atoms at the crack-tip surface, surface diffusion of adsorbed atoms to a preferred surface site, adsorption of the adatoms into the metal matrix, and followed by diffusion of hydrogen atoms to a position in front of the crack-tip. Nevertheless if hydrogen is indeed the basis of the embrittlement during SCC, the kinetics may still be influenced, if not controlled, by such processes as hydrogen permeation or stress induced rupture of the oxide film.

The possible crack-advancement mechanisms, that is, dissolution and hydrogen ion reduction, will be controlled at a given potential by three subsidiary factors: the oxide rupture rate, the solution-renewal rate, and passivation rate including repassivation rate. In these experiments, it can be found that passivation rate at the stress

concentration region, which is common to both mechanisms, that is film rupture (activation control) and hydrogen-embrittlement (diffusion control) mechanism, is the rate controlling reaction in the stress corrosion process.

B. Crack Electrochemistry.

According to the polarization curves in Figures 24, 26, and 27, hydrogen gas formation and bubbling were observed near the corrosion potential region. Under the experimental results, two major cathodic reactions may be considered, i.e., reduction of oxygen and hydrogen,

$$0_2 + 2 H_2 0 + 4e^- --- > 4 OH,$$

and
$$H_2O + e^- -- > \frac{1}{2} H_2 + OH^-$$
.

If both cathodic reactions may take place, the effect of the depolarization can be considered. Because of this effect, the corrosion rate will increase.

Figure 24 shows that the polarization profiles inside the isolated crack differ from the bare surface specimen. Furthermore, the pH inside the crack is also different from that of the external surface. In the case of the bare surface specimen, no hydrogen gas bubbling was observed.

These results show that the chemical and electrochemical environment of the crack tip may be different from the bulk exterior environment.

There also may be the possibility of additional or alternative electrochemical and/or chemical reactions such as hydrogen reduction inside the crack.

Figure 24 shows that 0.1 wt.% NaNO₂ + 0.1 wt.% Na₂B₄O₇ inhibitors may affect the chloride attack inside the crack, although Figure 14 shows only a small effect of these inhibitors. This is because of the establishment of a special, more complex microchemical or electrochemical environment within the crack which is different from the bulk exterior environment. Although localized corrosion is complex and involves many processes which occur simultaneously, many suggestions can be considered for this reason. If accumulation, by migration, of chloride ions within the crevice, and hydrogen by hydrogen evolution are another significant factor (hydrogen evolution is the main factor based on the results of the anodic polarization), it is possible that electrochemical behaviors would depend upon [Cl⁻] and [H⁺].

In the case of a coupled crack, Figure 30 and 31 show that the cathodic reaction (probably oxygen reduction and hydrogen reduction) takes place outside the crack and a little anodic reaction as well as hydrogen reduction occurs inside the crack. Figure 31 also shows that the anodic profile of an isolated crack is different from the profile of a coupled crack. The evidence of a different corrosion potential, the active potential and the anodic profiles probably result from the hydrogen evolution reaction. This cathodic reduction may control this corrosion mechanism or suppress the anodic dissolution.

According to Pourbaix (6), the surfaces which are outside the crack and are in direct contact with NaCl solution, are often passivated by oxygen, and are acting as aerated cathodes where oxygen is being reduced to water, for example,

$$0_2 + 4 H^+ + 4 e^- --- > 2 H_2 0$$

The surfaces which are inside the crack are active and are acting as non-aerated anodes where the metal undergoes corrosion and hydrolyzes with a decrease of pH, for example,

A1
$$\longrightarrow$$
 A1³⁺ + 3e⁻
A1³⁺ + 3 H₂O \longrightarrow A1(OH)₃ + 3H⁺.

The experimental result shows the decrease of pH inside the coupled crack and indicates weak acidity inside the crack, and chloride ion inside the crack affects the anodic dissolution .

Rosenfeld (55) shows a general mechanism of real crack involving the effects of chloride ion and acidity,

Me +
$$H_2O$$
 - 2e --> MeO + $2H^+$,
Me + $2H_2O$ - 2e --> Me(OH)₂ + $2H^+$,
Me + $2CI^-$ - 2e --> Me $C1_2$ (ads) + H_2O -->
--> MeO + $2H^+$ + $2CI^-$.

Our experimental results show that hydrogen evolution and oxygen reduction (secondary) take place cathodically, and anodic dissolution may take place anodically (anodic condition).

Pickering and Frankenthal (24) showed that large potential drops attributed to constrictions are caused by trapped hydrogen gas bubbles. For our experimental results, the following two cathodic processes can be considered. (1) Hydrogen evolution and (2) ionization of oxygen.

These may proceed by independent but parallel stages and are related

to one another only as they provide an overall electrochemical potential on the corroding surface. However, the hydrogen evolution reaction may take an important role as the main controlling cathodic process.

The hydrogen evolution process possesses high diffusion mobility and a high rate of migration in an electric field. An increase in the rate of hydrogen evolution with consequent evolution of hydrogen bubbles will decrease the thickness of the diffusion layer of liquid ajacent to the surface of the metal, because of the additional mixing. As a result, the limiting diffusion current for oxygen reduction also will increase, as is evident from Equation (34). The presence of hydrogen bubbles on the metal surface may decrease oxygen diffusion, either as a result of a smaller electrolyte cross section, or by removal of oxygen from the metal surface by entrapment with the evolved bubbles of In our experimental results, the principal effect of hydrogen evolution on the limiting diffusion current density for oxygen has been suggested to consist of a decrease in the thickness of the diffusion layer as a result of increased agitation caused by hydrogen evolution.

Uhlig (58) suggested the importance of hydrogen evolution in a different role as a controlling factor. When aluminum dissolves anodically, both Al⁺³ and Al⁺ are formed, initially the univalent ion which then reduces water to form the trivalent ion. During formation of a surface oxide film, the hydrogen evolution reaction takes place simultaneously at the anode as well as at the cathode. In the anodic dissolution process, hydrogen evolution is responsible for increased local corrosion action. Many actions of hydrogen as well as migration are probably responsible for the potential drop as well as

separation of the anodic and cathodic sites.

Another experimental result in the case of an isolated crack, shows that the current density is independent of the concentration of Cl⁻ ion, i.e., the rate of corrosion inside the crack is controlled by a cathodic process. When aluminum dissolves anodically, both Al³⁺ and Al⁺ may be formed. Initially, the univalent ion then reduces water to form the trivalent ion,

A1 +
$$H_2^0$$
 --> $A10H_{ads}$ + H^+ + e^- ,

 $A10H_{ads}$ + $5H_2^0$ + H^+ --> $A1^{3+}$ $6H_2^0$ + $2e^ 2A10H_{ads}$ + H_2^0 --> $A1_2^0$ + $4H^+$ + $4e^-$

or $A1^+$ + $2H_2^0$ ---> $A1^{+2}$ + H_2 + $20H^-$.

During these processes, in the rate-determining steps, these reactions do not involve complexes with Cl ion.

C . Mathematical Model

Several models for crevice corrosion or corrosion cracking have been proposed (21),(22),(25) which yield distributions of current, voltage, and composition in the crevice and nearby regions. The results indicate that the approach shows promise, especially in predicting crevice gap/depth ratios that are the most critical for localized attack. Porous electrode theory (63) can also be used to predict the depth at which the anodic reaction may be driven by an external cathodic current. Ohmic drop restricts the penetration of current into a small-gap, occluded region. At greater depths in the gap, the metal is isolated from the external Newman (64) calculated the depth to which a reaction surface reactions. Turnbull (65) showed improved mathmay penetrate the walls of pipe. ematical modelling of mass transport of oxygen in a crevice or crack for an estimation of the oxygen concentration. Diffusion and acid hydrolysis were included in a mathematical model for crevice corrosion by Galvele (66).

A sophisticated model for stress corrosion cracking of titanium was developed by Beck; (76) transport limitations, wall reactions and nonlinear kinetics were included in the model. Alkire and Hebert (21) developed improved mathematical modelling for initiation of corrosion of pure aluminum. His model accounts for electrode reactions of aluminum, oxygen and hydronium ion; and for transport by unsteady state diffusion and migration.

In our research, inside the crack, hydrogen evolution reaction takes place cathodically and anodically, although the reaction is a cathodic process. The electrode potential of the metal inside the crack is lower than the hydrogen equilibrium potential in the relevant

solution. The anodic corrosion reaction is not the only possible one; a cathodic evolution of hydrogen according to $2H^+ + 2e^- - H_2$ also may occur inside the crack under the anodic condition. Our results show that near the corrosion potential, only cathodic evolution of hydrogen may take place and hinders the anodic dissolution so that Pickering and Ateya's (25) mathematical model may be useful and can describe the mass transfer of the electrolyte taking place by molecular diffusion and ionic migration according to the Nernst-Einstein relation. From the ideas discussed in an earlier section (theoretical background), the following model can be written.

According to Pickering and Ateya,

$$J_{H}^{+} = -D_{H}^{+} \left(\frac{dC_{H}^{+}}{dx} + C_{H}^{+} + \frac{F}{RT} \frac{d\emptyset}{dx} \right) = \frac{1}{F}, \tag{45}$$

$$J_{C1}^{+} = -D_{C1}^{-} \left(\frac{dC_{C1}^{-}}{dx} - C_{C1}^{-} \frac{F}{RT} \frac{d\emptyset}{dx} \right) = 0, \quad (46)$$

where D_H^+ is the diffusivity of H^+ ion, D_{C1}^- is the diffusivity of C1, C is the concentration of the indicated species, \emptyset is the local electrical potential in the crack, and i is the local current density of the hydrogen evolution reaction; T is the absolute temperature, F is the Faraday constant, and R is the gas constant. The equation of electroneutrality is

$$\sum_{i} C_{i} = 0, \tag{47}$$

i.e.,
$$C_{H} + = C_{C1} - = C.$$
 (47)

The experimental results also show that after a few hours, the potential and current attain a steady-state condition. Acorroding to the Pickering model,

$$C = C_0 \exp\left(\frac{F \emptyset}{R T}\right). \tag{48}$$

Modifying Equation(48), by Equation(47) and substituting in Equation(45) gives

$$J_{H}^{+} = -2 D_{H}^{+} C_{O} \frac{F}{R T} \frac{d \emptyset}{d x} \exp \left(\frac{F \emptyset}{R T}\right). \tag{49}$$

Pickering derived the following equation,

$$\emptyset = \frac{R T}{F} \ln \frac{\cosh \left[\left(L - x \right) / X \right]}{\cosh \left[L / x \right]}, \tag{50}$$

where

$$X = (D_{H} + C_{O} F a / i_{S}),$$

$$i_{S} = i_{O} \exp \left(\frac{\beta F}{R T}\right), \text{ or } i = i_{S} \left(\frac{C}{C_{O}}\right) \exp \left(\frac{\beta F \phi}{R T}\right),$$

where $\boldsymbol{\beta}$ is the transfer coefficient of the hydrogen evolution reaction, and $\boldsymbol{\emptyset}$ is the local electrical potential in the crack and solution. Figure 35 shows the experimental results of the open circuit corrosion potential vs a function of time inside the real crack. According to Figure 35, the potential difference from outer surface is about 40 mV. Mathematically, the potential difference $\boldsymbol{\emptyset}$ can be calculated from Equation (50), that is,

$$\emptyset = \frac{R T}{F} \ln \frac{\cosh \left[\left(L - x \right) / X \right]}{\cosh \left[\left(L / X \right) \right]}, \tag{50}$$

within the crack. Values for the relevant parameters are as follows: $X = (D_H + C_O F a/i_S)$, $D_H + + 5 \times 10^{-5} cm^2/sec$, $\frac{RT}{F} = 25mV$. The crack length (L) is 1 cm, and crack width (a) is 0.01 cm. $C_O = 0.17 mole/1$, F = 96500 c/mole, i_S can be obtained from the experimental results (Figures 26 and 27). From the experimental data (Figure 26),

$$i_s = 20 \,\mu\text{A/cm}^2 = 20 \, \times \, 10^{-6} \,\mu\text{A/cm}^2$$
,
 $X = (D_H + C_o \, F \, a \, / \, i_s) = 0.64$
Thus, the potential
 $\phi = \frac{R \, T}{F} \, \ln \, \frac{\cosh \, [\, (L - \times \,) \, / \, X \,]}{\cosh \, [\, (L/X \,) \,]} = 18 \, \text{mV}$

According to the calculation, $\emptyset = 18$ mV, about 20 mV, which this theoretical value is not in very good agreement with the experimental value.

Another important mathematical model with a different approach has been proposed by Doig and Melville (69), (70), (73).

They show that when stress corrosion cracks, growing by enhanced anodic disolution, are subjected to an external polarization, an electrode potential distribution is established within the crack. Figure 37 shows the schematic diagram of a crack of width w in the Z direction and length x in the X direction and width y in the Y direction.

The width y is very much greater than the width w so that it may be considered to be of infinite length. In our experiment (Figure 37), following crack was used for analysis

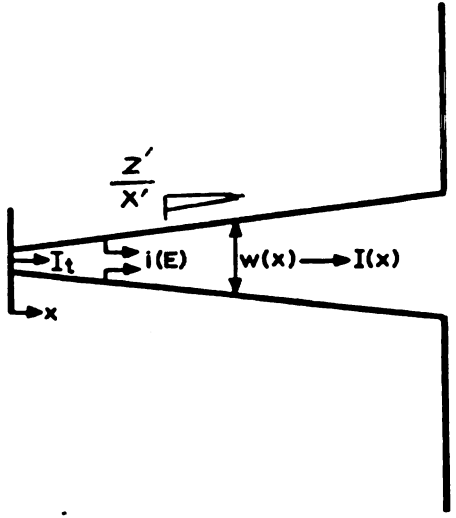


Fig 37 Schematic representation of the crack

However, $\frac{Z'}{X'}$ <<0 so that we may assume that the effect of variation of crack width may be neglected. Figure 38 shows the Evans polarization diagram.

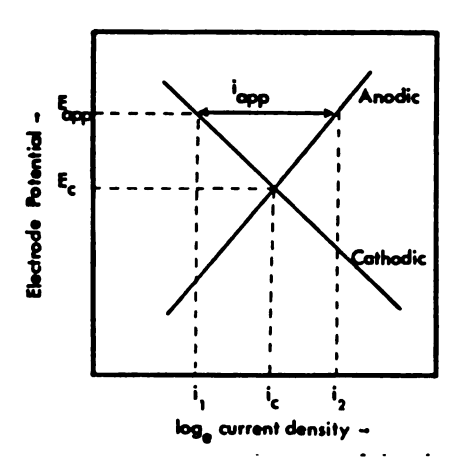


Figure 38 Schematic Polarization Diagram of the Electrochemical Reactions Occurring at the Specimen Surface Showing the Influence of Potentiostatic Polarization

Ec is the corrosion potential at external surface, i is the corrosion current density at potential E_c and E_x is the potential at position x within a crack (V). According to Doig and Flewitt $^{(73)}$, the net anodic i app at E_{app} is given by

$$i_{app} = i_{c} \left[exp \left(\frac{E_{app} - E_{c}}{d} \right) - exp \left(\frac{E_{app} - E_{c}}{-\beta} \right) \right].$$
 (51)

More generally, the net current density, $\mathbf{i}_{\mathbf{x}}$, at any potential $\mathbf{E}_{\mathbf{x}}$ is given by

$$i_{x} = i_{c} \left[\exp \left(\frac{E_{x} - E_{c}}{\Delta} \right) - \exp \left(\frac{E_{x} - E_{c}}{-\beta} \right) \right]. \tag{52}$$

According to Doig and Flewitt, the net anodic current flow within the crack at a distance x from the free surface is the integrated sum of the net anodic current generated on the crack surface at distance greater than X,

$$\frac{\mathrm{d} \, \mathbf{i}_{\mathrm{f}}}{\mathrm{d} \, \mathbf{x}} = 2 \, \mathbf{i}_{\mathbf{x}},\tag{53}$$

and

$$i_f = -wc \left(\frac{d E_x}{d x} \right). \tag{54}$$

Consequently, from Equation (53) and the differential Equation (54), we obtain

$$\frac{d^2 E_x}{d X^2} = \frac{-2 i c}{W c} \left[\exp \left(\frac{E_x - E_c}{d} \right) - \exp \left(\frac{E_x - E_c}{-3} \right) \right]. \quad (55)$$

In order to apply this model to real experimental conditions, it was modified, following Melville's (70,71) line of reasoning, According to Melville, the variation of potential is described under more general conditions. If E(x) is the potential of the specimen relative to the solution at a position, X, in the crack, there is a change dI, in the current down the crack over a length, dx, given by,

$$dI = 2 ti (E) dx. (56)$$

Ohms law gives the change in the potential, dE of the solution over a length dx as

$$dE = -\frac{I}{t W C} dx. ag{57}$$

If I(x) is the current down the crack, and C is the conductivity of the solution,

$$\frac{dE}{dx} = -\frac{I}{TWC}, \qquad (58)$$

then

$$\frac{d^2E}{dx} = \frac{2 i (E)}{E}, \qquad (59)$$

and

$$-\frac{d^2E}{dx^2} = \frac{dE}{dx} - \frac{d}{dE} \left(\frac{dE}{dx} \right). \tag{60}$$

If the potential remains close to the free corrosion potential for the passivated sides of the crack, E_{c} , the function i(E), describing the electrochemical reactions on the crack sides may be approximated by

$$i(U) = KU, \tag{61}$$

where $U = (E - E_c)$, and

$$K = \frac{d \mathbf{1}}{d E} \Big|_{E=E_C} = \frac{d \mathbf{1}}{d \mathbf{U}} \Big|_{\mathbf{U}=\mathbf{0}}$$
 (62)

The second order differential Equation (60), then is applied to Equation (61),

$$\frac{d^2 U}{d x^2} = \chi^2 U,$$

where

Integration of Equation (62) yields

$$\frac{d U}{d x} = (U^2 + b)^{1/2}, \tag{64}$$

where b is a constant to be determined from the boundary conditions,

$$x = \ln \left[\frac{U + (U^2 + b)^{1/2}}{U + (U + b)^{1/2}} \right], \tag{65}$$

and

$$U = 0$$
, at $x = 1$. Equation (65) gives

$$U(x) = U_0 \frac{\sinh (L - x)}{\sinh L}. \tag{66}$$

From the experimental data (Figure 21),

$$K = \frac{1}{4.95 \times 10^{-2}}$$
 A m²/ V

The crack width (w) is 0.1 mm = 0.1 x 10^{-3} , the total crack length (L) is 1 cm = 1 x 10^{-2} m and % = (2 K/w) is 449.46, hence

$$\frac{U(x)}{U_{0}} = \frac{\sinh^{\eta} L(1-x/L)}{\sinh^{\eta} L} = 0.2587$$

If we find the U(x) value, U_0 can be calculated.

According to the experimental data (Figure 35), U(x) is about -0.040 V, and U_0 (potential at cract tip) is about -0.155 V. It is impossible to obtain experimentally the potential at the tip of the crack. However, potential at the crack tip of crack can be calculated, if polarization curves for the materials are presented, and if it may be assumed that the sides of the crack behave in a similar fashion to the outside surfaces of the specimen.

Melville (71) also has developed an analytical method of solution for the calculation of the variation in potential with stress corrosion cracks where there is a simultaneous variation in the current density with potential along the sides of the crack and a variation in the width of the crack along its length. According to Melvilles modified mathematical model,

$$dI = 2 t i (E) dx, (67)$$

where E(x) is the potential of the specimen relative to the electrolyte, and i(x) is the corrosion current density. Then

$$dE = \frac{I(x)}{t C w(x)} dx, \qquad (68)$$

where I(x) is the current down the crack, C is the conductivity of the electrolyte. Further

$$\frac{dI}{dx} = 2 t i(E) = t C w(x) \frac{d^2 E}{dx^2} + t C \frac{dw}{dx} \frac{dE}{dX}, \quad (69)$$

$$w = w_0 + bx, \tag{70}$$

$$i(E) = i_0 + a(E - E_0), \text{ and}$$
 (71)

$$a = \frac{d i}{d E} \qquad (72)$$

From these equations, we have

C
$$(w_0 + bx) - \frac{d^2 E}{dx^2} + C b - \frac{dE}{dX} - 2 [i_0 + a(E - E_0)] = 0,$$
 (73)

which on substitutions for

$$V = E - E_0 + i_0/a,$$
 (74)

$$y = x + w_0/b, (75)$$

$$a = 8a/Cb, (76)$$

reduces to

$$y^{2} \frac{d^{2}V}{dy^{2}} + y \frac{dV}{dy} - \frac{1}{4} a y V = 0,$$
 (77)

By using the Transformed Bessel Equation, equation (77), can be solved. In general,

$$y^{2} \frac{d^{2} V}{d y^{2}} + (2p + 1) y \frac{d V}{d y} + (d^{2} y^{2} + \beta^{2}) V = 0.$$
 (76)

A general solution of this equation is

$$V = y^{-p} \left[C_1 J_{q/r} \left(\frac{\lambda}{r} y^r \right) + C_2 y_{q/r} \left(\frac{\lambda}{r} y^r \right) \right], \tag{77}$$

with p = 0, r = 1/2, and q=0. Therefore,

$$V = C_1 J_0 (a^{1/2} y^{1/2}) + C_2 K_0 (a^{1/2} y^{1/2}),$$
 (78)

where $J_0(\lambda^{1/2} y^{1/2})$ and $K_0(\lambda^{1/2} y^{1/2})$ are zero order Bessel functions.

Under free corrosion conditions, the potential at the crack mouth is close to the free corrosion potential $\mathbf{E}_{\mathbf{C}}$, and the boundary conditions used are that

$$E = E$$
 = E at $x = 1$, and $I = I$ at $x = 0$.

In the general case where both w(x) and i(E) vary, putting $i_0 = 0$ and with boundary conditions that $E = E_0 = E_c$ at x = 1 and

$$1 = t C w_1 dE/dx = I_t$$
, $x = 0$, we have

$$E = E_{c} - \frac{I_{t}}{t \cdot C \cdot w_{o}} \frac{2y_{o}}{d^{1/2}} \left[\frac{J_{o}(x_{o}^{1/2} y_{1}^{1/2}) K_{o}(x_{o}^{1/2} y_{1}^{1/2})}{J_{1}(x_{o}^{1/2} y_{1}^{1/2}) K_{o}(x_{o}^{1/2} y_{1}^{1/2})} - \frac{1}{2} \left[\frac{J_{o}(x_{o}^{1/2} y_{1}^{1/2}) K_{o}(x_{o}^{1/2} y_{1}^{1/2})}{J_{1}(x_{o}^{1/2} y_{1}^{1/2}) K_{o}(x_{o}^{1/2} y_{1}^{1/2})} \right]$$

$$\frac{K_{o} \left(\lambda^{1/2} \ y_{1}^{1/2} \right) I_{o} \left(\lambda^{1/2} \ y_{1}^{1/2} \right)}{K_{1} \left(\lambda^{1/2} \ y_{0}^{1/2} \right) I_{o} \left(\lambda^{1/2} \ y_{1}^{1/2} \right)}], \tag{79}$$

where $y_0 = w_0/b$ and $y_1 = (1 + w_0/b)$. This may be evaluated at $y = y_0$ to give the potential at the crack tip as ,

$$E = E_c - \frac{I_t I}{t C w_0} g (\Gamma, w_1),$$
 (90)

where $w_1 = w_1/w_0$, and w_1 and w_0 are the widths of the crack at the mouth and crack tip, respectively. Then

$$g(\Gamma, w_1) = \frac{2}{\Gamma^{1/2}(w_1 - 1)} \left[\frac{\int_0^1 (\Gamma^{1/2} w_1^{1/2}) K_0(\Gamma^{1/2})}{I_1(\Gamma^{1/2}) K_0(\Gamma^{1/2} w_1^{1/2})} - \frac{1}{\Gamma^{1/2}(\Gamma^{1/2} w_1^{1/2})} \right]$$

$$\frac{K_{o}(\Gamma^{1/2} w_{1}^{1/2}) J_{o}(\Gamma^{1/2})}{K_{1}(\Gamma^{1/2}) J_{o}(\Gamma^{1/2} w_{1}^{1/2})},$$
(91)

where
$$T = y_0 = \frac{8 \text{ a w}_0}{\text{C h}^2}$$
.

Values of the parameter, Γ can be obtained directly from Eq.(74) using a = di/dE or from a logarithmic plot of current density against potential, from which a becomes

$$a = \frac{di}{dE} = [i (E) ln (10) \frac{d(log i)}{dE}]$$

According to our experiment.

 $C = 0.5 (\Omega m)^{-1}$, $w_1 = 0.1 mm$ (the crack width at point x) $w_0 = 0.01 mm$ (the width of crack tip)

$$a = \frac{d1}{dE} = 10 \text{ A/Vm}^2.$$

Value of g(Γ , W_1) which can be obtained from the calculations is

$$g(\Gamma, W_1) = 0.365.$$

The potential difference, that is, $E-E_c=\emptyset$ can also be obtained using

$$\emptyset = \frac{I_t}{t} \frac{1}{CW_0} g \left(\prod_{i=1}^{n} w_i \right). \quad \text{If } I_t \text{ is about } 320 \times 10^{-2} \text{ A/m}^2, \text{ then}$$

$$\frac{I_t 1}{t C w_0} = 64 \text{ mV}.$$

Therefore.

$$\emptyset = E - E_0 = -\frac{I_t I}{t C w_0} g (T, W_1) = -64 \times 0.365 = -23.36 \text{ mV}$$

According to the calculation $\emptyset = 23.36$ mV, and experimental value was founded to be $\emptyset = 35-45$ mV. The real potential drop is larger than that calculated by the Equation (79) but the difference between the experimental and calculated values is not large, although one also may take into account a variation in the conductivity of the electrolyte in the crack by making the substitution, $Cw = C_0W + PX$, where the term in PX taken into account the variation of the product of conductivity. According to these calculations, the effect of the variation in crack width plays a significant role.

VI CONCLUSION

- (1) The electrode potential at the tip of a stress corrosion crack which is growing by an anodic dissolution mechanism is lower than the bulk corrosion potential, i.e., the electrode potential at the crack tip is more active than at the crack mouth. Because of this effect, there are additional or alternative electrochemical reactions, such as hydrogen evolution reaction as well as anodic dissolution within the crack.
- (2) There is a potential difference between the bulk and the crack tip. Because of this difference, the electrochemical drive force becomes more favorable for the development of corrosion inside the crack. Futhermore, enhanced anodic dissolution of the crack tip, together with the corrosion reactions on the crack surface, will result in composition changes within the crack.
- (3) Because of the observation of H₂ gas formation within the crack under an active condition, the hydrogen evolution reaction takes place within the crack. Because of the hydrogen evolution reaction, it may be suggested that the environment-controlled component in stress corrosion cracking probably results from the diffusion-controlled mechanism (hydrogen enhanced embrittlement) as well as activation reaction-controlled mechanism (slip dissolution mechanism).
- (4) Because of the high concentration (1 wt.% 3 wt.%) of NaCl, corrosion attack on 7075 T6 Aluminum Alloy is quite severe. A passivator, such as nitrite and chelating agents, were studied for their ability to inhibit the chloride ion penetration into the aluminum surface. In our experiments, however, anodic polarization curves in Figures 14, 16 and 17 indicated no discontinuities which normally are associated with film formation and no passivation. It may be suggested that the passive film formed by NaNO₂

and chelating agents in small inhibitor concentrations is still weak and not very effective against chloride attack when chloride ions are present in high concentration without having a high concentration of inhibitors. On the other hand, multi-functional inhibitors such as nitrite-borax with small amounts of surfactant such as mercaptobenzothiazole (MBT) or aminomethyl-propanol, are excellent inhibitors. The surfactant interferes in the dissolution reaction and blocks active chloride ion and hydrogen ion by interacting synergistically with the passive film produced by the borax-nitrite, which results in development of a stronger and thicker protective film.

(5) According to Figure 9, the polarization behavior of the bare surface is dependent on chloride content. The polarization curves also show that the anodic dissolution kinetics of the bare surface do not follow Tafels

Law because of not simple charge-transfer controlled process. Furthermore, passivation does not occur by a dissolution process.

On the other hand, Figures 30 and 31 show that the anodic dissolution kinetics of the crevice surface follow Tafels Law and dependence on chloride content. This is expected for a simple charge-transfer rate-controlled anodic dissolution reaction. This reaction also does involve complexes of chloride anion.

(6) In neutral electrolytes in which oxygen is the principal cathodic depolarizer, concentration plays a substantial part both in the corrosion process taking place as result of the microelements and the emergence of the macroelement.

According to Figures 10 and 26, the magnitude of the limiting diffusion current density for cathodic reduction inside the crack is the same as that of the bare surface (about $10\,\mu\text{A/cm}^2$). Inside the crack, the principal effect of hydrogen evolution on the limiting diffusion current density for

oxygen has been suggested to consist of a decrease in the thickness of the diffusion layer as a result of increased agitation caused by hydrogen evolution. If this is true, the oxygen inside the crack is consumed quite rapidly, in the cathodic reaction, i.e., the drop in oxygen concentration or oxygen depletion occurred and this should lead in NaCl electrolytes to a change in the kinetics of the cathodic process. It is suggested that oxygen may play an insignificant part.

(7) Of considerable importance in corrosion cracking are the geometrical factors, since the width and depth of clearance determine the distribution of the potential and the effectiveness of the macroelements.

The mathematical results show the crack width affects the potential drop inside the crack because of the existence of electric potential gradients. Furthermore, the experimental result shows the decrease of pH inside the crack and indicates weak acidity inside the crack because of precipitation and hydrolysis equilibria of the corrosion products. Since access of fresh acid into the narrow recess from the body is impeded, the difference in the value of pH of the electrolyte inside the crack and the external surface is maintained. This changes the values of the potentials of the metals inside the crack and outside the crack and brings about the formation of a concentration cell.

Figure 35 shows the experimental results of the potential distribution inside the crack with stress. As the width of the crack diminishes, corrosion acquires a local character, because of electric potential gradients, acidification of the medium and action of chloride ion.

REFERENCES

- M. Khobaib, "Development of Corrosion Inhibitors",
 AFML-TR-79-4127, Air Force Wright Aeronautical Laboratories,
 Wright-Patterson AFB OH, Sept., 1979.
- M. Khobaib, "Bilge Inhibitors "AFWAL-TR-81-4186, Air
 Force Wright Aeronautical Laboratories, Wright-Patterson AFB,
 OH, Feb 1980.
- 3. C. C. Nathan, "Corrosion Inhibitors," NACE, Houston, TX 1974
- 4. U. R. Evans, Trans. Faraday Soc. 30, 417 (1954).
- 5. I. L. Rosenfeld and I. K. Marshakov, Corrosion 20, 115 (1964).
- 6. M. Pourbaix, in "Localized Corrosion", R. W. Staehle et al., eds., Pl2, NACE, Houston, TX (1974).
- 7. E. McCafferty, <u>J. Electrochem. Soc.</u> 121, 1007 (1974).
- 8. M. G. Fontana and N. D. Greene, "Corrosion Engineering," 2nd edn.,
 McGraw-Hill, New York (1978).
- 9. R. C. Alkire and G. Nicolaides, <u>J. Electrochem. Soc.</u> 121, 183 (1974).
- 10. R. C. Alkire and D. W. Siitari, <u>J. Electrochem. Soc.</u> <u>129</u>, 481 (1982).
- 11. G. S. Eklund, J. Electrochem. Soc. 129, 170 (1976).
- 12. F. P. Ford, J. Met. Sci., July (1978), P.326
- 13. K. Khobaib, C. T. Lynch, and F. W. Vahldiek, <u>Corrosion</u> 36, 285 (1981)
- 14. E. N. Pugh, Metallurgica 63, 3 (1961).
- 15. E. N. Pugh, <u>Trans. Am. Soc. Metals.</u> 62, 238 (1967).
- 16. W. K. Boyd, Proc. Conf. "Fundamental Aspects of Stress Corrosion Cracking", NACE Houston (1969).

- 17. J. D. Harston and J. C. Scully, Corrosion 26, 387 (1970).
- 18. P. R. Swann, <u>Corrosion</u> 19, 102 (1963).
- 19. P. R. Swann, J. Inst. Metals 88, 478 (1959)
- 20. T. P. Hoar, J. Electrochem. Soc. 120, 1013 (1973).
- 21. R. Alkire and K. Hebert, J. Electrochem. Soc. 130, 1001 (1983).
- 22. F. D. Bogar and R. T. Foley, <u>J. Electrochem. Soc.</u> 119, 462 (1983).
- 23. M. J. Pryor, in "Localized Corrosion", R. W. Staehle et. al., Eds, P2, NACE, Houston, TX (1974).
- 24. H. W. Pickering and R.P. Frankenthal, <u>J. Electrochem. Soc.</u> 119, 1297 (1972).
- 25. H. W. Pickering and B. G. Ateya, <u>J. Electrochem. Soc.</u> 122, 1018 (1974).
- 26. A. A. Seys and M. J. Brabers, <u>Corrosion</u> <u>30</u>, 47 (1974).
- 27. D. Siitari and R. Alkire, J. Electrochem. Soc. 126, 15 (1979).
- 28. U. R. Evans and C. Edeleanu, <u>Trans. Faraday Soc.</u> 47, 1121 (1951).
- 29. R. C. Alkire and D. Siitari, <u>J. Electrochem. Soc.</u> <u>129</u>, 488 (1982).
- 30. E. McCafferty, J. Electrochem. Soc. 129, 385 (1979).
- 31. J. A. V. Butler, <u>Trans. Faraday Soc.</u> 28, 379 (1932).
- 32. J. O. M. Bockris and A. K. N. Reddy, "Modern Electrochemistry",
 Vol. 2, Plenum Press, New York, (1970).
- 33. J. O. M. Bockris, "Modern Aspects of Electrochemistry", Academic Press, New York, (1954).
- 34. J. A. V. Butler, Pro. Roy. Soc. London. A157, 423 (1936).
- 35. M. Stern and A. L. Geary, J. Electrochem. Soc. 104, 56 (1957).

- 36. M. Stern, <u>J. Electrochem. Soc.</u> 102, 602 (1955).
- 37. M. Stern, <u>J. Electrochem. Soc.</u> <u>14</u>, 440 (1958).
- 38. M. Stern, J. Electrochem. Soc. 104, 559 (1957).
- 39. S. Barnatt, J. Electrochem. Soc. 99, 549 (1952).
- 40. J. Newman, "Electrochemical Systems", Prentice-Hall, Englewood Cliffs (N.J) (1973).
- 41. S. R. Novak and S. T. Rolfe, <u>J. Material</u>. <u>4</u>,701 (1969).
- 42. Shi-Qun Li, Scripta Met. 13, 1063 (1979).
- 43. W. G. Clark and J. D. Landes, in "Stress Corrosion New Approaches" STP 610, ASTM P108.
- 44. Shi-Qum Li, Corrosion . 36, 475 (1980).
- 45. R. T. Foley and T. H. Nguyen, J. Electrochem. Soc. 120, 464 (1982).
- 46. R. T. Foly and T.H. Nguyen, J. Electrochem. Soc. 127, 2563 (1930).
- 47. K. Bhansali, C. T. Lynch, F. Vahldiek and R. Summitt,
 "Effect of Multifunctional Inhibitors on Crack Propagation Rate
 of High Strength Steel in Corrosive Environments ", Conf. Effect of
 Hydrogen on Mechanical Behavior of Materials, Moran, WY, 7-11 Sept.
 1975.
- 48. C. T. Lynch, F. Vahldiek, K. J. Bhansali and R. Summitt,

 "Inhibition of Environmentally Enhanced Crack Growth Rates in

 High Strength Steels "Symp. Environment Sensitive Fracture of

 Engineering Materials, AIME Meeting, Chicago, IL, 26 Oct. 1977.
- 49. J. M. West, "Basic Corrosion and Oxidation". John Wiley & Sons, New York, 1980.
- 50. M. Khobaib, L. Quakenbush and C.T. Lynch, Corrosion, 39, 7 (1983).

- 51. J. A. Davis, in "Localized Corrosion", R.W.Staehle et al.,
 Eds, P168, NACE, Houston, TX (1974).
- 52. D. Davies, J.P. Dennison, and M.L.Mehta, Corrosion 27, 371 (1971).
- 53. J. A. Smith, M.H. Peterson and B.F. Brown, <u>Corrosion</u> <u>26</u>, 536 (1970).
- 54. J. W. Oldfield and W.H.Sutton, Brit. Corros. J. 13, (1978)
- 55. I L. Rosenfeld, in "Localized Corrosion", R.W. Staehle et al.,
 Eds. P373, NACE, Houston, TX (1974) .
- 56. W. D. France and N. D. Greene, Corrosion 24, 247 (1968).
- 57. D. A. Vermilyea and C. S. Tedmon, <u>J. Electrochem. Soc</u>. <u>117</u>, 437 (1970).
- 58. H. H. Uhlig, "Corrosion and Corrosion Control," 2nd Ed., John Wiley 1971.
- 59. F. O. Ford and T. P. Hoar, <u>J. Electrochem. Soc.</u> 28, 1325 (1980).
- 60. E. Raijola and A. Davidson, J. Am. Chem. Soc. 78, 556 (1956).
- 61. M. J. Johnson, ASTM STP Vol. 516, P262 (1972).
- 62. K. D. Efrird and E. D. Verink, Jr., Corrosion 33, 328 (1977).
- 63. J.Newman and W. Tieman, in "Advances in Electrochemistry and Electrochemical Engineering, "Vol. 11, H.Gerischer and C.W. Tobias, eds., Wiley Interscience, New York (1978).
- 64. J. Newman, in "Localized Corrosion", R. Staehle, ed., NACE,
 Houston (1974).
- 65. A Turnbull, <u>Brit. Corros. J.</u> <u>15</u>, 4 (1980).
- 66. J. R. Galvele, J. Electrochem. Soc. 123, 464 (1976).
- 67. R. Alkire and K. Hebert, <u>J. Electrochem. Soc.</u> 116, 177 (1969).
- 68. R. Alkire and K. Hebert, <u>J. Electrochem. Soc.</u> 130, 1007 (1983).

- 69. P. Doig and P. E. J. Flewitt, Met. Trans. 9A, 357 (1978).
- 70. P. H. Melville, Brit. Corrosion J. 14, 15 (1979).
- 71. P. H. Melville, Brit. Corrosion J. 15, 26 (1980).
- 72. Michigan State University Water Department, private communication
 Junuary (1984).
- 73. P. Doig and P.E.J.Flewitt, Corrosion 37, 378 (1981)
- 74. Metals Handbook, 8th Edition, Vol. 1, p. 948, ASM (1961).
- 75. R. Summitt and F.T. Fink, "Experimental Determination of Environmental Corrosion Severity", AFWAL-TR-80-4102, Air Force Wright Aeronautical Laboratories, Wright-Patterson AFB, OH, June, 1980.
- 76. T.R. Beck and E.A. Grens, J. Electrochem. Soc. 116, 177 (1969).
- 77. M. Pourbaix, "Atlas of Electrochemical Equilibria in Aqueous Solutions", NACE, Houston, p. 499 (1966).
- 78. B.F. Brown and R.T. Foley, Corrosion 36, 673 (1980).
- 79. G.S. Havlland, Mechanical Engineering, Oct. 17 (1983).